2012

Performance optimization of wind turbines

Zijun Zhang
University of Iowa

PERFORMANCE OPTIMIZATION OF WIND TURBINES

by

Zijun Zhang

An Abstract

Of a thesis submitted in partial fulfillment of the
requirements for the Doctor of Philosophy degree
in Industrial Engineering
in the Graduate College of
The University of Iowa

May 2012

Thesis Supervisor: Professor Andrew Kusiak

ABSTRACT

Improving performance of wind turbines through effective control strategies to reduce the power generation cost is highly desired by the wind industry. The majority of the literature on performance of wind turbines has focused on models derived from principles versed in physics. Physics-based models are usually complex and not accurate due to the fact that wind turbines involve mechanical, electrical, and software components. These components interact with each other and are subjected to variable loads introduced by the wind as well as the rotating elements of the wind turbine.

Recent advances in data acquisition systems allow collection of large volumes of wind energy data. Although the prime purpose of data collection is monitoring conditions of wind turbines, the collected data offers a golden opportunity to address most challenging issues of wind turbine systems. In this dissertation, data mining is applied to construct accurate models based on the turbine collected data. To solve the data-driven models, evolutionary computation algorithms are applied. As data-driven based models are non-parametric, the evolutionary computation approach makes an ideal solution tool. Optimizing wind turbines with different objectives is studied to accomplish different research goals.

Two research directions of wind turbines performance are pursued, optimizing a wind turbine performance and optimizing a wind farm performance. The goal of single wind turbine optimization is to improve wind turbine efficiency and its life-cycle. The performance optimization of a wind farm is to minimize the total cost of operating a wind farm based on the computed turbine scheduling strategies.

The methodology presented in the dissertation is applicable to processes besides wind industry.

Abstract Approved: _____
Thesis Supervisor

_____
Title and Department

_____
Date

PERFORMANCE OPTIMIZATION OF WIND TURBINES

by

Zijun Zhang

A thesis submitted in partial fulfillment
of the requirements for the Doctor of
Philosophy degree in Industrial Engineering
in the Graduate College of
The University of Iowa

May 2012

Thesis Supervisor: Professor Andrew Kusiak

Graduate College
The University of Iowa
Iowa City, Iowa

CERTIFICATE OF APPROVAL

_____

PH.D. THESIS

_____

This is to certify that the Ph.D. thesis of

Zijun Zhang

has been approved by the Examining Committee
for the thesis requirement for the Doctor of Philosophy
degree in Industrial Engineering at the May 2012 graduation.

Thesis Committee: _____
Andrew Kusiak, Thesis Supervisor

_____
Yong Chen

_____
Pavlo Krokhmal

_____
Albert Ratner

_____
Kate Cowles

To My Parents and Family

No pain, no palm; no thorns, no throne; no gall, no glory; no cross, no crown

William Penn

ACKNOWLEDGMENTS

I would like to express my sincere gratitude to my advisor Professor Andrew Kusiak, for his devotion to this research. He has been the most instrumental person for my academic and research achievements. He provided the motivation, encouragement, guidance and advice which have prepared me for the challenging life that lies ahead. I was extensively exposed to the research of advanced modeling and optimization theories as well as real-world applications while working in the Intelligent Systems Laboratory. This invaluable experience has allowed me to maintain a balance between theory and practice leading to realistic solutions.

I would like to thank Professor Yong Chen, Professor Pavlo Krokhmal, Professor Albert Ratner and Professor Kate Cowles for serving on my Ph.D. Dissertation Committee and providing valuable suggestions and feedback on my research.

I am also grateful for the financial support from Iowa Energy Center and MidAmerican Energy Company. The energy experts from Iowa Energy Center and MidAmerican Energy Company have offered me invaluable information for this research.

I thank all the members of the Intelligent Systems Laboratory who have worked with me and provided advice, reviews, and suggestions. Special thanks to my previous colleagues: Dr. Zhe Song, who worked with me to solve challenging problems in wind energy and Robert A. Hamel, who provided access to industrial data.

And finally, and most importantly, I would like to express my sincere gratitude to my parents, who solidly supported me in pursuing my Ph.D. degree.

ABSTRACT

Improving performance of wind turbines through effective control strategies to reduce the power generation cost is highly desired by the wind industry. The majority of the literature on performance of wind turbines has focused on models derived from principles versed in physics. Physics-based models are usually complex and not accurate due to the fact that wind turbines involve mechanical, electrical, and software components. These components interact with each other and are subjected to variable loads introduced by the wind as well as the rotating elements of the wind turbine.

Recent advances in data acquisition systems allow collection of large volumes of wind energy data. Although the prime purpose of data collection is monitoring conditions of wind turbines, the collected data offers a golden opportunity to address most challenging issues of wind turbine systems. In this dissertation, data mining is applied to construct accurate models based on the turbine collected data. To solve the data-driven models, evolutionary computation algorithms are applied. As data-driven based models are non-parametric, the evolutionary computation approach makes an ideal solution tool. Optimizing wind turbines with different objectives is studied to accomplish different research goals.

Two research directions of wind turbines performance are pursued, optimizing a wind turbine performance and optimizing a wind farm performance. The goal of single wind turbine optimization is to improve wind turbine efficiency and its life-cycle. The performance optimization of a wind farm is to minimize the total cost of operating a wind farm based on the computed turbine scheduling strategies.

The methodology presented in the dissertation is applicable to processes besides wind industry.

TABLE OF CONTENTS

LIST OF TABLES

LIST OF FIGURES

LIST OF NOMENCLATURE

Nomenclature for CHAPTER 5

T	Scheduling horizon
t	Time unit (one hour in this study), t = 1, 2, 3, …, T
I	Number of wind turbines installed at a wind farm
i	Wind turbine index
D_t	Grid demand at time t
$P_{i,t}$	Generated power of wind turbine i at time t
P_C	Rated power of wind turbines
$f_i(v_t, \theta_i)$	Power curve (logistic function) of wind turbine i
θ_i	Parameter vector of a logistic function, $\theta_i = (\theta_{1,i}, \theta_{2,i}, \theta_{3,i}, \theta_{4,i})$
v_t	Average wind speed at time t
v_{ci}	Cut-in wind speed
v_{co}	Cut-out wind speed
$I(\cdot)$	Indicator function
p_t	Penalty for compensating the power shortage at time t
$s_{i,t}$	Operational status (on or off) of wind turbine i at time t, denoted as 0 or 1.
K	Energy needed to start up a wind turbine
B_t	Electricity spot price at time t
ΔP_t	Power shortage (the demand minus generated wind power) at time t
c	Estimated operations and maintenance cost of a wind turbine to generate a unit of power
C_{ps}	Opportunity cost due to power shortage
C_{pc}	Compensation cost due to power shortage
C_{om}	Operations and maintenance cost of a wind farm (all turbines in a wind farm)
TC	Cost associated with a schedule: TC_b is the cost of a baseline schedule; TC_c is the cost of a computed schedule

$Gain$	The gain of running an optimized schedule over the baseline schedule
N_t	Number of tribes
N_p	Number of particles in a tribe
m	Tribe index
h	Particle index
j	Iteration number in the particle swarm algorithm
ψ	Dimensionality of the search space
x_{hm}^{j}	Position of particle h in tribe m at iteration j
v_{hm}^{j}	Velocity of particle h in tribe m at iteration j
$\hat{x}_{hm}^{j}$	Particle h is a local best in tribe m at iteration j
$\hat{g}_{m}^{j}$	The best of tribe m
$f(x_{hm}^{j})$	Fitness value of particle h in tribe m at iteration j
$\hat{g}_{q}^{j}$	The best of a random tribe $q \neq m$
$f(\hat{g}_{q}^{j})$	Fitness value of a tribe's best
g_{b}^{j}	Global best of all particles
r_1^{j}, r_2^{j}	Random vectors generated from uniform distribution in the interval [0,1]
ω	Inertia of the particle swarm algorithm
δ_1, δ_2	Constants used to update particle's velocity
α	Constant used in the communication function
ρ	Parameter controlling the structure of a small world network
$N(0,1)$	Normal distribution with mean 0 and standard deviation 1
S_m	Selected particles to communicate among tribes during the search process
k, λ	Shape and scale parameters of Weibull distribution
$G1$, $G2$	Two groups of wind turbines, each including wind turbines with identical power curves
$X_{G1,t}$, $X_{G2,t}$	Number of wind turbines turned on at time t in group $G1$ or group $G2$
μ_{w1}, μ_{w2}	Average wind speeds of data sets 1 and 2, respectively

μ_{e1}, μ_{e2} Average electricity prices of data sets 1 and 2

μ_{d1}, μ_{d2} Average grid demands of data sets 1 and 2

Nomenclature for CHAPTER 6

T Scheduling horizon

t Time window (30-min in this study), t = 1, 2, 3, …, T

I Number of wind turbines installed at a wind farm

i Wind turbine index

D_t Grid demand at time t

$P_{i,t}$ Generated power of wind turbine i at time t

$E(P_{i,t})$ Expectation of generated power of wind turbines in a wind speed scenario

υ_t Average wind speed at time t

υ_{ci} Cut-in wind speed

υ_{co} Cut-out wind speed

$\hat{\upsilon}$ Estimated wind speed by the prediction model

τ The setting of generator torque of a wind turbine

β The setting of blade pitch angle of a wind turbine

$I(\cdot)$ Indicator function

p_t Penalty for compensating the power shortage at time t

$s_{i,t}$ Operational status (on or off) of wind turbine i at time t, denoted as 0 or 1.

K Energy dragged by idle wind turbines

B_t Electricity spot price at time t

ΔP_t Power shortage (the demand minus generated wind power) at time t

c Levelized unit operations and maintenance cost of a wind turbine to generate a unit of power (MW) per 30-min

C_{oc} Opportunity cost due to power shortage

C_{cc} Compensation cost due to power shortage

C_{om}	Operations and maintenance cost of a wind farm (all turbines in a wind farm)
C_{ic}	Cost due to the idle condition of wind turbines
TC	Cost associated with a schedule: TC_{BMS} is the cost of a computed schedule based on base model; TC_{SOS} is the cost of a computed schedule based on stochastic optimization model; TC_{PIS} is the cost of a computed schedule under perfect information; TC_{BS} is the cost of a baseline schedule
∂	A set of wind speed scenarios
Q	Sampling interval of the data
S	The sub-interval of a wind speed interval associated with a wind speed scenario ∂_h
n	Number of data points in a dataset
$\hat{y}$	Predicted value of a parameter in model validation
y	Observed value of a parameter in model validation
h	Index of wind speed scenarios
j	Iteration number in the particle swarm algorithm
l	Index of swarm locations in migrated particle swarm optimization
b	Number of locations in migration procedure of migrated particle swarm optimization
m	Number of particles in flight procedure of migrated particle swarm optimization
x_l^j	Position of particle l at iteration j
v_l^j	Velocity of particle l at iteration j
$\hat{x}_l^j$	The local best of particle l at iteration j
$\hat{g}^j$	The global best of particles at iteration j
$fit(x_l^j)$	Fitness value of particle l at iteration j
$fit(\hat{x}_l^j)$	Fitness value of the local best of particle l at iteration j
$fit(\hat{g}^j)$	Fitness value of the global best
r_1^j, r_2^j	Random vectors generated from uniform distribution in the interval [0,1]

ω	Inertia of the particle swarm algorithm
c_1, c_2	Constants used to update particle's velocity
$U(0,1)$	Continuous uniform distribution between 0 and 1
SI	Solution index

CHAPTER 1

INTRODUCTION

Renewable energy has been vigorously debated and pursued in the past decade. The growing public awareness of the environmental concerns, limited energy supply, and uncertain energy prices has spearheaded this debate.

Wind energy has experienced a remarkable expansion in the past years. The global cumulative capacity of wind power generation has increased 20 times in a ten year period and is expected to grow even faster in the future. In 2008, the U.S. Department of Energy announced an ambitious goal for wind energy to produce 20% of electricity by 2030. However, the challenge for wind energy generation is to be cost competitive with the energy produced from the conventional sources. The cost of wind generated power is largely derived from the turbine installation cost and the operation and maintenance (O&M) cost. Therefore, reducing the cost of installation and O&M makes wind power more cost-attractive. In this dissertation, performance of wind turbines is studied with the aim of reducing the O&M cost and thus lowering the cost of wind power generation.

To improve wind turbine performance, models of wind turbines are investigated. Although various approaches have been studied to model conventional power systems, most of them are not applicable to modeling wind turbine systems. The main reason is that the static and dynamic characteristics of large-scale wind turbines differ from the conventional power plant systems. Therefore, novel theories for modeling wind turbine systems are needed.

To solve emerging problems in the rapidly expanding wind energy industry, wind energy research has intensified in recent years. The published literature with wind energy can be categorized into, design of wind turbines (Laino *et al.* 1993; Saranyasoontorn and Manuel 2004), the design and reliability of wind farms (Barthelmie *et al.* 2007; Mora *et al.* 2007; Leite *et al.* 2007), control of wind turbines (Senjyu *et al.* 2006; Ko *et al.* 2008; Johnson *et al.* 2006; Munteanu *et al.* 2005), the prediction of wind power (Ko *et al.* 2008;

Mutlu *et al.* 2009), wind energy conversion (Kusiak *et al.* 2009b; Kusiak *et al.* 2009c) and condition monitoring of wind turbines (Kusiak *et al.* 2009d; Kusiak *et al.* 2009e). Although the wind turbine efficiency topic has been studied in the literature, several shortcomings can be noted. The wind power generation cost can be considered from two perspectives, the efficiency of power generation and the O&M cost of the wind turbine. Therefore, simply improving the efficiency of wind power generation cannot reduce the power generation cost as the cost of turbine consumed mechanical components may increase. Another shortcoming is that improving the performance model of a wind turbine does not easily scale up to that of a wind farm. Numerous factors, such as electricity demand, wind speed, and electricity price might impact the performance of a wind farm. Scheduling wind farms needs to be investigated. Moreover, the majority of the published studies about control of a wind turbine system involve Physics-based models. Since such models usually involve stringent assumptions, they do not adequately model working systems.

Three research goals are set for this dissertation. The first goal is to develop nonlinear and non-parametric models accurately capturing performance of wind turbines. The wind turbine performance is expressed by the amount of the generated power and the level of turbine vibration. Since wind turbine vibration impact performance and life-cycle of wind turbine components, such as a gearbox, it is considered as an indicator of mechanical component usage. The second goal is to optimize wind turbine performance based on the developed models. Unlike the previous two goals that concentrate on a single turbine, the third goal is to improve performance of a wind farm.

1.1 Wind Turbine Vibration and Power Generation

In the published literature, wind turbine vibration and power generation have been studied as two independent topics. The published research on wind turbine vibration has primarily focused on the models derived from the first principles. Leithead and Connor

(2000) studied dynamics of variable speed wind turbines and design of models to control wind turbines. Fadaeinedjad *et al.* (2008) investigated the impact of voltage sag on vibration of the wind turbine tower. They used three simulation programs, TrubSim, FAST and Simulink, to model wind turbines. Murtagh *et al.* (2008) investigated control wind turbine vibration by incorporating a passive control device. A passive control method using a tuned mass damper to mitigate vibrations of the blades and tower of a wind turbine was introduced. Hansen *et al.* (2006) discussed the estimation of aeroelastic damping of operational wind turbine modes based on experiments. Hansen *et al.* (2003) also presented analysis of vibrations in a three-blade wind turbine. Molinas *et al.* (2010) addressed extending the life of a gearbox by smoothing the transient generator torque to control vibration. Although first principles based models provided solid foundation of understanding the nature of wind turbine vibration, the real wind turbine vibration cannot be fully reflected due to the assumptions and the diverse source of wind turbine vibration (Wowk 1991).

Predicting wind power is an important direction of the wind energy research since wind power prediction is critical to power system reliability and handling variability of the generated power (Bathurst *et al.* 2002). Long-term wind speed and power prediction is of interest to management of energy distribution (Barbounis *et al.* 2006). Short-term prediction of wind turbine parameters is key to anticipatory control of wind turbines (Senjyu *et al.* 2006) and on-line monitoring (Kusiak *et al.* 2009d, Kusiak *et al.* 2009e).

Numerous approaches for predicting wind speed and power generated by wind turbines have been developed. Potter and Negnevitsky (2006) presented an adaptive neuro-fuzzy system to forecast wind speed considering both wind speed and direction. Boukhezzar *et al.* (2006) presented the estimation of wind speed based on the aerodynamic torque. Louka *et al*. (2008) applied Kalman filters as a post-processing method to enhance wind speed prediction. Flores *et al*. (2005) employed neural networks for wind speed prediction in time-scales can vary from 1 minute to an hour and designed

a control system for active power generation. El-Fouly *et al*. (2008) developed a linear time-series based models to predict both wind speed and direction. Damousis *et al*. (2004) used a fuzzy logic model trained by a genetic algorithm to predict wind speed and power over 0.5 to 2 hour horizons.

Based on the predicted wind speed, wind power models are conducted for wind power prediction. Sideratos and Hatziargyriou (2007) presented an advanced statistical method for wind power forecasting 48 hours ahead based on artificial intelligent techniques. Bessa *et al.* (2009) reported the adopting entropy concepts to the training of neural network to build hourly based power prediction model. Kariniotakis *et al.* (1996) developed a recurrent high order neural network for building power prediction models based on 10-minute average data.

Besides the power prediction, wind power models are also discussed in the power optimization research. Boukhezzar and Siguerdidjane (2009) presented a non-linear controller for optimizing the power of the DFIG (Doubly Fed Induction Generator). Wang and Chang (2004) investigated an intelligent power extraction algorithm for improving the performance of wind turbine systems. Morimoto *et al.* (2005) researched the maximization of wind-turbine-generated power by controlling the current vector of the interior, permanent-magnet, synchronous generator. Muljadi and Butterfield (2001) addressed operating a variable-speed wind turbine with pitch control to maximize power while minimizing the loads. Moyano *et al.* (2009) adopted an operation strategy to optimize wind power on a wind park control level.

In the published literature, statistical, Physics-based and control theory based wind power models are widely discussed. However, the drawback of such models is also obvious. Assumptions, delay of feedback loop and delay of measuring wind speed impair the results of power estimation.

1.2 Wind Farm Scheduling Problem

The ultimate goal of wind energy research is to save cost of operating wind farms. Progress on scheduling wind turbines is highly demanded by the wind industry. However, due to variability of electricity prices, grid demand, wind speed as well as heterogeneity of wind turbines, determining a sequence of activating or de-activating turbines in a wind farm is a challenge.

A commercial wind farm usually involves a large number of wind turbines (e.g., 100 or more) and each wind turbine performs uniquely even if all turbines are produced by the same manufacturer. Various reasons could contribute to the heterogeneity (difference in performance) of wind turbines. The location of a turbine, terrain, turbine-turbine interactions, different component suppliers and maintenance regimes are example factors contributing to this heterogeneity. Thus, for a wind farm operator, it is necessary to know which turbine is less efficient so that it could be turned on or off at appropriate time. Power curves constructed from field data are good indicators of turbine's actual performance (Manwell, *et al.* 2002) and therefore could be incorporated into an optimization model to assist operators in scheduling wind turbines.

This topic of scheduling wind turbines is new and it differs from dispatching power generated by traditional power plants. One of the reasons is that fuel (the wind) is free and therefore the desire to keep wind turbines running makes scheduling wind turbines seemingly less important. Yet, as the number of wind farms is growing, operating them at maximum capacity is not always possible and profitable. Power curtailment, fluctuation of electricity price, and heterogeneity of wind turbines need to be considered while determining the capacity at which a wind farm should be operated. Classical scheduling models have usually been studied in the context of manufacturing applications (Ouelhadj and Petrovic, 2009). However, scheduling wind farms has not been investigated.

The published literature related to wind farm scheduling only focuses on determining the power generation schedule of a wind farm integrated with other power plants, such as coal-fired plants, hydroelectric plants, where the total grid demand is usually fixed or known before (Ren and Jiang, 2009; Siahkali and Vakilian, 2009). A wind farm is treated as a power generation unit in the scheduling. Scheduling wind turbines of a wind farm is ignored in the previous research.

1.3 Computational Intelligence

New theories and advances in computational intelligence offer alternatives to model energy systems and solve complex optimization problems.

In combustion energy, Chu *et al.* (2003) applied a neural network approach to speed up the trial-and-error process of obtaining optimal operating points optimizing combustion process. Rusinowski *et al.* (2002) focused on finding an optimal travelling rate of the grid and an optimal height of the fuel layer. Büche *et al.* (2002) applied an evolutionary computation algorithm to find an optimal design of a burner to reduce NOx emissions as well as pressure fluctuation. Wang *et al.* (1997) applied a naïve intelligent control algorithm to determine the best air supply for a boiler. Cass *et al.* (1997) combined the neural network and evolutionary computation techniques to determine an optimal fuel/air ratio.

In wind energy, Kusiak *et al.* (2009a) applied data mining and evolutionary computation to optimize the control of wind turbines. Li *et al.* (2008) introduced a hybrid genetic and immune algorithm to solve the optimization problem of internal electric connection system of large offshore wind farms. Prats *et al.* (2000) applied fuzzy control techniques to improve wind energy capture for variable speed and variable pitch wind turbines. Sareni *et al.* (2009) developed multi-objective genetic algorithm to study the optimal design of a small passive wind turbine generator by considering the size, power generation and other issues.

Modeling and optimization based on computational intelligence usually require expensive computations. Therefore, appropriate parameter selection strategies are needed to select more useful parameters from a large dataset to save the computational cost.

1.4 Meta-control of Wind Turbine Performance with Data Mining

Supervisory Control and Data Acquisition (SCADA) system routinely collect wind turbine data sensed by numerous sensors mounted on the wind turbines and store them to a database. The large volume of SCADA data contains rich information of wind turbine systems and can be utilized to analysis, modeling, optimization and diagnosis of wind turbine systems.

An emerging science, data mining, which offers advantage in data analysis and modeling is applied to study the SCADA data. The successful applications and advantages of data mining can be observed from the previous literature and our research. Ogilvie *et al.* (1998) applied an association-rule algorithm to look for strong relations among the measured parameters. The inducted rules were intended to build an expert system. Lu *et al.* (2005) applied a data mining approach to forecast electricity market price spikes based on the various parameters that influence the price, which can be used to schedule a power production. Other successful applications of data mining in manufacturing, marketing, and medical informatics were reported by (Harding *et al.* 2006; Berry and Linoff 2004; Shah *et al.* 2006). In our previous research, the modeling capability of data mining has been proven in various applications such as combustion systems (Kusiak and Song 2008; Song and Kusiak 2010) as well as heating, ventilation, and air conditioning systems (Kusiak *et al.* 2010a,b). Therefore, in the research of single wind turbine system, data mining algorithms are employed to develop models precisely depict wind turbine performance. Next, the data driven based wind turbine models are integrated to construct a wind farm model for the study of scheduling a wind farm.

Both wind turbine control and wind farm scheduling are optimization problems. As data driven models are invisible and canonical optimization algorithms are incompatible to solve them, more advanced optimization methods, computational intelligence, are considered to obtain the optimal solution in this study.

At present, there is no standard approach to evaluate wind turbine performance. In this dissertation, performance of wind turbine systems is described by two parts, the generated wind power and wind turbine vibration. Wind turbines are controlled to achieve to objectives, maximization of power and minimization of wind turbine vibration.

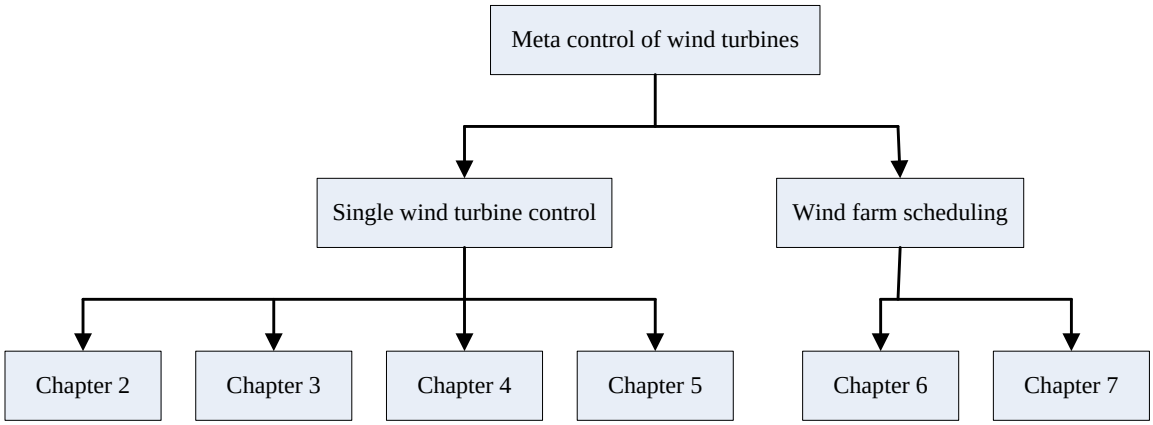

Figure 1.1 Structure of the dissertation.

Figure 1.1 shows the dissertation structure. Two major research topics are introduced in this dissertation. The first research topic presented in Chapters 2 – 5 focus on the control of a single wind turbine. To model wind turbine systems in the first research topic, seven data mining algorithms, Neural Network (NN), Neural Network Ensemble (NNE), Support Vector Machine (SVM), Classification and Regression Tree (CART), Boosting Tree (BT), Random Forests (RF) and k Nearest Neighbors (kNN) are utilized. Chapter 6 and 7 present the second research topic, control wind turbines from a wind farm perspective.

In Chapter 2, the optimization of wind turbine performance based on an anticipatory control model is discussed. Both maximizing wind power generation and minimizing the drive-train and tower vibration are considered in the optimization. The drive-train and tower vibration is represented by the vibratory acceleration of drive-train and tower measured with accelerometers.

Chapter 3 introduces an adaptive approach to wind turbine control. It is designed to achieve a balance between power optimization and smooth drive train control in response to the changes in wind speed and electricity demand. The smoothing of the drive train is accomplished by minimizing the torque ramp rate.

In Chapter 4, a new power optimization constraint constructed based on control chart theory is introduced to the optimization of wind turbine power generation process. Two optimization objectives, maximizing wind power and minimizing the power ramp rate, are discussed. To prove that the framework of wind turbine control in Chapter 2 – 4 can be extended to other applications, Chapter 5 presents the application of the framework in the optimization of pump systems in a wastewater processing plant.

Chapter 6 presents a model to schedule wind turbines in a wind farm. A scheduling model determines activation/deactivation status of individual wind turbines to cope with the varying electricity prices, wind speed, and grid demand. Due to the complexity of the scheduling model, an enhanced particle swarm algorithm is introduced to compute the optimal solution. In Chapter 6, the power generation process of various wind turbines is simply described by power curve models. More advanced models can accurately depict the power generation process are needed to develop a more applicable wind farm scheduling model. Therefore, in Chapter 7, data mining algorithms are employed to develop wind power generation models for the wind farm scheduling problem.

CAPTER 2

CONTROL OF WIND TURBINE POWER AND VIBRATION WITH A DATA DRIVEN APPROACH

2.1 Introduction

Improving performance of wind turbines is of interest to the wind energy industry as it provides an opportunity to reduce the cost of generating electricity. This cost is largely determined by the efficiency of wind turbines and maintenance of the equipment (U.S. Department of Energy 2008).

This chapter investigates the optimization of wind turbine performance in based on an anticipatory control model (Kusiak *et al.* 2009a; Camacho and Bordons 1999; Rossiter 2003). Both maximizing wind power generation and minimizing the drive-train and tower vibration are considered in the optimization. The drive-train and tower vibration is measured with accelerometers. The task of modeling the power generation process and wind turbine vibration is challenging. In conventional analysis, the first principles and aerodynamics are frequently applied. However, assumptions made by the classical analysis approach limit its practical applications. In this chapter, a data-driven approach is utilized to model power generation and turbine vibration. The sources of wind turbine vibration are diverse (Wowk 1991). The focus here is on vibrations attributed to the control of wind turbines, e.g., control of the blade pitch and the generator torque.

The performance optimization model is derived from data, and it includes constraints. As data-driven models are usually non-linear and non-parametric, conventional optimizers cannot solve them. A particle swarm optimization algorithm (Kennedy and Eberhart 1995; Shi and Eberhart 1998; Abido 2002) is applied here do solve this challenging problem. Solutions of this optimization problem are the optimal settings of the controllable parameters, generator torque and blade pitch angle.

2.2 Data Description and Processing

In this research, data collected from supervisory control and data acquisition (SCADA) systems installed at a large wind farm is utilized. The sampling frequency of data collected over a period of one month is 0.1 Hz (this is the highest frequency permitted for research). Though the SCADA system collects data on over 120 parameters, a subset of parameters is used in this research. The domain knowledge and the results from the previous studies are used to select most relevant parameters. Table 2.1 demonstrates the sample data used in this research.

Table 2.1 Sample dataset

Time Stamp	Power	Wind Speed	Blade Pitch Angle	…	Tower Acceleration	Drive-Train Acceleration
11/1/2009 12:00:30 AM	-2	2.33	83.07	…	332.30	4.28
11/1/2009 12:00:40 AM	-2.5	2.46	83.07	…	74.75	4.81
11/1/2009 12:00:50 AM	-2.4	2.59	83.07	…	18.12	6.25
11/1/2009 12:01:00 AM	-2.5	2.86	83.07	…	89.14	8.46
11/1/2009 12:01:10 AM	-2.5	2.93	83.07	…	125.79	11.68
…	…	…	…		…	…

To enhance accuracy of the data-driven models, the data is pre-processed to exclude data caused by sensor failures, transmission errors, and failures of various subsystems. These errors usually appear as the data exceeding physical constraints or missing values. The data quality also impacts accuracy of the models extracted by data-driven approaches. As the accelerometers are sensitive to noise, the Daubechies wavelet (Daubechies 1992) is applied to de-noise and smooth the measured drive-train and tower acceleration data. In particular, two threshold schemes of Daub 5 wavelets with 5 levels,

Fix_Soft and Fix_Hard (Kobayashi 1998; Tang *et al.* 2000), are considered to obtain an acceptable threshold setting. Fix thresholding uses a fixed threshold multiplied by a small factor. Hard and soft thresholding could potentially produce different de-noising results. Hard thresholding is the usual process of setting to zero for the elements with absolute values lower than the threshold. Soft thresholding is an extension of hard thresholding, first setting to zero the elements with absolute values lower than the threshold, and then reducing the nonzero coefficients towards zero. The entropy type of the wavelet analysis can be accomplished with SURE (Stein's Unbiased Risk Estimate) (Stein 1981) which uses function (2.1).

$$\text{Entropy threshold} = \sqrt{2\log_e(n\log_2(n))} \tag{2.1}$$

To increase de-noising efficiency, the best tree algorithm (Coifman and Wickerhauser 1992) is applied.

The dataset from 11/1/2009 12:00:40 AM to 11/2/2009 4:09:40 AM is selected to perform the comparative analysis of two threshold settings. The following four metrics, the Mean Square Error (MSE), the Standard Deviation of Square Error (SD of SE), the Maximum of Square Error (Max SE), and the Minimum of Square Error (Min SE), are used to evaluate the two threshold settings (see (2.2) – (2.5)).

$$\text{MSE} = \frac{1}{n}\sum_{i=1}^{n}(\hat{y}_i - y_i)^2 \tag{2.2}$$

$$\text{SD of SE} = \frac{1}{n}\sqrt{\sum_{i=1}^{n}(\frac{1}{n}\sum_{i=1}^{n}(\hat{y}_i - y_i)^2 - (\hat{y}_i - y_i)^2)^2} \tag{2.3}$$

$$\text{Max SE} = \max\{(\hat{y}_i - y_i)^2\} \tag{2.4}$$

$$\text{Min SE} = \min\{(\hat{y}_i - y_i)^2\} \tag{2.5}$$

Table 2.2 summarizes the comparative analysis of two threshold settings for de-noising the drive-train acceleration. Table 2.3 illustrates the same results for de-noising the tower acceleration. As illustrated in both tables, the threshold setting, Fix_Hard, is

more suitable for de-noising the two accelerations, and therefore it is selected for further study.

Table 2.2 Statistics of de-noising drive-train acceleration with two threshold settings

Threshold	MSE	SD of SE	Max SE	Min SE
Fix_Hard	16.1052	28.0168	316.0088	0
Fix_Soft	31.6875	64.2476	786.8944	0

Table 2.3 Statistics of de-noising tower acceleration with two threshold settings

Threshold	MSE	SD of MSE	Max SE	Min SE
Fix_Hard	99.1767	161.2681	1840.8441	0
Fix_Soft	141.5024	262.0488	5098.8578	0

The dataset after pre-processing is split into two parts, the training and the test dataset. The training dataset includes data from 11/1/2009 12:00:30 AM to 11/7/2009 5:58:30 PM, around 10000 points. The test dataset contains about 5000 data points, from 11/7/2009 5:59:10 PM to 11/8/2009 7:52:30 AM.

2.3 Dynamic Modeling and Prediction for Anticipatory Control

The anticipatory control of wind turbine vibration and power generation discussed in this chapter includes three data-driven models, a power generation model, a drive-train vibration model, and a tower vibration model. The power generation model describes the dynamic process of extracting power from the wind, while the other two models represent turbine vibration. Two controllable parameters, the generator torque and the blade pitch

angle, are utilized to control the performance of the wind turbine. The concept of anticipatory control falls into the category of model predictive control (MPC) (Camacho and Bordons 1999; Rossiter 2003). It extends the MPC scheme by including controllable and non-controllable parameters. It aims at generation of control settings ahead of the current process.

2.3.1 Modeling Power Generation

The dynamic process of power generation is represented by the four-tuplet (v, τ, β, P), where v represents the wind speed (non-controllable parameter), τ is the generator torque (controllable parameter), β is the blade pitch angle (controllable parameter), and P is the power generated by the wind turbine (response parameter). The value of the response parameter, P, is impacted by the non-controllable and controllable parameters shown in (2.6).

$$P(t) = f(v(t), v(t-\mathrm{T}), \tau(t), \tau(t-\mathrm{T}), \beta(t), \beta(t-\mathrm{T})) \tag{2.6}$$

where t is the current time, T represents the sampling time of data (10-s data), and $f(\cdot)$ is the function describing the wind turbine energy conversion learned by the data-mining algorithms.

To extract the data-driven model, six data-mining algorithms, neural network (Siegelmann and Sontag 1994; Liu 2001; Smith 1993), neural network ensemble (Hansen and Salamon 1990), support vector machine (Schölkopf *et al.* 1999; Steinwart and Christmann 2008), k nearest neighbor (Shakhnarovish *et al.* 2005), boosting regression tree (Friedman 2001; Friedman 2002) and random forest regression (Breiman 2001), are considered the most suitable algorithm is selected.

Four metrics (2.7) – (2.10), the mean absolute error (MAE), standard deviation of absolute error (SD of AE), mean absolute percentage error (MAPE) and standard deviation of absolute percentage error (SD of APE), are employed to evaluate the performance of candidate algorithms.

$$\text{MAE} = \frac{1}{n}\sum_{i=1}^{n}|\hat{y}_i - y_i| \tag{2.7}$$

$$\text{SD of AE} = \sqrt{\frac{1}{n}\sum_{i=1}^{n}(|\hat{y}_i - y_i| - \frac{1}{n}\sum_{i=1}^{n}|\hat{y}_i - y_i|)^2} \tag{2.8}$$

$$\text{MAPE} = \frac{1}{n}\sum_{i=1}^{n}(|\frac{\hat{y}_i - y_i}{y_i}|)\times 100\% \tag{2.9}$$

$$\text{SD of APE} = \sqrt{\frac{1}{n}\sum_{i=1}^{n}(|\frac{\hat{y}_i - y_i}{y_i}| - \frac{1}{n}\sum_{i=1}^{n}|\frac{\hat{y}_i - y_i}{y_i}|)^2}\times 100\% \tag{2.10}$$

The training and test data introduced in Section 2.2 is used in the comparative analysis. The test dataset is used to determine the performance and robustness of the data-driven models. Table 2.4 presents the test results derived by the data-driven models. As shown in Table 2.4, models extracted by three algorithms, neural network ensemble, neural network and k nearest neighbor, exhibit similar performance. However, the MAPE (0.0096) and SD of APE (0.0155) offered by the neural network model are slightly better than the MAPE and SD of APE of the other two. Hence, the neural network is selected as a more suitable algorithm to build the power generation model.

Table 2.4 Accuracy of power generation models extracted with six algorithms

Algorithm	MAE	SD of AE	MAPE	SD of APE
Neural Network Ensemble	4.2907	3.2428	0.0100	0.0176
Neural Network	4.4378	3.4114	0.0096	0.0155
Support Vector Machine	22.0804	15.8217	0.0647	0.0754
Boosting Regression Tree	34.8634	45.6751	0.0939	0.2827
Random Forest (Regression)	97.6282	86.4113	0.1317	0.1205
k Nearest Neighbor	6.4009	7.1931	0.0139	0.0218

Figure 2.1 and Figure 2.2 illustrate the prediction accuracy of the model developed by the neural network algorithm for the first 300 points from the test set.

Figure 2.1 is the run chart, and Figure 2.2 presents the scatter plot of the observed and the predicted values.

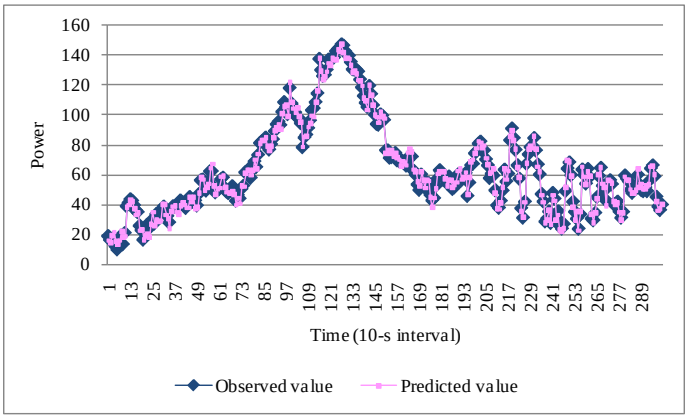

Figure 2.1 The power corresponding to the first 300 observed and power model predicted points

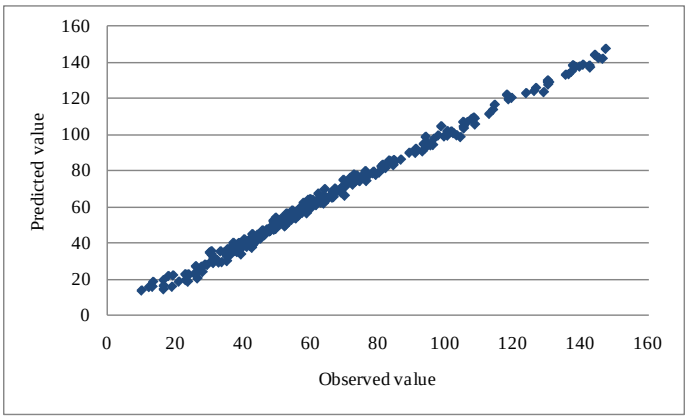

Figure 2.2 The predicted and observed value of the first 300 test points

2.3.2 Modeling Wind Turbine Vibration

In this research, vibrations of the drive-train are measured by the accelerometer installed at the bottom of a nacelle. The tower acceleration is measured by the accelerometer located at the connection of the nacelle and the tower. The wind turbine

vibrations are largely due to the air passing through the wind turbine and the forces originated by the control system impacting the generator torque and the blade pitch angle. Based on the domain knowledge and the past research, six parameters, the generator torque, blade pitch angle, wind speed, wind deviation, drive-train acceleration, and tower acceleration, are selected to model wind turbine vibration (see Table 2.5). In Table 2.5, the drive-train acceleration and the tower acceleration are the response parameters. The generator torque and the blade pitch angle are controllable parameters, while the wind speed and wind deviation are non-controllable parameters.

Table 2.5 Parameter list for modeling wind turbine vibration

Parameter	Symbol
Drive-train acceleration	A_d
Tower acceleration	A_t
Generator torque	τ
Blade pitch angle	β
Wind speed	v
Wind deviation	w_d

Wind turbine vibration is a dynamic process. To model the drive-train acceleration that portrays the vibration in the drive-train system, the current and the past states of parameters need to be considered. In this section, the past three states of controllable and non-controllable parameters are included in the training and testing dataset mentioned in Section 2.2 to build the models of drive-train acceleration.

Parameter selection is performed to reduce the dimensionality of the dataset and simplify the structure of the model. The wrapper genetic algorithm (Witten and Frank 2005; Kohavi and John 1997) is applied for parameter selection based on the training dataset of Section 2.2. Table 2.6 illustrates the parameters used in the selection process

and the selected parameters, where, t is the current time, and T represents the time unit (10-s in this chapter).

Table 2.6 List of parameters before and after parameter selection

Pool of parameters				Selected parameters			
Parameter	Symbol	Parameter	Symbol	Parameter	Symbol	Parameter	Symbol
Wind speed at time t	$v(t)$	Generator torque at time t	$\tau(t)$	Wind speed at time t	$v(t)$	Blade pitch angle at time t – 3T	$\beta(t - 3T)$
Wind speed at time t – T	$v(t - T)$	Generator torque at time t – T	$\tau(t - T)$	Wind speed at time t – 2T	$v(t - 2T)$		
Wind speed at time t – 2T	$v(t - 2T)$	Generator torque at time t – 2T	$\tau(t - 2T)$	Wind speed at time t – 3T	$v(t - 3T)$		
Wind speed at time t – 3T	$v(t - 3T)$	Generator torque at time t – 3T	$\tau(t - 3T)$	Wind deviation at time t – 3T	$w_d(t - 3T)$		
Wind deviation at time t	$w_d(t)$	Blade pitch angle at time t	$\beta(t)$	Generator torque at time t	$\tau(t)$		
Wind deviation at time t – T	$w_d(t - T)$	Blade pitch angle at time t – T	$\beta(t - T)$	Generator torque at time t – T	$\tau(t - T)$		
Wind deviation at time t – 2T	$w_d(t - 2T)$	Blade pitch angle at time t – 2T	$\beta(t - 2T)$	Generator torque at time t – 3T	$\tau(t - 3T)$		
Wind deviation at time t – 3T	$w_d(t - 3T)$	Blade pitch angle at time t – 3T	$\beta(t - 3T)$	Blade pitch angle at time t – T	$\beta(t - T)$		

The model of the drive-train acceleration is expressed in (2.11) using the selected parameters and the past states of the drive-train acceleration itself.

$$A_d(t) = f(v(t), v(t-2\mathrm{T}), v(t-3\mathrm{T}), \beta(t-\mathrm{T}), \beta(t-3\mathrm{T}), \tau(t), \tau(t-\mathrm{T}), \tau(t-3\mathrm{T}), w_d(t-3\mathrm{T}), A_d(t-\mathrm{T})) \quad (2.11)$$

The notation of Table 2.5 and Table 2.6 is used in model (2.11).

Data-mining algorithms of Section 2.3.1 are used to model drive-train acceleration. The training and test datasets used here are the same as in Section 2.2. Table 2.7 illustrates the test results of the drive-train acceleration models derived by the six data-mining algorithms. The neural-network ensemble algorithm provides lower values of MAPE and SD of APE than the other five algorithms, and it is selected to model the drive-train acceleration.

Table 2.7 Accuracy of drive-train acceleration models extracted with six algorithms

Algorithm	MAE	SD of AE	MAPE	SD of APE
Neural Network Ensemble	2.8376	4.4902	0.0517	0.0608
Neural Network	2.8929	4.4559	0.0569	0.0621
Support Vector Machine	11.4550	8.0720	0.3742	0.4128
Boosting Regression Tree	3.3508	4.9792	0.0686	0.0674
Random Forest (Regression)	14.5029	12.6100	0.3148	0.1947
k Nearest Neighbor	4.3069	5.6329	0.0920	0.0850

Figure 2.3 presents results produced for the first 300 points by the drive-train acceleration model extracted by the neural network ensemble algorithm. Figure 2.4 illustrates the observed value and predicted value of these 300 points.

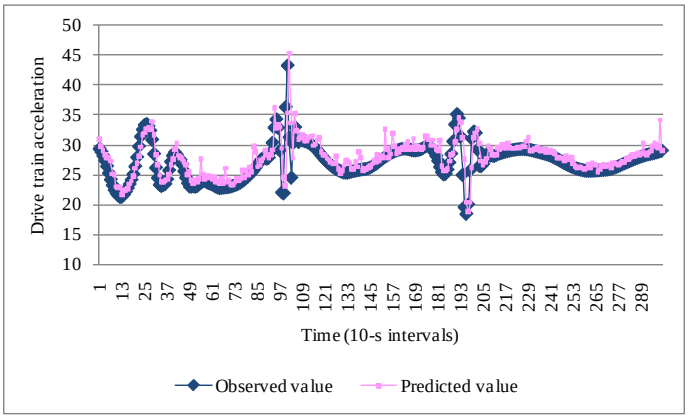

Figure 2.3 Results for the first 300 points used to test the drive-train acceleration model

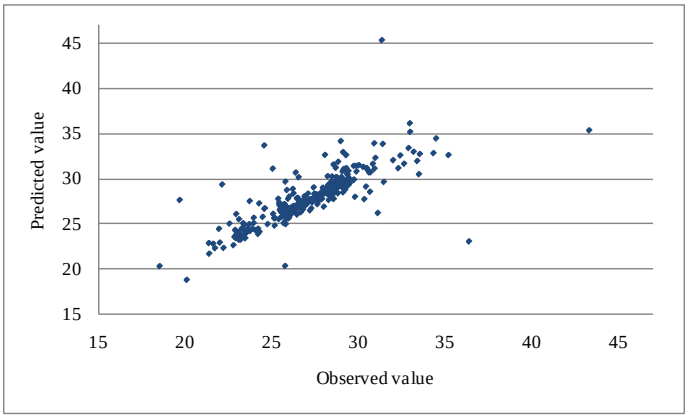

Figure 2.4 The predicted and observed value of the first 300 test points

To establish the tower acceleration model, same parameter selection procedure and data mining algorithm for developing the drive train acceleration model are applied. Table 2.8 lists the parameters selected for modeling tower acceleration.

Table 2.8 Selected parameters for modeling tower acceleration

Parameter	Symbol	Parameter	Symbol
Wind speed at time t	$v(t)$	Generator torque at time t	$\tau(t)$
Wind speed at time $t - \mathrm{T}$	$v(t-\mathrm{T})$	Generator torque at time $t - 2\mathrm{T}$	$\tau(t-2\mathrm{T})$
Wind speed at time $t - 2\mathrm{T}$	$v(t-2\mathrm{T})$	Generator torque at time $t - 3\mathrm{T}$	$\tau(t-3\mathrm{T})$
Wind speed at time $t - 3\mathrm{T}$	$v(t-3\mathrm{T})$	Blade pitch angle at time $t - \mathrm{T}$	$\beta(t-\mathrm{T})$

The model of the tower acceleration is expressed as (2.12).

$$A_t(t) = f(v(t), v(t-\mathrm{T}), v(t-2\mathrm{T}), v(t-3\mathrm{T}), \beta(t-\mathrm{T}), \tau(t), \tau(t-2\mathrm{T}), \tau(t-3\mathrm{T}), A_t(t-\mathrm{T})) \quad (2.12)$$

where the notation is the same as in model (2.11).

Table 2.9 presents the testing results of the models extracted by different data-mining algorithms. The neural network ensemble and the neural network offer the best performance in estimating tower acceleration. Since the MAPE for the neural network ensemble is slightly better than that of the neural network, the neural network ensemble is chosen to build the tower acceleration model. Figure 2.5 illustrates the observed and predicted values of the tower acceleration for the first 300 test points using the neural-network ensemble model. The scatter plot in Figure 2.6 demonstrates the relationship between the predicted and observed values for the same 300 points.

Table 2.9 Accuracy of the tower acceleration models extracted with six algorithms

Algorithm	MAE	SD of AE	MAPE	SD of APE
Neural Network Ensemble	4.2667	8.7580	0.0637	0.1021
Neural Network	4.3324	8.7523	0.0649	0.1000
Support Vector Machine	54.1059	19.8097	1.3150	1.0944
Boosting Regression Tree	7.0456	10.2048	0.1089	0.1285
Random Forest (Regression)	12.6052	14.3985	0.2652	0.4624
k Nearest Neighbor	12.8249	12.2709	0.2407	0.2074

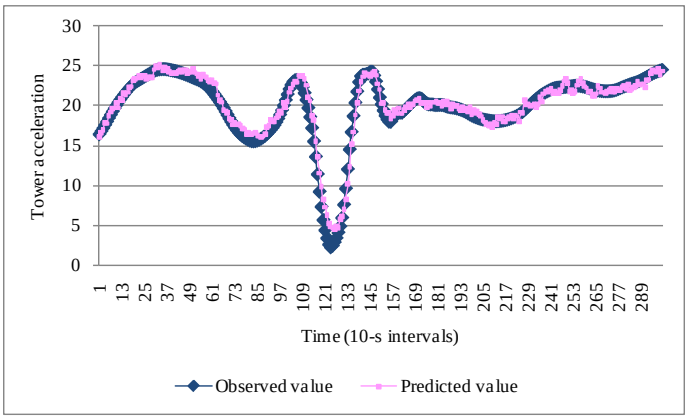

Figure 2.5 Test results of the tower acceleration model for first 300 points

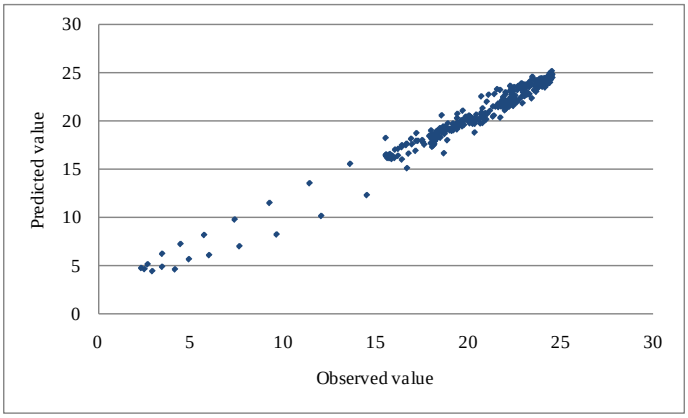

Figure 2.6 The predicted and observed value of the tower acceleration for first 300 test points

2.3.3 Prediction Based on Data-driven Models

To realize anticipatory control, the values of the generated power and the wind turbine vibration need to be predicted a step ahead (here 10-s). Based on the dynamic models (2.6), (2.11), and (2.12) of Section 2.3.1 and 2.3.2, the models for one-step ahead predictions are formulated in (2.13) – (2.15).

$$P(t+\mathrm{T}) = f(v(t+\mathrm{T}), v(t), \beta(t+\mathrm{T}), \beta(t), \tau(t+\mathrm{T}), \tau(t)) \tag{2.13}$$

$$\begin{aligned} A_d(t+\mathrm{T}) = f(&v(t+\mathrm{T}), v(t-\mathrm{T}), v(t-2\mathrm{T}), \beta(t), \beta(t-2\mathrm{T}), \\ &\tau(t+\mathrm{T}), \tau(t), \tau(t-2\mathrm{T}), w_d(t-2\mathrm{T}), A_d(t)) \end{aligned} \tag{2.14}$$

$$\begin{aligned} A_t(t+\mathrm{T}) = f(&v(t+\mathrm{T}), v(t), v(t-\mathrm{T}), v(t-2\mathrm{T}), \beta(t), \tau(t+\mathrm{T}), \\ &\tau(t-\mathrm{T}), \tau(t-2\mathrm{T}), A_t(t)) \end{aligned} \tag{2.15}$$

where the notation is the same as in Section 2.3.2.

2.3.3.1 Modeling Wind Speed Based on the Time-series Method

The values of all parameters in Eqs (2.13) – (2.15) can be measured or computed except the wind speed at time t + T. A model for wind speed prediction at time t + T needs to be developed. In this research, the time-series model (see (2.16)) for wind speed prediction is developed based on its past states.

$$v(t) = f(v(t-\mathrm{T}), v(t-2\mathrm{T}), v(t-3\mathrm{T}), ..., v(t-n\mathrm{T})) \tag{2.16}$$

Eight past states of the wind speed are considered as candidates for inclusion in the model. The wrapper approach of Section 2.3.2 is applied to select the most suitable parameters. Among the eight past states, only the 7th state, $v(t - 7\mathrm{T})$, is considered as an unnecessary parameter. Thus, Eq (2.16) is reformulated as (2.17).

$$\begin{aligned} v(t) = f(&v(t-\mathrm{T}), v(t-2\mathrm{T}), v(t-3\mathrm{T}), v(t-4\mathrm{T}), \\ &v(t-5\mathrm{T}), v(t-6\mathrm{T}), v(t-8\mathrm{T})) \end{aligned} \tag{2.17}$$

To build model (2.17) from the data, six data-mining algorithms are utilized. The performance of these algorithms is summarized in Table 2.10. As The neural network

algorithm provides the lowest value of all the four metrics, MAE, SD of AE, MAPE and SD of APE. Hence, it is selected for modeling wind speed.

Table 2.10 Accuracy of wind speed prediction models extracted with six algorithms

Algorithm	MAE	SD of AE	MAPE	SD of APE
Neural Network Ensemble	0.3624	0.3518	0.0448	0.0400
Neural Network	0.3620	0.3518	0.0447	0.0399
Support Vector Machine	0.3931	0.3516	0.0512	0.0450
Boosting Tree	0.4367	0.3846	0.0551	0.0464
Random Forest	1.0870	0.8108	0.1297	0.0806
k-NN	0.4240	0.3963	0.0529	0.0464

Figure 2.7 illustrates wind speed prediction results for the first 300 test points.

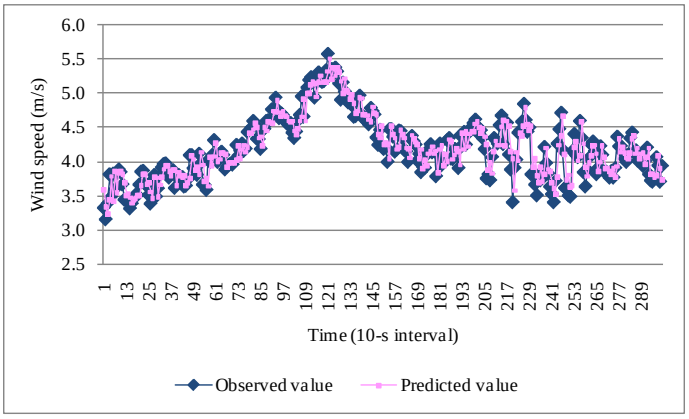

Figure 2.7 Prediction results from the wind speed prediction model for the first 300 points

2.3.3.2 One-step Ahead Prediction

A model for one-step ahead prediction of the generated power, the drive-train acceleration, and the tower acceleration is discussed (see Eqs (2.13) – (2.15)). The model is tested with the test dataset introduced in Section 2.2. Table 2.11 presents the values of

four metrics (defined in Section 2.3.1) for one-step ahead wind speed prediction. The value of MAPE for predicting generated power at t + T = 10-s is 0.0096 (see Table 2.11), which is almost identical to the accuracy of the power prediction at time t (see Table 2.4). The accuracy of predicting drive-train acceleration (MAPE = 0.0785) at t + T = 10-s is also close to that at the current time (MAPE = 0.0517). The MAPE for predicting tower acceleration at t + T = 10-s is higher (MAPE = 0.1054) relative to its predicted value at time t (MAPE = 0.0637). In general, the prediction accuracy of the three models in 10-s ahead prediction is better than 90%, which presents an acceptable result. Figures 2.8 – 2.10 illustrate the first 300 results for of the three parameters, generated power, drive-train acceleration, and tower acceleration.

Table 2.11 Results of one-step ahead prediction

Parameter	MAE	SD of AE	MAPE	SD of APE
Generated power	4.5592	3.5510	0.0096	0.0142
Drive-train acceleration	4.1247	5.7525	0.0785	0.0815
Tower acceleration	6.5365	9.9910	0.1054	0.1425

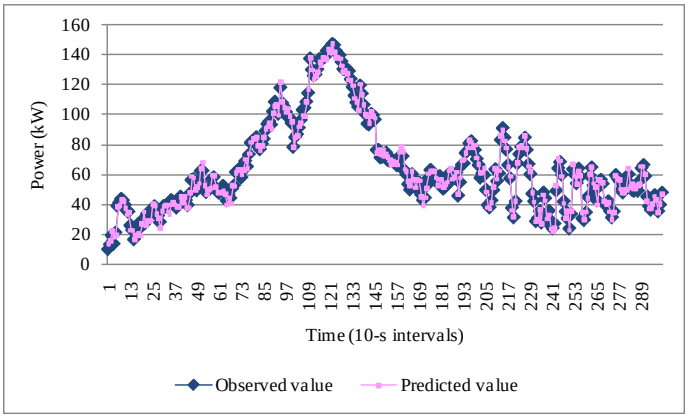

Figure 2.8 First 300 points of one-step ahead prediction of the generated power

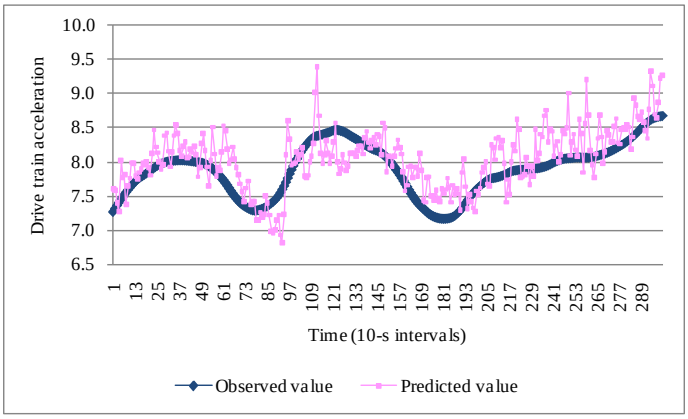

Figure 2.9 The results of one-step ahead prediction of the drive-train acceleration for first 300 points

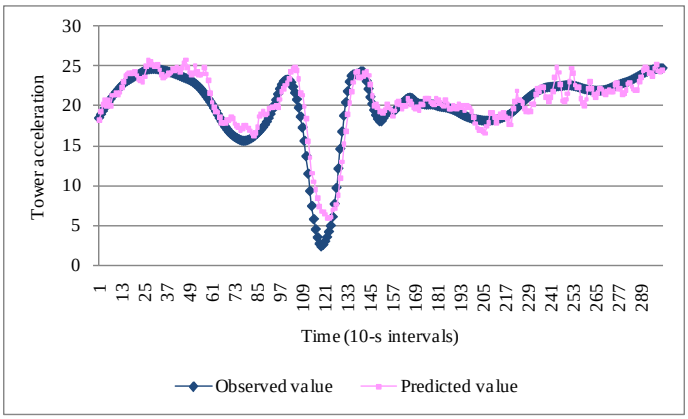

Figure 2.10 The results of one-step ahead prediction of the tower acceleration for the first 300 points

2.4 Multi-objective Optimization

2.4.1 Anticipatory Control Process

The process of anticipatory control is implemented as an iterative, finite horizon optimization of wind turbine performance. The anticipatory control model generates control settings for the wind turbine at the current time *t* and *t* + T. For example, assume the optimal settings of controllable parameters, the generator torque and the blade pitch

angle for time t and t + T are $\tau(t)^*$, $\tau(t + \mathrm{T})^*$, $\beta(t)^*$ and $\beta(t + \mathrm{T})^*$. The wind speed at time t + T can be obtained from model (2.17). The power generated at time t and t + T is computed from (2.18) and (2.19). The optimal drive-train acceleration is expressed in (2.20) – (2.21) and the optimal tower acceleration is formulated in (2.22) – (2.23).

$$P(t)^* = f(v(t), v(t-\mathrm{T}), \beta(t)^*, \beta(t-\mathrm{T}), \tau(t)^*, \tau(t-\mathrm{T})) \tag{2.18}$$

$$P(t+\mathrm{T})^* = f(v(t+\mathrm{T}), v(t), \beta(t+\mathrm{T})^*, \beta(t)^*, \tau(t+\mathrm{T})^*, \tau(t)^*) \tag{2.19}$$

$$\begin{aligned} A_d(t)^* = f(&v(t), v(t-2\mathrm{T}), v(t-3\mathrm{T}), \beta(t-\mathrm{T}), \beta(t-3\mathrm{T}), \tau(t)^*, \\ &\tau(t-\mathrm{T}), \tau(t-3\mathrm{T}), w_d(t-3\mathrm{T}), A_d(t-\mathrm{T})) \end{aligned} \tag{2.20}$$

$$\begin{aligned} A_d(t+\mathrm{T})^* = f(&v(t+\mathrm{T}), v(t-\mathrm{T}), v(t-2\mathrm{T}), \beta(t)^*, \beta(t-2\mathrm{T}), \tau(t+\mathrm{T})^*, \\ &\tau(t)^*, \tau(t-2\mathrm{T}), w_d(t-2\mathrm{T}), A_d(t)^*) \end{aligned} \tag{2.21}$$

$$\begin{aligned} A_t(t)^* = f(&v(t), v(t-\mathrm{T}), v(t-2\mathrm{T}), v(t-3\mathrm{T}), \beta(t-\mathrm{T}), \tau(t)^*, \\ &\tau(t-2\mathrm{T}), \tau(t-3\mathrm{T}), A_t(t-\mathrm{T})) \end{aligned} \tag{2.22}$$

$$\begin{aligned} A_t(t+\mathrm{T})^* = f(&v(t+\mathrm{T}), v(t), v(t-\mathrm{T}), v(t-2\mathrm{T}), \beta(t)^*, \tau(t+\mathrm{T})^*, \\ &\tau(t-\mathrm{T})^*, \tau(t-2\mathrm{T}), A_t(t)^*) \end{aligned} \tag{2.23}$$

where the notation is the same as in Section 2.3.2.

To implement the anticipatory control approach, the settings at time t + T are computed based on the current status parameters. Once the wind turbine is operated with the computed control strategies, the status of the wind turbine will be sampled, and the sampled data will be stored in a database as the inputs for the next optimization step. This procedure is repeatedly implemented to realize the anticipatory control.

2.4.2 Multi-objective Optimization Model

To optimize the wind turbine performance, the power generated in the interval t to t + T can be maximized as an expression of a linear combination of $P(t)^*$ and $P(t + \mathrm{T})^*$ (Kusiak *et al.* 2009a). This can be transformed as minimization of the linear combination of $|P(t)^* - \min\{1500, 2.625v(t)^3\}|$ and $|P(t + \mathrm{T})^* - \min\{1500, 2.625v(t)^3\}|$ shown in (2.24).

$$T_p = w_p \mid P(t)^* - \min\{1500, 2.625v(t)^3\} \mid + \\ (1-w_p) \mid P(t+\mathrm{T})^* - \min\{1500, 2.625v(t)^3\} \mid \quad (2.24)$$

where T_p is the weighted sum, the w_p is the weight coefficient (between 0 and 1) and the $\min\{1500, 2.625v(t)^3\}$ is the boundary of theoretical maximum power that can be obtained from the wind kinetic energy (Kusiak *et al.* 2009a).

Like the maximization of the generated power, the minimization of drive-train acceleration and the tower acceleration is formulated as (2.25) and (2.26).

$$T_D = w_D A_d(t)^* + (1-w_D) A_d(t+\mathrm{T})^* \quad (2.25)$$

$$T_T = w_T A_t(t)^* + (1-w_T) A_t(t+\mathrm{T})^* \quad (2.26)$$

where T_D is the weighted sum of minimized drive-train acceleration at time t and time t + T, T_T is the weighted sum of minimized tower acceleration at time t and time t + T, w_D and w_T are the two weights between 0 and 1.

The objective function C for optimizing the wind turbine performance is expressed in (2.27) as the weighted sum of (2.25) and (2.26).

$$C = (w_1 T_D + w_2 T_T + w_3 T_P) / \sum_{i=1}^{3} w_i \quad (2.27)$$

where w is the weight coefficient in [0, 1].

To define the feasible ranges of the parameters, constraints (2.28) – (2.31), are defined.

$$\max\{0, \mathrm{currentSetting} - 40\} \le \tau(t)^* \\ \le \min\{100, \mathrm{currentSetting} + 40\} \quad (2.28)$$

$$\max\{0, \mathrm{currentSetting} - 40\} \le \tau(t+\mathrm{T})^* \\ \le \min\{100, \mathrm{currentSetting} + 40\} \quad (2.29)$$

$$\max\{-0.57, \mathrm{currentSetting} - 15\} \le \beta(t)^* \\ \le \min\{90.61, \mathrm{currentSetting} + 15\} \quad (2.30)$$

$$\max\{-0.57, \mathrm{currentSetting} - 15\} \le \beta(t+\mathrm{T})^* \\ \le \min\{90.61, \mathrm{currentSetting} + 15\} \quad (2.31)$$

In this study, the value of generator torque is normalized to [min = 0, max = 100%]. In addition, the maximum rate of change of the generator torque is limited to 40%. Therefore, the upper and lower bound for generator torque can be determined as min{100, CurrentSetting + 40} and max{0, CurrentSetting – 40}. To control the blade pitch angle, the maximum value of blade pitch angle is set to 90.61 degrees and the minimum value is fixed at – 0.57 degree. The two values are obtained from the maximum and minimum values of the blade pitch angle included in the dataset. The maximum rate of the blade pitch angle change is 15 degrees. Then the upper bound and lower bound of the blade pitch angle control can be expressed as max{– 0.57 , CurrentSetting – 15} and min{90.61, CurrentSetting + 15}.

The optimization model is formulated in (2.32).

$$
\begin{aligned}
&\min_{\tau(t)^*,\beta(t)^*,\tau(t+\mathrm{T})^*,\beta(t+\mathrm{T})^*} C(\cdot)\\
&\text{subject to}\\
&A_d(t)^* = f(v(t), v(t-2\mathrm{T}), v(t-3\mathrm{T}), \beta(t-\mathrm{T}), \beta(t-3\mathrm{T}), \tau(t)^*, \tau(t-\mathrm{T}),\\
&\qquad \tau(t-3\mathrm{T}), w_d(t-3\mathrm{T}), A_d(t-\mathrm{T}))\\
&A_d(t+\mathrm{T})^* = f(v(t+\mathrm{T}), v(t-\mathrm{T}), v(t-2\mathrm{T}), \beta(t)^*, \beta(t-2\mathrm{T}), \tau(t+\mathrm{T})^*,\\
&\qquad \tau(t)^*, \tau(t-2\mathrm{T}), w_d(t-2\mathrm{T}), A_d(t)^*)\\
&A_t(t)^* = f(v(t), v(t-\mathrm{T}), v(t-2\mathrm{T}), v(t-3\mathrm{T}), \beta(t-\mathrm{T}), \tau(t)^*,\\
&\qquad \tau(t-2\mathrm{T}), \tau(t-3\mathrm{T}), A_t(t-\mathrm{T}))\\
&A_t(t+\mathrm{T})^* = f(v(t+\mathrm{T}), v(t), v(t-\mathrm{T}), v(t-2\mathrm{T}), \beta(t)^*, \tau(t+\mathrm{T})^*,\\
&\qquad \tau(t-\mathrm{T})^*, \tau(t-2\mathrm{T}), A_t(t)^*)\\
&P(t)^* = f(v(t), v(t-\mathrm{T}), \beta(t)^*, \beta(t-\mathrm{T}), \tau(t)^*, \tau(t-\mathrm{T}))\\
&P(t+\mathrm{T})^* = f(v(t+\mathrm{T}), v(t), \beta(t+\mathrm{T})^*, \beta(t)^*, \tau(t+\mathrm{T})^*, \tau(t)^*)\\
&v(t) = f(v(t-\mathrm{T}), v(t-2\mathrm{T}), v(t-3\mathrm{T}), v(t-4\mathrm{T}), v(t-5\mathrm{T}),\\
&\qquad v(t-6\mathrm{T}), v(t-8\mathrm{T}))\\
&P_a(t)^* \le \min\{1500, 2.625v(t)^3\}\\
&P_a(t+\mathrm{T})^* \le \min\{1500, 2.625v(t+\mathrm{T})^3\}\\
&\max\{0, \text{currentSetting} - 40\} \le \tau(t)^* \le \min\{100, \text{currentSetting} + 40\}\\
&\max\{0, \text{currentSetting} - 40\} \le \tau(t+\mathrm{T})^* \le \min\{100, \text{currentSetting} + 40\}\\
&\max\{-0.57, \text{currentSetting} - 15\} \le \beta(t)^* \le \min\{90.61, \text{currentSetting} + 15\}\\
&\max\{-0.57, \text{currentSetting} - 15\} \le \beta(t+\mathrm{T})^* \le \min\{90.61, \text{currentSetting} + 15\}
\end{aligned}
\tag{2.32}
$$

where $C(\cdot)$ is the objective function that transforms the multi-objective model to a single-objective model (see (2.24) – (2.27)). The remaining notation is the same as in Section 2.3.2. The four controllable parameters are the solutions to the optimization model.

Solving the optimization model (2.32) is a challenge for classical optimization algorithms. A particle swarm optimization (PSO) algorithm (Kennedy and Eberhart 1995; Shi and Eberhart 1998; Abido 2002) is applied to solve this problem.

To implement the PSO algorithm, some parameters need to be initialized, such as the number of particles. In this study, the number of particles is arbitrarily fixed at 10. The inertial parameter, ω, which controls the impact of previous velocity on the current velocity in the velocity function, should also be determined. Usually it is a value between 0 and 1. In this chapter, it is set to 0.5. Besides this parameter, in the velocity function, there are another two constants c_1 and c_2, which require an assignment of values. Here, c_1 and c_2, are both arbitrarily set to 2 in this study.

2.5 Case Study and Computational Results

In this section, the computational results of optimizing the wind turbine performance with the PSO algorithm are presented. Before computing the optimal solutions for the wind turbine control, the value of the weights used in the objective of model (2.32) should be determined. In Eqs (2.24) – (2.26), the weights, w_P, w_D and w_T, are all assigned the value 0.5. This value indicates the equal importance of the three objectives, generated power, drive-train acceleration and tower acceleration at time t + T. Two cases of weight assignments are studied to show different wind turbine control preference. In Case 1, the $w_1 = 1$ and $w_2 = w_3 = 0$. In this case, the wind turbine is supposed to be controlled in maximizing the generated power. In Case 2, the $w_1 = 0$ and $w_2 = w_3 = 0.5$. This case translates to a circumstance whereby the preference of controlling the wind turbine reduces the turbine vibration. In this part, a multi-point

optimization is introduced. It is based on data from 11/8/2009 7:47:10 AM to 11/8/2009 8:03:50 AM (about 16 minutes) in the dataset.

2.5.1 Stopping Criteria of the PSO

The number of iterations of the PSO to converge needs to be determined. Three instances of the dataset used in Section 2.5 are randomly selected to show the convergence speed of the PSO algorithm. The standardized best global fitness based on function (2.33) is employed to evaluate the convergence of the PSO algorithm. Figure 2.12 illustrates the number of iterations the PSO needs to converge in Case 1 for all three instances. Figure 2.13 shows the similar concept for Case 2.

$$\frac{\hat{g}^{j}}{\max\{\hat{g}^{1500}\}} \tag{2.33}$$

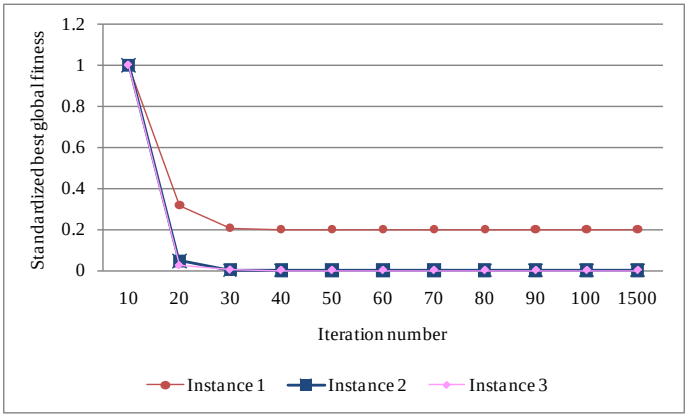

Figure 2.11 Convergence of the PSO algorithm for three instances of Case 1

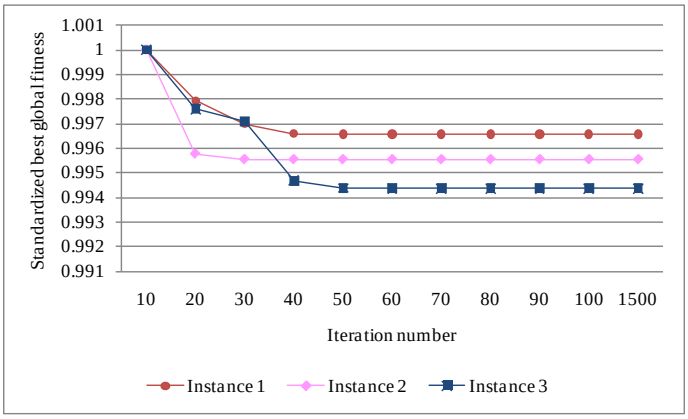

Figure 2.12 Convergence of the PSO algorithm for three instances of Case 2

Figures 2.11 and 2.12 illustrate that the PSO converges within 50 iterations. However, to set a more conservative setting criterion the iteration limit of 100 is applied.

2.5.2 Case 1 (w1 = 1 and w2 = w3 = 0)

This section addresses the multi-point optimization result for Case 1 based on the data points of Section 2.5. Table 2.12 summarizes the optimization results of anticipatory control for these data points. Since in this case the wind turbine is controlled with the preference being to maximize only the generated power, the weight coefficient for maximizing the power generation model is set to 1, and for minimizing wind turbine vibration to 0. As shown in Table 2.12, the gain of maximizing power at time t + T can approach 37.49%. However, the drive-train acceleration and tower acceleration both increase. The power advantage comes from the increased generator torque. Figures 2.13 and 2.14 illustrate the optimized control strategies at time t + T versus the observed control strategies.

Table 2.12 Summary of multi-point optimization of Case 1

Objective	Original Value (Mean)	Optimized Value (Mean)	Gain (Mean)
Generated power	1089.0740	1497.3160	37.49%
Drive-train acceleration	53.1174	65.4381	23.20%
Tower acceleration	54.5172	85.3627	56.58%

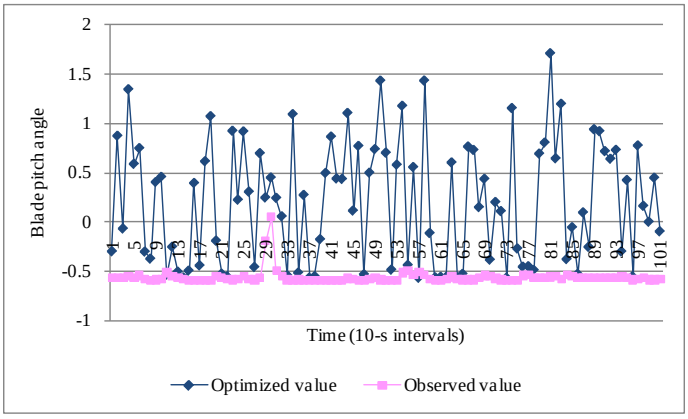

Figure 2.13 Optimized vs observed blade pitch angle for Case 1

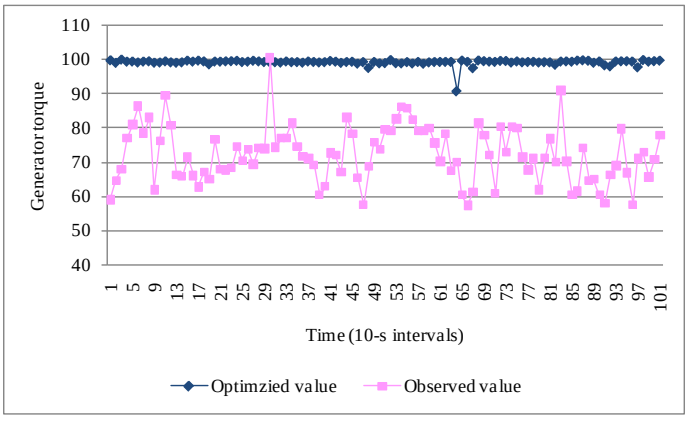

Figure 2.14 Optimized vs observed generator torque for Case 1

2.5.3 Case 2 (w1 = 0 and w2 = w3 = 0.5)

Case 2 represents a control preference emphasizing reduction of wind turbine vibration rather than increasing the power output. In this case, the weight assigned to maximizing power is w_1= 0, and the weights assigned to mitigating drive-train and tower acceleration are w_2 = w_3 = 0.5. Table 2.13 summarizes the optimization results of anticipatory control for Case 2. The vibration is reduced by 2.07% and 4.63% for the drive-train and the tower, respectively, at time t + T. The generated power is reduced by 9.42%. Figures 2.15 and 2.16 demonstrate the optimized value and observed value of the blade pitch angle and generator torque at time t + T.

Table 2.13 Summary of multi-point optimization in Case 2

Objective	Original Value (Mean)	Optimized Value (Mean)	Gain
Generated power	1089.074	986.4936	-9.42%
Drive-train acceleration	53.11743	52.01851	-2.07%
Tower acceleration	54.51721	51.99516	-4.63%

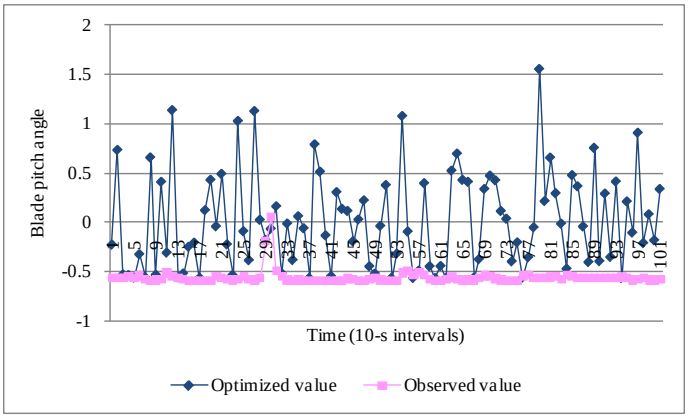

Figure 2.15 Optimized vs observed blade pitch angle for Case 2

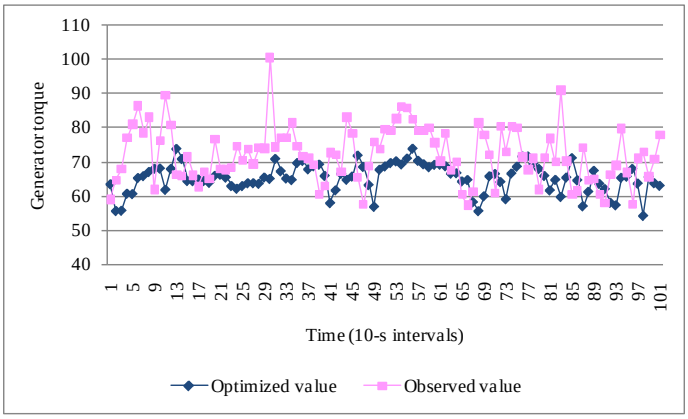

Figure 2.16 Optimized vs observed generator torque for Case 2

2.6 Summary

An anticipatory control model for optimizing performance of wind turbines was discussed in this chapter. It was set to accomplish three goals, increasing the power extracted from the wind, and mitigating vibration of the drive-train system and the tower. By considering these goals, the power generation model, drive-train acceleration model, tower acceleration model and the time-series wind speed prediction model were derived to establish this optimization model. Data-driven approaches were applied to constrict these models from wind farm data. A comparative analysis was performed to assess the performance of data-driven models derived by different data-mining algorithms and select the best performing model. To solve the constructed optimization model, a particle swarm optimization algorithm was applied.

Two strategies of anticipatory control were implemented, control of a wind turbine by emphasizing maximization of power generation and reduction of wind turbine vibration. Single point and multi-point optimization results were presented. As the generator torque and power are correlated, the increased generator torque improves the power generated. However, as shown in the optimization results, increasing torque led to

a higher acceleration of the drive-train and the tower. To reduce vibration of the drive-train and tower, an optimization strategy resulting in reduced generator torque was recommended.

CAPTER 3

ADAPTIVE CONTROL OF A WIND TURBINE WITH DATA MINING AND SWARM INTELLIGENCE

3.1 Introduction

In this chapter, an adaptive approach to wind turbine control is presented. It is designed to achieve a balance between power optimization and smooth drive train control in response to the changes in wind speed and electricity demand. The smoothing of the drive train is accomplished by minimizing the torque ramp rate rather than controlling the rotor speed presented in (Kusiak *et al.* 2009a). The former reduces extreme loads, which translates into a lower maintenance and operation cost. To model the turbine, a data-driven approach is introduced. To realize the adaptive turbine control, estimates of future electricity demand and wind power to be produced at the same time are desired. A time-series model extracted by a data-driven approach predicts the future wind power. A simulation model is used to generate the future demand due to the lack of demand data in this research.

SCADA (Supervisory Control and Data Acquisition) data from turbines installed at a large wind farm (150 MW) has been used in this research. To develop and validate the models proposed in this research, 0.1 Hz (10-s) data from three randomly selected wind turbines are used.

3.2 Problem Formulation

3.2.1 Adaptive Control

The framework of adaptive wind turbine control is illustrated in Figure 3.1. In this chapter, a wind turbine is optimized subject to the following two objectives: power maximization and minimization of the torque ramp rate. A weighted linear combination of the two objectives is used in the bi-objective optimization model. The values of two

weights are impacted by the amount (excess or deficit) of the generated power and the projected power demand.

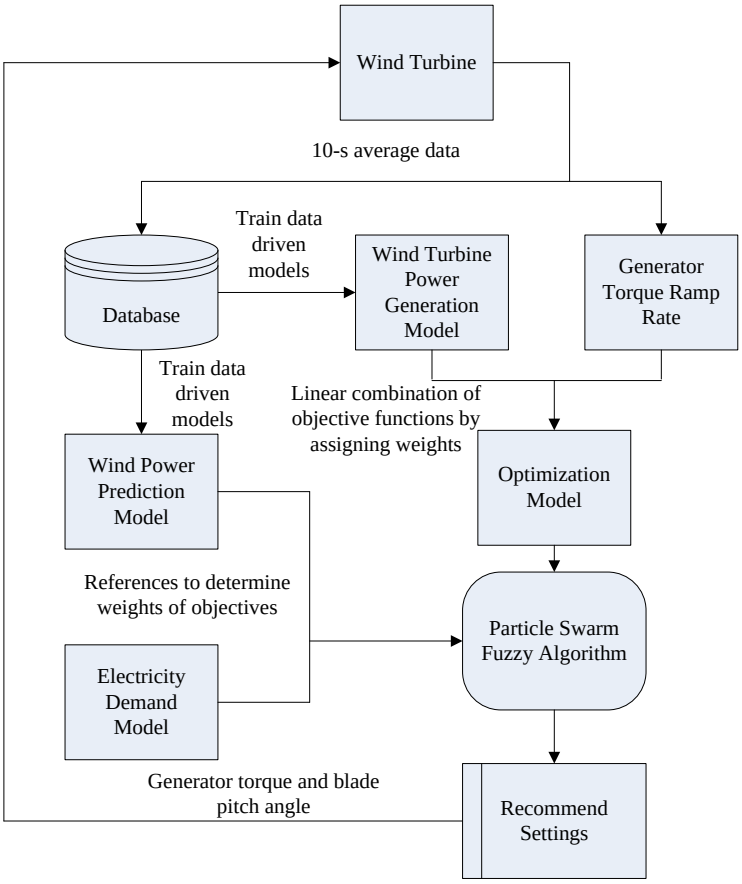

Figure 3.1 The framework of adaptive wind turbine control

As illustrated in Figure 3.1, three models, the wind turbine power generation model, the wind power prediction model and the electricity demand model, are established to realize the adaptive control framework. The wind power prediction model and the electricity demand model are utilized as references in determining values of the weights of the objectives. The wind turbine power generation model aims to accurately estimate the power generated from a wind turbine with the control settings. Establishing accurate models of power generation and power prediction is challenging, and in this chapter, it is accomplished with data-mining algorithms that have been successfully

applied in other domains, e.g., industry and service (Berry and Linoff 2004; Shevade *et al.* 2000).

The energy of the wind and the electricity demand are variable, and therefore the weights assigned to the two corresponding objectives need to be adjusted accordingly. A novel optimization algorithm, the Particle Swarm Fuzzy Algorithm, is developed to determine the weights of the two objectives and solve the optimization model that is composed of data-driven models developed in this chapter. Two controllable parameters, blade pitch angle and generator torque, are the solution to the optimization problem, and they are considered the recommended settings for the control system of a wind turbine to manipulate wind turbines.

To maintain good quality of data-driven models, a re-learning scheme is applied to the models using the continuously collected data.

3.2.2 Wind Turbine Power Generation Model

The power conversion of a wind turbine is represented by the 4-tuplet (υ, τ, β, y), where υ represents the wind speed (non-controllable parameter), τ is the generator torque (controllable parameter), β is the blade pitch angle (controllable parameter), and y is the power generated by the wind turbine (response parameter). The value of the response parameter, y, is impacted by the non-controllable and controllable parameters as shown in (3.1).

$$y_t = f(\upsilon_t, \upsilon_{t-T}, \tau_t, \tau_{t-T}, \beta_t, \beta_{t-T}) \tag{3.1}$$

where t is the current time, T represents the sampling time of data (10-s data), and $f(\cdot)$ is the function describing the wind turbine energy conversion process learned by the data-mining algorithms.

3.2.2.1 Algorithm Selection

To build the model (3.1), the following seven data-mining algorithms have been considered: Neural Network (Siegelmann and Sontag 1994; Liu 2001; Smith 1993), Neural Network Ensemble (Hansen and Salamon 1990), k-Nearest Neighbor (Shakhnarovish *et al.* 2005), Support Vector Machine (Schölkopf *et al.* 1999; Steinwart and Christmann 2008), Boosting Tree (Regression) (Friedman 2001; Friedman 2002), Classification and Regression Tree (Breiman *et al.* 1984), and Random Forest (Regression) (Breiman 2001).

Table 3.1 describes the industrial data selected from three wind turbines to conduct the research discussed in this chapter. The data are partitioned into three datasets: training dataset, test dataset, and validation dataset. Turbine 1 provides the training and test datasets, and the data from Turbines 2 and 3 are used to validate the models derived by various data-mining algorithms. The training dataset is used to extract models by the data-mining algorithms. The test dataset is applied to test the accuracy of the models and selection of the best-performing data-mining algorithm. The validation dataset examines the robustness of the data-driven model established by the selected algorithm.

Table 3.1 Data description

Turbine No.	Training Dataset	Test Dataset	Validation Datasets
1	11/4/2008 4:37:20 AM to 11/4/2008 2:37:20 PM, 11/4/2008 4:49:30 PM to 11/5/2008 2:49:30 AM, 11/18/2008 3:19:50 AM to 11/18/2008 1:19:50 PM, 10803 data points	11/18/2008 2:48:40 PM to 11/19/2008 12:48:40 AM, 12/30/2008 3:25:20 AM to 12/30/2008 1:25:10 PM, 7201 data points	Not applicable
2	Not applicable	Not applicable	11/18/2008 2:52:00 PM to 11/19/2008 12:51:50 AM, 12/30/2008 3:25:40 AM to 12/30/2008 1:25:30 PM, 7200 data points
3	Not applicable	Not applicable	11/18/2008 2:53:30 PM to 11/19/2008 12:53:20 AM, 12/30/2008 3:25:50 AM to 12/30/2008 1:25:40 PM, 7200 data points

The four metrics (3.2) – (3.5), the mean absolute error (MAE), the standard deviation of absolute error (SD of AE), the mean absolute percentage error (MAPE), and the standard deviation of absolute percentage error (SD of APE), are applied to evaluate the performance of the data-driven models.

$$\text{MAE} = \frac{1}{n}\sum_{i=1}^{n}|\hat{y}_i - y_i| \tag{3.2}$$

$$\text{SD of AE} = \sqrt{\frac{1}{n}\sum_{i=1}^{n}(|\hat{y}_i - y_i| - \frac{1}{n}\sum_{i=1}^{n}|\hat{y}_i - y_i|)^2} \tag{3.3}$$

$$\text{MAPE} = \frac{1}{n}\sum_{i=1}^{n}(|\frac{\hat{y}_i - y_i}{y_i}|)\times 100\% \tag{3.4}$$

$$\text{SD of APE} = \sqrt{\frac{1}{n}\sum_{i=1}^{n}(|\frac{\hat{y}_i - y_i}{y_i}| - \frac{1}{n}\sum_{i=1}^{n}|\frac{\hat{y}_i - y_i}{y_i}|)^2}\times 100\% \tag{3.5}$$

Comparative analysis of the test results of the models built by the data-mining algorithms is shown in Table 3.2. The model derived by the Neural Network algorithm outperforms all models in estimating the power generated by a wind turbine. The corresponding values of MAPE (0.02) and SD of APE (0.07) are the lowest in Table 3.2. Thus, the Neural Network algorithm will be used to construct the wind turbine power generation model.

Table 3.2 Test results of the models derived by seven data-mining algorithms

Algorithms	MAE	SD of AE	MAPE	SD of APE
Neural Network	11.00	9.09	0.02	0.07
Neural Network Ensemble	10.70	9.04	0.03	0.17
k-Nearest Neighbor (*k*=5)	15.20	15.38	0.04	0.15
Support Vector Machine	26.20	16.68	0.08	0.45
Boosting Tree	30.10	45.64	0.06	0.28
CART Regression	135.00	116.23	0.19	0.20
Random Forest Regression	121.00	110.74	0.18	0.56

Figure 3.2 illustrates the first 100 values of the observed (measured) power and the power predicted by the neural network model.

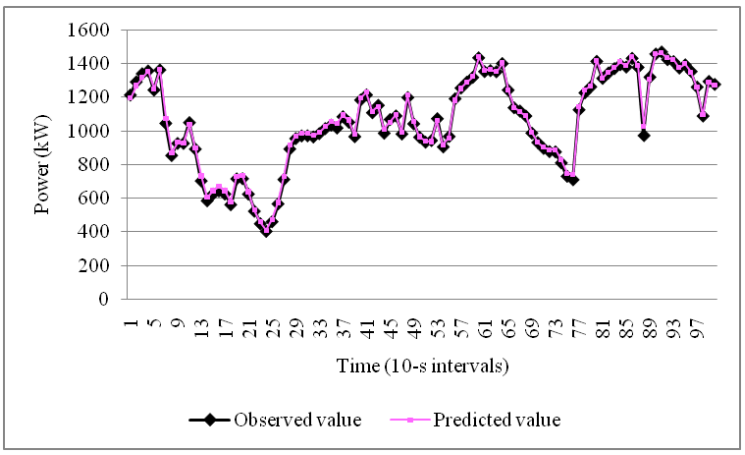

Figure 3.2 The first 100 points of test results produced by the neural network model

3.2.2.2 Model Validation

The validation dataset is used here to assess the robustness of the neural network extracted model in Section 3.2.2.1. Two validation datasets are used: Dataset 1 is collected from wind turbine 2, and validation dataset 2 is collected from wind turbine 3. The details of the two validation datasets are presented in Table 3.1. The four metrics (3.2) – (3.5) are used to assess the accuracy of the power model with the results presented in Table 3.3. The MAPE for validation dataset 1 is 0.05, and the MAPE for validation dataset 2 is 0.03. Although the accuracy of this model tested on two different turbines is lower than the accuracy reported in Table 3.2, it is still impressive considering that the model was built from the data generated at Turbine 1 and tested on Turbines 2 and 3.

Table 3.3 Prediction accuracy results produced
by the neural network model

Validation Datasets	MAE	SD of AE	MAPE	SD of APE
Validation Dataset 1 (Turbine No.2)	19.74	14.08	0.05	0.53
Validation Dataset 2 (Turbine No.3)	12.16	9.09	0.03	0.40

Figure 3.3 presents the first 100 values of the observed generated power and the power predicted by the neural network model for validation dataset 1.

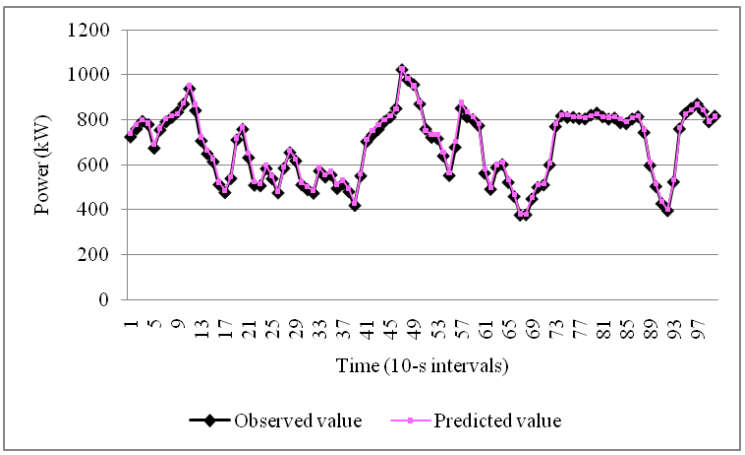

Figure 3.3 The first 100 points of the generated power based on validation dataset 1

Figure 3.4 illustrates the first 100 values of the observed generated power and the power predicted by the neural network model using validation dataset 2.

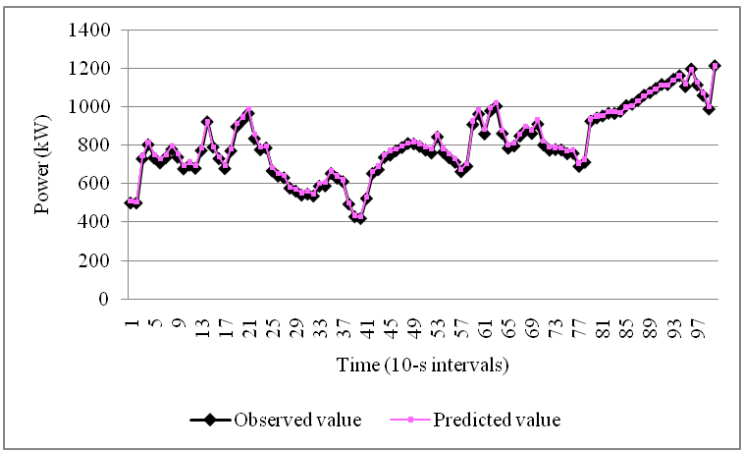

Figure 3.4 The first 100 points of the observed power and the power predicted by the neural network model

3.2.3 Wind Power Prediction Model

To determine wind turbine power at time *t*, the time-series prediction model with the structure presented in (3.6) is utilized.

$$y_t = f(y_{t-T}, ..., y_{t-5T}, \upsilon_{t-T}, ..., \upsilon_{t-5T}) \tag{3.6}$$

where the notation is the same as in model (3.1).

The time-series prediction model employs the past observed events to determine its future values. In the candidate model (3.6), the past states of the generated power itself and wind speed at time periods t – T to t – 5T are considered. A parameter selection strategy, the wrapper with a random search approach (Witten and Frank 2005; Kohavi and John 1997), is applied to select the most significant parameters. The parameters, y_{t-T}, y_{t-2T}, y_{t-3T}, y_{t-5T} and υ_{t-5T}, are selected, and model (3.6) is instantiated as model (3.7).

$$y_t = f(y_{t-T}, y_{t-2T}, y_{t-3T}, y_{t-5T}, \upsilon_{t-5T}) \tag{3.7}$$

where the notation is the same as in model (1).

3.2.3.1 Algorithm Selection

The seven data-mining algorithms of Section 3.2.2.1 are applied to build power prediction models. The training dataset of Table 3.1 is utilized to extract models, and the test dataset (Table 3.1) is used to test their accuracy at time *t*.

Table 3.4 presents the test results (expressed with the metrics (3.2) – (3.5)) of the power prediction models derived by the seven data-mining algorithms. The Neural Network and the Neural Network Ensemble provided results with a MAPE of 0.06. However, since the values of MAE, SD of AE and SD of APE of the Neural Network Ensemble are all smaller than those of the Neural Network, the Neural Network Ensemble is considered for building the power prediction model.

Table 3.4 Test results of power prediction by data-driven models

Algorithms	MAE	SD of AE	MAPE	SD of APE
Neural Network	21.24	34.09	0.06	0.41
Neural Network Ensemble	20.52	32.73	0.06	0.34
k-Nearest Neighbor (*k*=17)	28.83	46.18	0.09	0.68
Support Vector Machine	44.13	39.42	0.14	0.88
Boosting Tree	40.55	54.99	0.09	0.46
CART Regression	138.87	118.39	0.22	0.43
Random Forest Regression	140.90	123.77	0.23	0.83

Figure 3.5 illustrates the results for the first 100 points of power prediction by the Neural Network Ensemble using validation dataset 1.

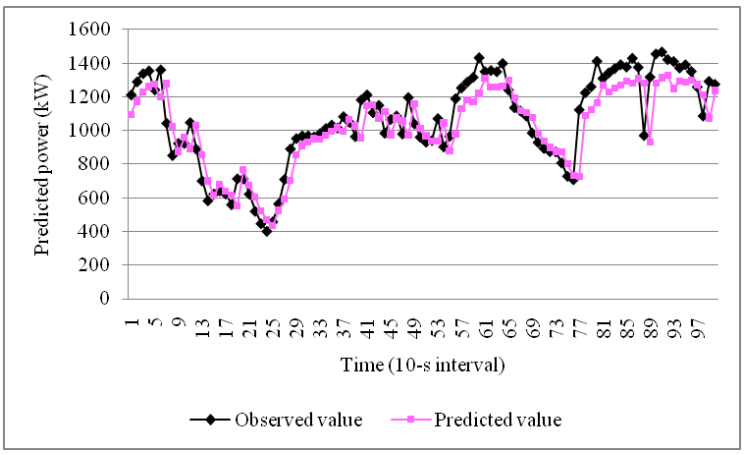

Figure 3.5 The first 100 test points of the observed power and the power predicted by the neural-network ensemble

3.2.3.2 Model Validation

The validation dataset used in Section 3.2.2.2 is used here to assess the robustness of the neural-network ensemble model. Table 3.5 presents the validation results of this model. Compare the MAPE listed in Table 3.4 and in Table 3.5. It is obvious that this time-series data-driven model is feasible, and its performance is consistent in power prediction.

Table 3.5 Prediction accuracy results of the power predicted by the neural-network ensemble

Validation Datasets	MAE	SD of AE	MAPE	SD of APE
Validation Dataset 1 (Turbine No.2)	13.97	22.47	0.06	0.51
Validation Dataset 2 (Turbine No.3)	20.93	36.15	0.07	1.00

Figure 3.6 shows the first 100 points of the observed power and the power predicted by the neural network ensemble for validation dataset 1.

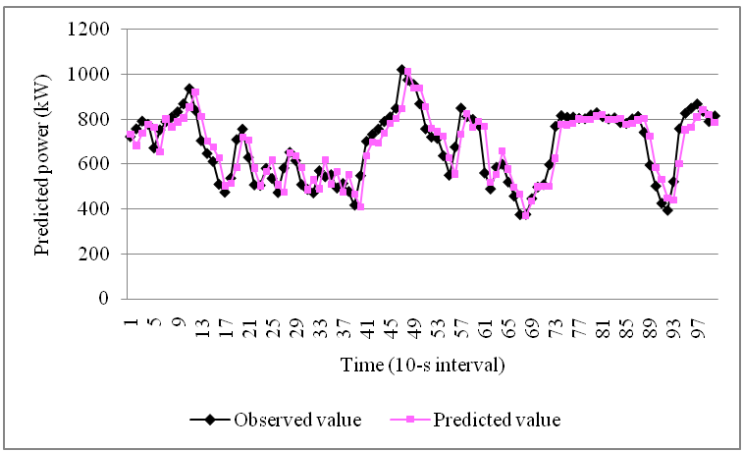

Figure 3.6 The first 100 points of the observed power and the power predicted by the neural network ensemble

Figure 3.7 illustrates the first 100 points of the observed power and the power predicted by the neural network ensemble for validation dataset 2.

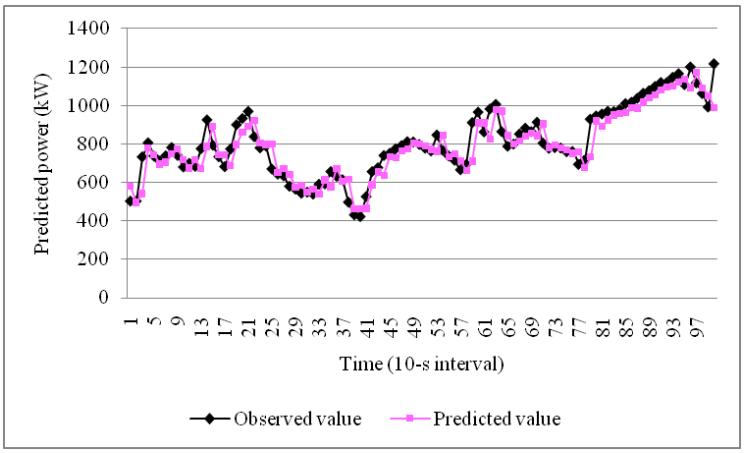

Figure 3.7 The first 100 validation results of power prediction for validation dataset 2

3.2.4 Electricity Demand Simulation Model

Power demand is of significance in optimizing the energy produced by a wind turbine. Predicting power demand belongs to another research domain and therefore is

not discussed in this chapter. It should be stressed, however, that the data-mining algorithms discussed in this chapter can be used to generate power demand models.

Two basic demand simulation models are developed to generate daily power demand at 10-s intervals based on the previous literature (Swider 2007) and the daily electricity consumption by HVAC (Heating Ventilating and Air Conditioning) systems. It is known that modeling customer demand is a challenge, as it depends on factors such as the type of the buildings, the region size, the time of day, and so on. The two types of demand models used in this chapter are discussed next.

3.2.4.1 Demand Model M1

The demand model M1 is established to describe a pattern that simulates the usage of electricity in a micro-grid dominated by business offices (see Figure 3.8).

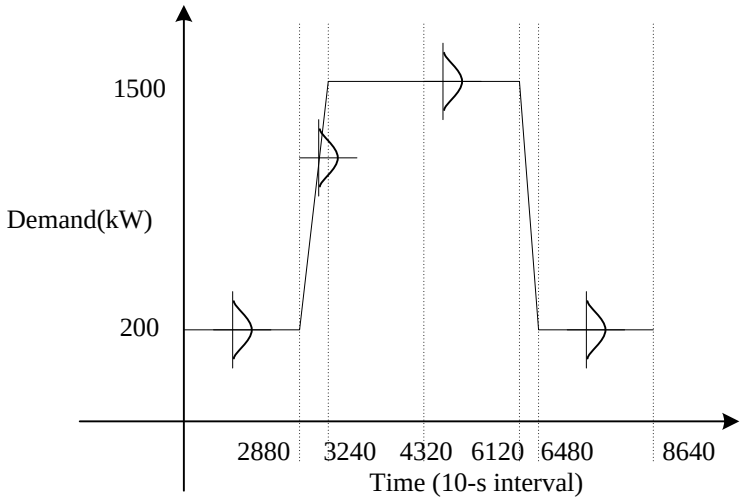

Figure 3.8 Electricity demand pattern of model M1

The vertical axis of Figure 3.8 represents the electricity demand and its maximum of 1500 kW. This arbitrary value of demand should match the generation of a single wind turbine. The horizontal axis represents the time measured in 10-s intervals, the same as

the data frequency used to develop the models in Section 3.2.2. In this model, each demand value is a random number generated from a normal distribution with the mean following the pattern (solid line) in Figure 3.8. The standard deviation is arbitrarily fixed at 50.

As presented in Figure 3.8, the mean demand reflects a scenario where the mean electricity demand is low (200 kW) in the evening after office hours (specifically, 6:00 PM) and in the early morning before office hours (specifically, 8:00 AM). After 8:00 AM, the mean demand increases and reaches a maximum at 9:00 AM. Between 9:00 AM and 5:00 PM, the mean demand remains constant, and it begins to decline after 5:00 PM because the staff leaves the office.

This demand model M1 is expressed in (3.8) – (3.9).

$$D_1 \sim N(\mu_1, \sigma^2) \tag{3.8}$$

$$\mu_1 = \begin{cases} 200 & \text{if } t_0 \le t < t_1 \\ \dfrac{D_{1,\max} - D_{1,\min}}{t_2 - t_1} t + \dfrac{D_{1,\min} t_2 - D_{1,\max} t_1}{t_2 - t_1} & \text{if } t_1 \le t < t_2 \\ 1500 & \text{if } t_2 \le t < t_3 \\ -\dfrac{D_{1,\max} - D_{1,\min}}{t_4 - t_3} t + \dfrac{D_{1,\max} t_4 - D_{1,\min} t_3}{t_4 - t_3} & \text{if } t_3 \le t < t_4 \\ 200 & \text{if } t_4 \le t < t_5 \end{cases} \tag{3.9}$$

where D_1 presents the demand data generated from the normal distribution, μ_1 is the mean of the normal distribution, $D_{1,\min}$=200, $D_{1,\max}$=1500, t_0=0, t_1=2880 (8:00 AM), t_2=3240 (9:00 AM), t_3=6120 (5:00 PM), t_4=6480 (6:00 PM), t_5=8640 (12:00 PM) and σ=50.

In model M1, the demand data is generated from a normal distribution (3.8) and the mean demand computed. For the demand data generated from (3.8), two constraints (3.10) – (3.11) are used to prevent the value of demand becoming negative or exceeding the maximum capacity of the office space.

$$\text{LB} = \max\{0, D_1 \sim N(\mu_1, \sigma^2)\} \tag{3.10}$$

$$\text{UB} = \min\{D_{1,\max}, D_1 \sim N(\mu_1, \sigma^2)\} \tag{3.11}$$

Figure 3.9 shows a portion of the demand data generated from model (3.8) – (3.9) from 7:00 AM to 9:00 AM.

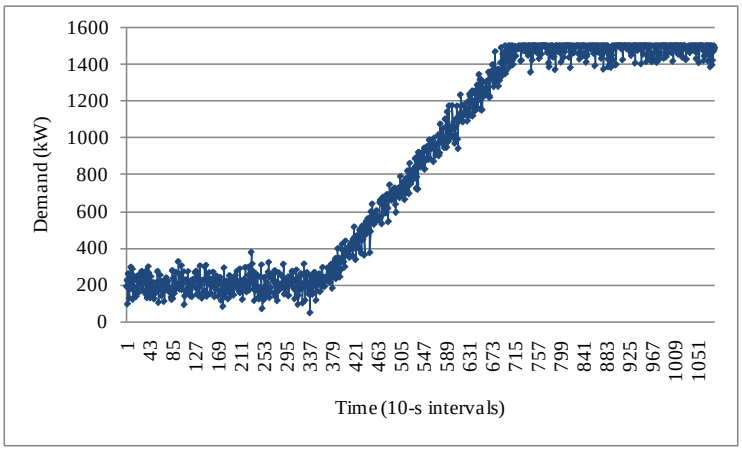

Figure 3.9 Simulated demand data from 7:00 AM to 9:00 AM based on using demand model M1

3.2.4.2 Demand Model M2

Demand model M2 represents a pattern that is non-linear rather than trapezoidal (see Figure 2.10) in the time period 8:00 AM to 6:00 PM. The remaining settings are identical to the model in Figure 2.9.

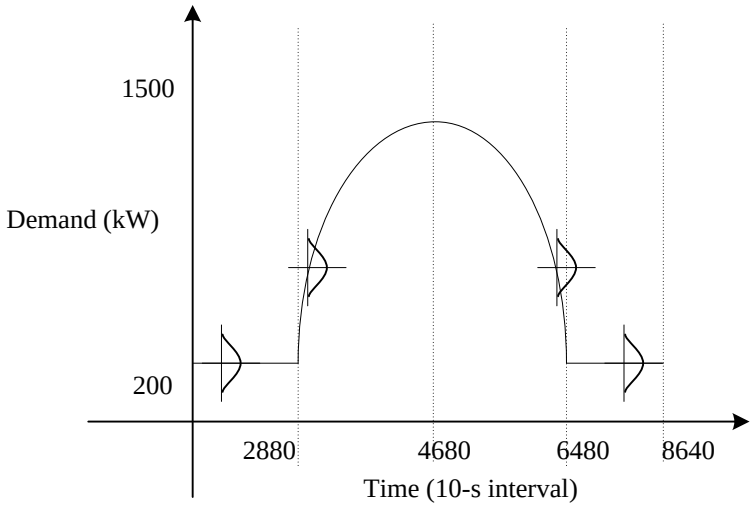

Figure 3.10 Power demand model M2

The demand model M2 is expressed in (3.12) – (3.13).

$$D_2 \sim N(\mu_2, \sigma^2) \tag{3.12}$$

$$\mu_2 = \begin{cases} 200 & \text{if } t_0 \le t < t_1 \\ -\dfrac{4(D_{2,\max} - D_{2,\min})}{(t_1 - t_2)^2} t^2 + \dfrac{4(D_{2,\max} - D_{2,\min})(t_1 + t_2)}{(t_1 - t_2)^2} t + \dfrac{(t_1 + t_2)^2 D_{2,\min} - 4t_1 t_2 D_{2,\max}}{(t_1 - t_2)^2} & \text{if } t_1 \le t < t_2 \\ 200 & \text{if } t_2 \le t < t_3 \end{cases} \tag{3.13}$$

where D_2 represents the generated demand data, μ_2 is the mean of the normal distribution, $D_{2,\min}$=200, $D_{2,\max}$=1500, t_0=0, t_1=2880 (8:00 AM), t_2=4680 (1:00 PM), t_3=6480 (6:00 PM), t_4=8640 (12:00 PM) and σ=50.

Like demand model M1, two constraints (3.14) – (3.15) are introduced to prevent unreasonable demand values.

$$\text{LB} = \max\{0, D_2 \sim N(\mu_2, \sigma^2)\} \tag{3.14}$$

$$\text{UB} = \min\{D_{2,\max}, D_2 \sim N(\mu_2, \sigma^2)\} \tag{3.15}$$

Figure 3.11 illustrates the data generated from demand model M2 between 7:00 AM and 9:00 AM.

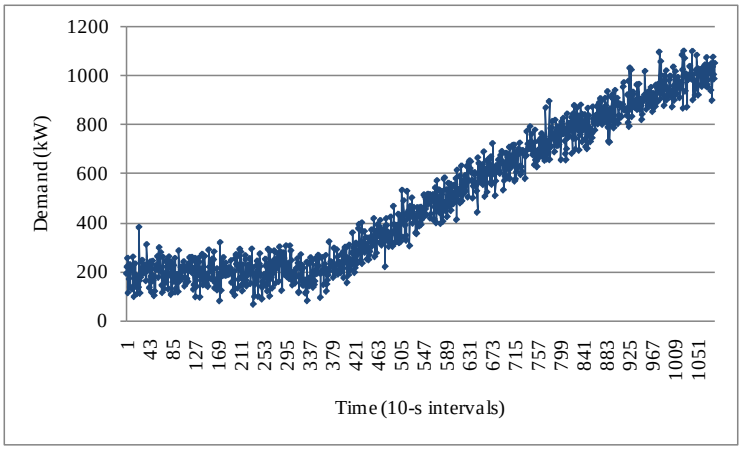

Figure 3.11 Demand data from 7:00 AM to 9:00 AM based on model M2

3.2.5 Optimization Model

The model considered in this chapter maximizes the power generated from a wind turbine and minimizes the generator torque ramp rate. Maximizing the generated power estimated by the model of Section 3.2.2 is equivalent to $|\min\{1500,\ 2.625\upsilon_t^3\} - y_t|$. Here, the difference between the maximum power that could be potentially generated by a wind turbine and the power output from the model is minimized. Two constraints are considered to construct this boundary, the maximum turbine capacity of 1500 kW, and the maximum energy that could be extracted from the wind according to Betz's law, expressed as $2.625\upsilon_t^3$ (Kusiak *et al.* 2009).

The torque ramp rate τ_{ramp} is expressed in (3.16).

$$\tau_{ramp} = \tau_t - \tau_{t-T} \tag{3.16}$$

where τ_t is the generator torque at time t, $\tau_{t-\mathrm{T}}$ is the generator torque at time t – T.

As the scales of the two objectives differ, the generated output is scaled as presented in (3.17).

$$\frac{|\min\{1500, 2.625\upsilon_t^3\} - y_t|}{\max\{|\min\{1500, 2.625\upsilon_t^3\} - y_t|\}} \max\{\tau_{ramp}\} \tag{3.17}$$

The bi-objective optimization model is expressed in (3.18).

$$
\begin{aligned}
&\min_{\tau_t,\beta_t}\{O\} \\
&s.t. \\
&O = \omega_2 \frac{|\min\{1500, 2.625\upsilon_t^3\} - y_t|}{\max\{|\min\{1500, 2.625\upsilon_t^3\} - y_t|\}} \max\{\tau_{ramp}\} + \omega_1 \tau_{ramp} \\
&y_t = f(\upsilon_t, \upsilon_{t-1}, \tau_t, \tau_{t-1}, \beta_t, \beta_{t-1}) \\
&\tau_{ramp} = \tau_t - \tau_{t-1} \\
&\max\{0, \tau_t^* - 20\} \le \tau_t \le \min\{100, \tau_t^* + 20\} \\
&\max\{-0.57, \beta_t^* - 2\} \le \beta_t \le \min\{90.61, \beta_t^* + 2\}
\end{aligned}
\tag{3.18}
$$

where O is the model's overall objective; β_t^* and τ_t^* are the settings of the blade pitch angle and the generator torque at time t; ω_1 and ω_2 are the weights of the two objectives determined by the particle swarm fuzzy algorithm – PSO (discussed in Section 3.3). The remaining notation is the same as in (3.1) and (3.16).

In model (3.8), two controllable parameters, β_t and τ_t, are utilized to realize the adaptive control of the wind turbine. As presented in model (3.18), to control the wind turbine conservatively, the ranges of the two controllable parameters are expressed in (3.19) and (3.20).

$$\max\{-0.57, \beta_t^* - 2\} \le \beta_t \le \min\{90.61, \beta_t^* + 2\} \tag{3.19}$$

$$\max\{0, \tau_t^* - 20\} \le \tau_t \le \min\{100, \tau_t^* + 20\} \tag{3.20}$$

The lower bound (-0.57) and the upper bound (90.61) for the blade pitch angle that cannot be exceeded are obtained from the industrial data used in this research. In addition, the increment (or decrement) of blade pitch angle is set in the range $(\beta_t^* - 2, \beta_t^* + 2)$. The value of the generator torque is expressed in percentage [0, 100], rather than N/m^2. The adjustment of the generator torque is done at increments (or decrements) in the range $(\tau_t^* - 20, \tau_t^* + 20)$.

3.3 The Particle Swarm Fuzzy Algorithm (PSFA)

In this research a wind turbine is controlled adaptively according to the predicted power generation and the power demand. The two control strategies impact the values of

the weights associated with the two objective functions of model (3.18). To relate the control strategy with the model objectives, a particle swarm fuzzy algorithm is developed.

The particle swarm fuzzy algorithm involves two phases. In the first phase, the weights of the two objectives are determined by a fuzzy algorithm (Mirzaeian *et al.* 2002) to ascertain the importance of two objectives (discussed in Section 3.2.5) in the optimization problem based on the predicted power and demand information. This algorithm is expressed by equations (3.21) – (3.24).

$$s_i = \begin{cases} f(y_{t-T}, y_{t-2T}, y_{t-3T}, y_{t-5T}, \upsilon_{t-5T}) & i = 1 \\ D_j \sim N(\mu_j, \sigma^2) \quad j = 1,2 & i = 2 \end{cases} \tag{3.21}$$

$$f(s_i) = \begin{cases} 0 & \text{if } s_i \geq T_{\max} \\ \dfrac{-s_i + T_{\max}}{T_{\max} - T_{\text{threshold}}} & \text{if } T_{\text{threshold}} \leq s_i \leq T_{\max} \\ 1 & \text{if } s_i \leq T_{\text{threshold}} \end{cases} \tag{3.22}$$

$$w_i = 1 - f(u_i) \qquad i = 1,2 \tag{3.23}$$

$$\omega_i = \frac{w_i}{\sum_{i=1}^{n} w_i} \qquad i = 1,2 \tag{3.24}$$

where s_i is the predicted power and demand from the power prediction model (3.6) and demand models (3.9) or (3.11), respectively; $f(s_i)$ is the membership function; w_i is the weight factor to determine the final weight; ω_i is the final weight used in the objective of the optimization model (3.18). $T_{\max}$ is the maximum wind turbine capacity (here 1500kW) and $T_{\text{threshold}}$ is arbitrarily fixed at 200 kW and expressed in the [0, 1] interval. If the predicted power is less than 200 kW, then $T_{\text{threshold}}$ indicates that the wind speed is low and the smoothing control of the generator torque is less significant than power maximization. Thus, the weight assigned to the torque smoothing objective in (3.18) will be close to 0. If customer demand is lower than 200 kW, this implies low energy demand, and the weight assigned to the generated power objective in (3.18) should be small. The

value of $T_{\max}$ indicates that the turbine's generation capacity has been attained or the demand level is at maximum. If the predicted power is greater or equal to 1500 kW, the control should focus on minimizing the torque ramp rate to prevent the fatigue of the drive train and thus reduce the maintenance cost. The demand, which is greater or equal to 1500 kW, implies a high level energy consumption and power maximization needs to be emphasized.

The second phase of the proposed algorithm involves the particle swarm optimization (PSO) algorithm (Kennedy and Eberhart 1995). In the PSO, each particle represents the candidate optimal solutions of model (3.18) and can be expressed as (x_i^j, v_i^j), where x_i^j is a two-dimensional vector $x_i^j = (\tau_t^j, \beta_t^j)$ at j^{th} iteration, and v_i^j is another two-dimensional vector $v_i^j = (v_\tau^j, v_\beta^j)$. The vector x_i^j represents the position of each particle at iteration *j*, and vector v_i^j represents the velocity associated with each particle at iteration *j*. The initial value of each dimension of the particle's position is generated from a uniform distribution, where τ_t^j is generated from $U[\max\{0, \tau_t^* - 20\}, \min\{100, \tau_t^* + 20\}]$ and β_t^j is generated from $U[\max\{-0.57, \beta_t^* - 2\}, \min\{90.61, \beta_t^* + 2\}]$. The initial values of the particle's velocity are all set at 0 at the initialization step. The optimization procedure is presented next.

Step 1. Determine the weights of fitness function $f(\cdot)$, which is the objective function of model (3.18) that takes the weights of objectives produced by the fuzzy algorithm.

Step 2. Initialize the particle size, n, the position of each particle, $x_i^j \in R^m$, and its velocity, $v_i^j \in R^m$, where, $i = 1, 2, ..., n$, m = 2 and j = 0.

Step 3. Initialize the local best $\hat{x}_i^j$ for each particle by $\hat{x}_i^j \leftarrow x_i^j$, and estimate the initial global best $\hat{g}^j$ by $\hat{g}^j \leftarrow \arg\ \min(f(x_i^j))$, where $i = 1, 2, ..., n$ and j = 0.

Step 4. Repeat until the stopping criterion is satisfied (j = iterations to stop in this research)

For each particle $1 \le i \le n$

Step 4.1. Create random vectors $r_1^j \in R^m$ and $r_2^j \in R^m$ by generating

$r_1^j, r_2^j \in U[0,1]$ for m = 1,2.

Step 4.2. Update the velocities of particles by

$v_i^j \leftarrow \omega v_i^j + c_1 r_1^j (\hat{x}_i^j - x_i^j) + c_2 r_2^j (\hat{g}^j - x_i^j)$ and update the particle positions by $x_i^j \leftarrow x_i^j + v_i^j$.

Step 4.3. Update the local best by $\hat{x}_i^j \leftarrow x_i^j$ if $f(x_i^j) \le f(\hat{x}_i^j)$.

Step 4.4. Update the global best by $\hat{g}^j \leftarrow x_i^j$ if $f(x_i^j) \le f(\hat{g}^j)$.

The above algorithm requires parameter initialization. The parameter, ω, is an inertial constant (Shi and Eberhart 1998). It controls the impact of the previous velocity on the current velocity, and usually it has a value between 0 and 1. It is fixed arbitrarily at 0.5 in this research. Parameters c_1 and c_2 are two constants that reflect how much the movement of particles is impacted by the local and global best. Both values are arbitrarily fixed at 2 (Abido 2002).

3.4 Industrial Case Study

3.4.1 Single-point Optimization

3.4.1.1 Description of the Data Point

In this section the particle swarm fuzzy algorithm is demonstrated for a single data point that has been randomly selected from the test dataset of Table 3.1. This data point is partially illustrated in Table 3.6.

Table 3.6 A data point selected to demonstrate single point optimization

Date	Time	Power (t)	… …	Generator Torque (t)	Generator Torque ($t-1$)	Blade Pitch Angle (t)	Blade Pitch Angle ($t-1$)	Demand (t)
12/30/2008	3:29:30 AM	1112.00	… …	76.90	77.59	1.07	3.49	225.72

The data in Table 3.6 reflects a scenario where the current power generated from a wind turbine is high and the simulated demand is low. The current settings of two controllable parameters are 76.90 for the generator torque and 1.07 for the blade pitch angle. The particle swarm fuzzy algorithm determines the weights of the objective function and the recommended control settings optimizing the two control objectives, the maximum power and the minimum torque ramp rate.

3.4.1.2 Convergence of the Particle Swarm Fuzzy Algorithm

In this experiment described next, convergence of the particle swarm fuzzy algorithm (PSFA) based on the data point of Table 3.6 is examined. Ten particles are created, and the stopping criterion is set to 1500 iterations. The convergence of the PSFA is evaluated from two perspectives. The first one is the convergence of the algorithm based on the fitness value. To simplify the evaluation procedure, a fitness value every five iterations from 5 – 100 and the fitness value at iteration 1500 are examined (see Figure 3.12). The horizontal axis in Figure 3.12 represents the number of iterations, and the vertical axis shows the standardized fitness value expressed in (3.25).

$$\frac{\hat{g}^{j}}{\min\{\hat{g}^{1500}\}} \tag{3.25}$$

according to the notation of Section 3.3.

As shown in Figure 3.12, the rapid drop of the standardized fitness value for the global best indicates the quick convergence of the PSFA. In the 1500 iterations, the standardized fitness value drops to 1 at the 50^{th} iteration (converges from 50^{th} iterations) and constantly keeps this value in the following iteration.

Figure 3.12 Standardized fitness value

The second perspective to assess the convergence of the PSFA is to compare the positions of the particles at the initial iteration and the iteration indicating convergence. The positions of the particles are described by two dimensions, generator torque and blade pitch angle, as shown in Figure 3.13. The squares in Figure 3.13 are the initial positions of the 10 particles, and the diamonds represent the positions of these particles at the convergence iteration (here, iteration 50).

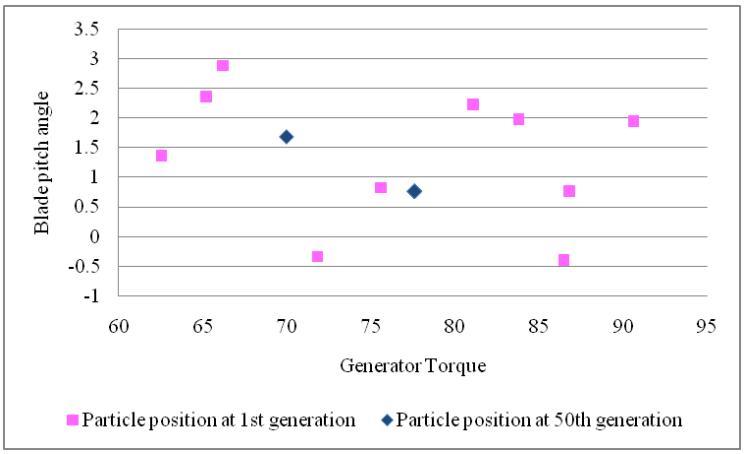

Figure 3.13 Positions of the initial iteration and the 50th iteration

As presented in Figure 3.13, most of the particles move from their initial positions towards the optimized positions in the neighborhood of the generator torque of 77.59 and blade pitch angle of 0.77. However, particles corresponding to the generator torque of about 69.96 and the blade pitch angle of about 1.68 can be noted.

3.4.1.3 Optimization Results

The optimization results based on this single point (Table 3.6) are illustrated in Table 3.7. The first column of Table 3.7 presents the recommended control strategy for the wind turbine. Here, the power generated is 1139.55 kW (slightly higher than original power output of 1112 kW shown in Table 3.6). The ramp rate of the generator torque is nearly zero. The two weights indicate the current control preference. Weight 1 is 0.97 and weight 2 is 0.03. The values of the weights indicate that the control preference focuses on the smoothness of the drive train rather than the maximization of the generated power.

Table 3.7 Results of the single-point optimization by the PSFA

Solution (Generator torque, Blade pitch angle)	Fitness of Global Best	Generated Power	Generator Torque Ramp Rate	Weight-Torque Ramp	Weight-Power
77.59,1.89	2.79E-05	1139.55	3.66E-06	0.97	0.03

3.4.2 Multi-point Optimization

To simulate and demonstrate the adaptive control approach of a wind turbine, the multi-point optimization based on selected data from the test dataset in Table 3.1 is introduced. This dataset reflects a scenario where the predicted power (supply) is higher than the demand at the beginning of the period, and then the power demand gradually exceeds the predicted power. It contains 300 data points from 12/30/2008 8:17:20 AM to

12/30/2008 9:07:10 AM. The demand data is generated from the two demand models M1 and M2 discussed in Section 3.2.4.

3.4.2.1 Stopping Criteria of the PSFA

Before running the multi-point optimization, an experiment is designed to evaluate the stopping criterion for the PSFA. Six data points, indexed as 20, 552, 1020, 1500, 1947 and 3155, are randomly selected from the test dataset of Table 3.1. The PSFA has run 1500 iterations for each point. Figure 3.14 illustrates the convergence of the PSFA for the six points. It is obvious that the PSFA converges quickly, most of the time within 60 iterations. However, to be more conservative, the number of iterations that the PSFA needs to run is set to 100.

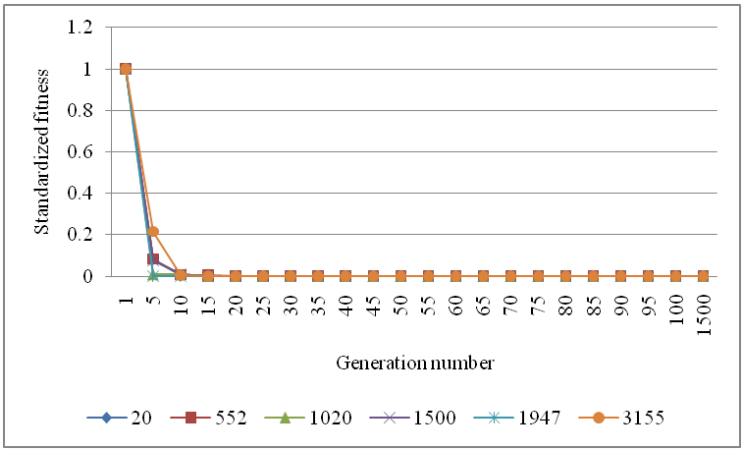

Figure 3.14 Convergence speed of six data points

3.4.2.2 Optimization Results Based on the Demand Model M1

In this section, the test dataset from 12/30/2008 8:17:20 AM to 12/30/2008 9:07:10 AM is merged with the demand data generated from model M1. Figure 3.15 illustrates the weight values assigned to the two objectives of model (3.18). As Figure

3.15 shows, weight 2 is initially lower than weight 1; however, over time weight 2 dominates weight 1. Since, in the PSFA, weight 2 and weight 1 are associated with the demand and predicted power, Figure 3.14 characterizes the scenario discussed before in Section 3.4.2. Figure 3.16 shows the optimized generator and the original torque ramp rate.

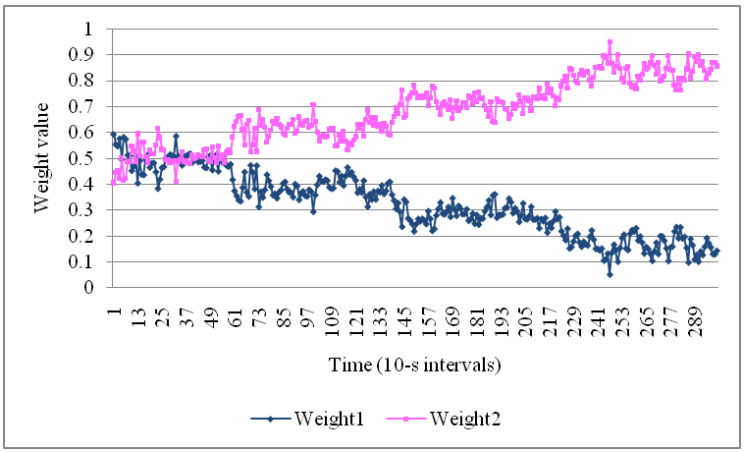

Figure 3.15 Estimated weights for two objectives

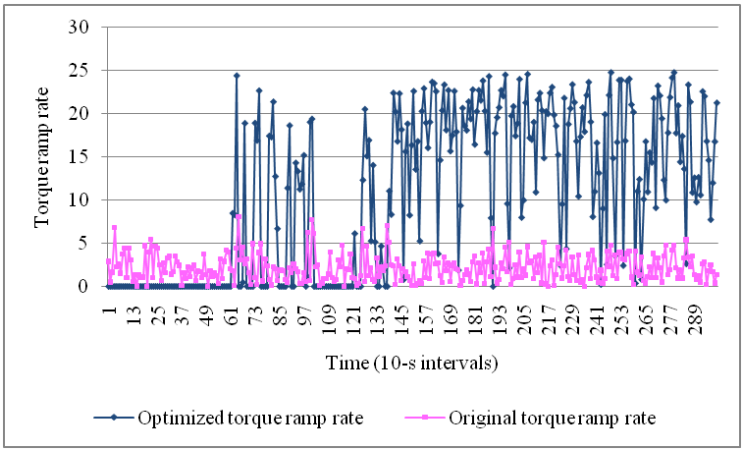

Figure 3.16 Comparison of the optimized torque ramp rate and original torque ramp rate

The optimized power generated from a wind turbine and the original power it produced is illustrated in Figure 3.17.

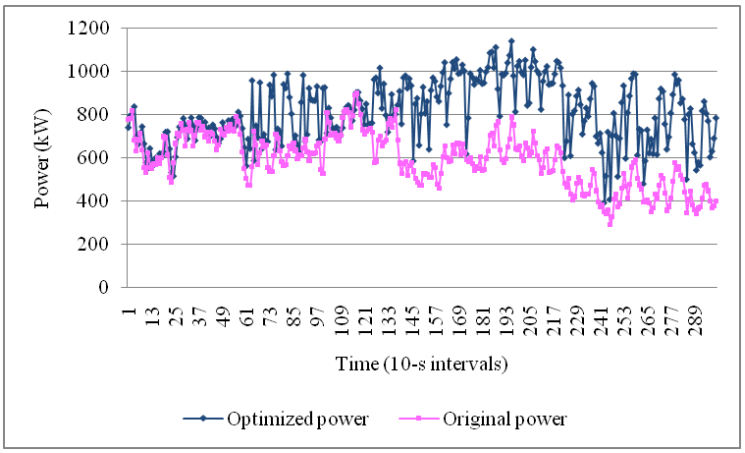

Figure 3.17 Comparison of the optimized and original power

Figures 3.16 and 3.17 clearly demonstrate the change in the wind turbine control strategies. As initially predicted, the power generated is higher than the demand; therefore, the wind turbine is controlled for torque smoothness. In this case, a higher weight is assigned to minimizing the generator torque ramp rate. However, the direction of the weights gets changed over time.

Figure 3.18 demonstrates that the original blade pitch angle remains essentially constant at about -0.53 degree.

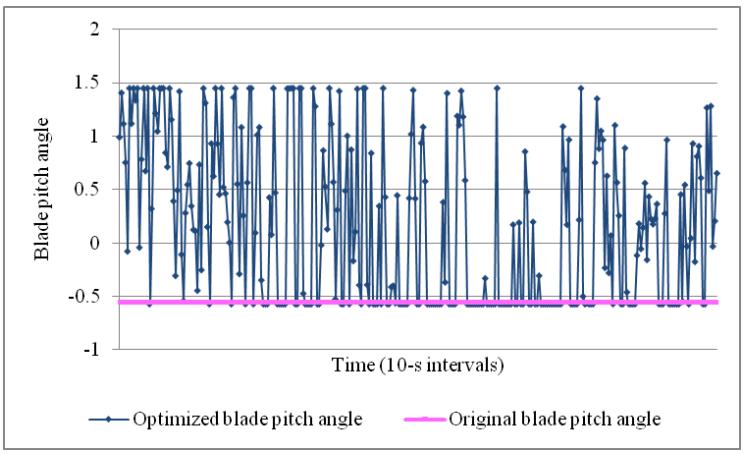

Figure 3.18 Comparison of the optimized and original blade pitch angle

3.4.2.3 Optimization Results Based on the Demand Model M2

The results of the multi-point optimization by the PSFA based on the selected dataset from 12/30/2008 8:17:20 AM to 12/30/2008 9:07:10 AM, merged with demand data generated from demand model M2, are presented. Figure 3.19 illustrates the weights of the two objectives (3.18) in the same time period.

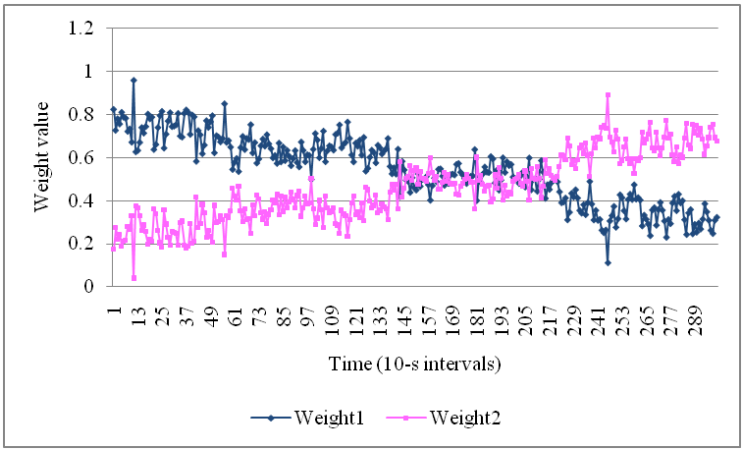

Figure 3.19 Estimated weights for two objectives

Figure 3.20 compares the torque ramp rate computed by the PSFA and the original torque ramp rate.

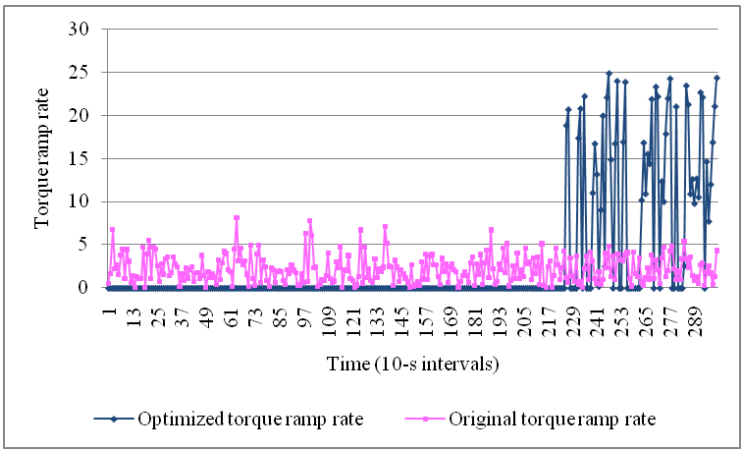

Figure 3.20 Comparison of the optimized and the original torque ramp rate

In Figure 3.20, the optimized ramp rate of the generator torque remains around zero until time period 12/30/2008 8:53:50 AM (220 shown in Figure 3.20). However, due to the change of weights for two objectives after the period 12/30/2008 8:53:50 AM (220), the optimized generator torque ramp rate begins to increase.

Figure 3.21 contrasts the optimized power with the original power output.

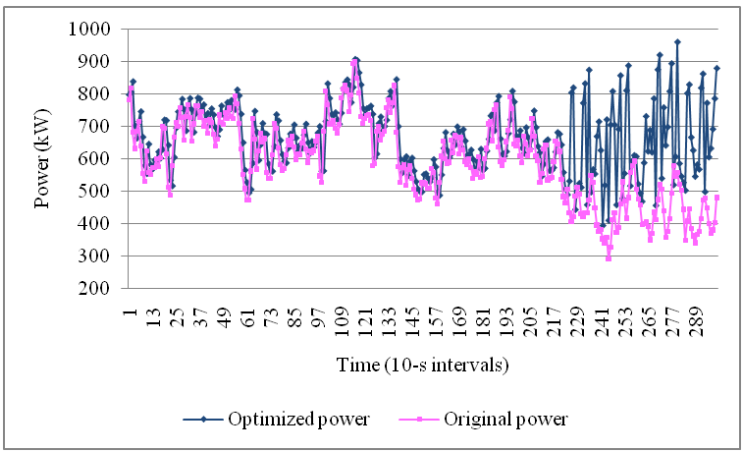

Figure 3.21 Comparison of the optimized and the original power

As shown in Figure 3.21, the optimized and original power follows a similar pattern until time period 12/30/2008 8:53:50 AM (220). After the period 12/30/2008 8:53:50 AM (220), a rise in optimized power is observed.

Figure 3.22 illustrates the recommended and the original set point of the blade pitch angle.

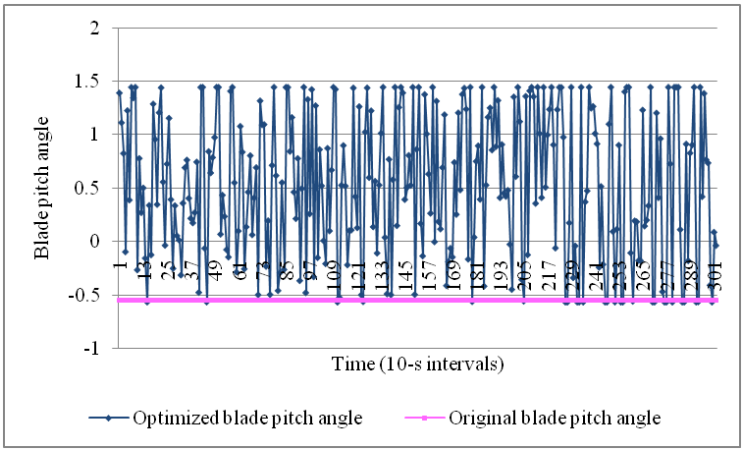

Figure 3.22 Comparison of optimized and original blade pitch angle

3.5 Summary

Adaptive control of a wind turbine to maximize power generation and minimize the torque ramp rate was presented in this chapter. Data-mining algorithms were utilized to generate non-parametric models of wind turbine power generation and the wind power prediction model. The two models were integrated into a model with a linear combination of weighted objectives. The weights associated with the objectives were estimated based on the predicted power and demand. The demand was generated from two simulation models. A novel optimization approach, the particle swarm fuzzy algorithm (PSFA), was developed to solve the model developed in this chapter.

Industrial data from three identical wind turbines of a large wind farm was utilized in this study. The data sampling frequency was 0.1 Hz. While the data from one turbine was used to develop and test data-driven models, the data of two other turbines was employed to validate these models. Comparative analysis of various data-mining algorithms was performed. The convergence and the stopping criterion of the PSFA were investigated.

The feasibility of adaptive control of wind turbines was demonstrated. In addition to the two objectives applied in this chapter, additional objectives, for example, mitigation of wind turbine vibrations, could be considered.

CAPTER 4

OPTIMIZATION OF WIND TURBINE POWER AND ITS VARIABILITY WITH AN ARTIFICIAL IMMUNE NETWORK ALGORITHM

4.1 Introduction

Due to variations in wind speed, wind farms exhibit different characteristics from conventional power plants. Two important goals are to maximize the generated power and to minimize its variability in order to meet the grid requirements. The variability of the generated wind power has become an essential issue in the management of wind-driven energy production.

Power ramp rate (PRR) expresses the change of power for a given time interval, e.g., a minute or an hour. The topic of PRR has been addressed in earlier research that has been published in the literature. Peterson and Brammer (1995) proposed a Lagrangian relaxation approach to address the thermal unit commitment problem associated with power systems. Kakimoto *et al.* (2009) discussed control of the ramp rate of a photovoltaic generator by using an electric double-layer capacitor. Svoboda *et al.* (1997) presented a Lagrangean relaxation approach for solving the short-term resource-scheduling problem with ramp constraints. Zheng and Kusiak (2009) applied data-mining algorithms to establish the multivariate time series model for predicting power ramp rate. The prediction of power ramp rate results at 10-min to 60-min intervals was demonstrated in their research. The significance of Power ramp rates in power systems in the presence of wind and solar generation has been recognized in the literature (Peterson and Brammer 1995; Kakimoto *et al.* 2009; Svoboda *et al.* 1997; Zheng and Kusiak 2009). Control of power ramp rates is beneficial to the power dispatching and grid management (Ling *et al.* 1989; Goosen *et al.* 2003; Xuan *et al.* 2005).

The operation of wind turbines for power production is a challenging topic, and several researchers have investigated this topic and published their results in the literature. Boukhezzar and Siguerdidjane (2009) designed a non-linear controller for optimizing the power of the DFIG (Doubly Fed Induction Generator). Abdelli *et al.* (2007) applied a multi-objective genetic algorithm to optimize the efficiency of a small-scale turbine. Wang and Chang (2004) investigated an intelligent power extraction algorithm for improving the performance of wind turbine systems. Munteanu *et al.* (2005) presented a control approach to optimize power production in low and high frequency scenarios. Morimoto *et al.* (2005) researched the maximization of wind-turbine-generated power by controlling the current vector of the interior, permanent-magnet, synchronous generator. Muljadi and Butterfield (2001) addressed operating a variable-speed wind turbine with pitch control to maximize power while minimizing the loads. Physics and parametric-based approaches to turbine modeling involve numerous assumptions that may limit their applicability. In this chapter, a model that maximizes the generated power and minimizes the power ramp rate is presented. Modeling the power generation process of a wind turbine with data-mining algorithms is an essential component of the overall model. The benefits of applying data mining in wind power modeling have been demonstrated in previous studies (Kusiak *et al.* 2010c; Kusiak *et al.* 2010d; Kusiak *et al.* 2009c). In this chapter, we have also addressed the important issue of the constraints used in power generation modeling. In the past, Betz' law (Kusiak *et al.* 2009a) has served as the basis for forming the constraints used in power optimization. A constraint derived from Betz' law is a boundary can never be achieved while regulating the power production of a wind turbine. Thus, a new power optimization constraint was studied in this research. The upper control limit of the control chart used in power monitoring (Kusiak *et al.* 2009e) was integrated with Betz' law to produce a more realistic constraint for power optimization.

The bi-objective optimization model formulated in this research involves a linear combination of weighted objectives, power and power ramp rate, which are maximized and minimized, respectively. This optimization model was developed with data-mining algorithms. A known computational intelligence algorithm, the artificial immune network algorithm (aiNet), was used to solve the formulated model. The value of the model was tested with three scenarios. The first scenario involves power maximization as the only objective. In the second scenario, the power and PRR objectives were treated as equally important. The third scenario focused on PRR minimization as the only objective. The optimization results were compared with the actual wind turbine data to show the improvement of wind turbine performance.

4.2 Modeling Power and PRRs

The analytical model of the power generated by a wind turbine, shown as equation (4.1), has been studied extensively, and the results have been reported in the literature (Boukhezzar *et al.* 2006).

$$P = \frac{1}{2}\rho\pi R^2 C_p(\omega R / v, \beta)v^3 \tag{4.1}$$

where ρ is the air flow density, R is the rotor radius, v is the wind speed measured by an anemometer, C_p (ωR / v, β) is the power coefficient function of the blade pitch angle β and the tip speed ratio expressed as ωR / v. In the tip speed formula, ω is the rotor angular speed.

In this chapter, data collected by Supervisory Control and Data Acquisition (SCADA) systems installed at operating 1.5 MW horizontal axis wind turbines was utilized. The dataset used in this research is split to two sub-sets, a training dataset and a test dataset. The training dataset was used to build a data-driven model, and the test dataset was used to validate the accuracy and robustness of the data-driven model. Table 4.1 characterizes the training dataset and the test dataset.

Table 4.1 Description of training and test datasets

Dataset	Start Time Stamp	End Time Stamp	Number of Observations
Training	10/23/2009 8:00 AM	10/30/2009 5:43 AM	60000 observations
Test	10/30/2009 5:43 AM	10/31/2009 18:00 PM	12301 observations

As shown in Table 4.1, the training dataset contains 60000 points that were collected from 8:00:30 A.M. on 10/23/2009 to 5:43:20 A.M. on 10/30/2009. The test dataset contains 12301 points that were collected from 5:43:30 A.M. on 10/30/2009 to 6:00:00 P.M. on 10/31/2009.

The SCADA system of the turbines considered in this research collects data on more than 120 parameters measured by different sensors. The domain knowledge and previous studies (Kusiak *et al.* 2010c; Kusiak *et al.* 2010d; Kusiak *et al.* 2009c; Boukhezzar *et al.* 2006) point to a subset of parameters related to the power generation. These parameters are listed in Table 4.2, where t is the current time and T is the sampling interval, which was 10 s in our study.

Table 4.2 Parameters selected for power modeling

Parameter	Symbol	Parameter	Symbol
Generated power at time t	P_t	Blade pitch angle at time $t-T$	β_{t-T}
Generated power at time $t-T$	P_{t-T}	Wind speed at time t	v_t
Generator torque at time t	τ_t	Wind speed at time $t-T$	v_{t-T}
Generator torque at time $t-T$	τ_{t-T}	Wind deviation at time t	d_t
Blade pitch angle at time t	β_t	Wind deviation at time $t-T$	d_{t-T}

Based on the parameters in Table 4.2, the data-driven model of power generation process is expressed in (4.2).

$$P_t = f_1(\tau_t, \tau_{t-T}, \beta_t, \beta_{t-T}, v_t, v_{t-T}, d_t, d_{t-T}) \tag{4.2}$$

where $f(\cdot)$ means the model extracted by data-mining algorithms discussed in the following.

Seven data-mining algorithms, Neural Network (NN) (Siegelmann and Sontag 1994; Liu 2001; Smith 1993), Neural Network Ensemble (NNE) (Hansen and Salamon 1990), Support Vector Machine (SVM) (Schölkopf *et al.* 1999; Steinwart and Christmann 2008), Boosting Tree (BT) (Friedman 2001; Friedman 2002), Random Forest (RF) (Breiman 2001), k Nearest Neighbor (kNN) (Shakhnarovish *et al.* 2005), and Classification and Regression Tree (CART) (Breiman *et al.* 1984), were utilized to extract the data-driven models from the training dataset. To develop NN and NNE models, five activation functions, identity, logistic, hyperbolic tangent, exponential, and sine were utilized. To produce high-performance NN or NNE models, 20 neural networks were generated. For the SVM algorithm, the kernel function was used as the Radial Basis Function (RBF). To implement kNN, the value of k was set to 3. Two software tools, Statistica and Weka, were used to train data driven models on a Quad-core processor computer with 4 GB memory. The test dataset was used to examine the accuracy of each data-driven model. A comparative analysis was performed to select the best-performing algorithm to train the data-driven model of power generation. Four metrics, the mean absolute error (MAE), standard deviation of mean absolute error (SD of AE), mean absolute percentage error (MAPE), and the standard deviation of absolute percentage error (SD of APE), were used to evaluate the performance of the data-mining algorithms; they are formulated as (4.3) – (4.6).

$$\text{MAE} = \frac{1}{n}\sum_{i=1}^{n}|\hat{y}_i - y_i| \tag{4.3}$$

$$\text{SDofAE} = \sqrt{\frac{1}{n}\sum_{i=1}^{n}(|\hat{y}_i - y_i| - \frac{1}{n}\sum_{i=1}^{n}|\hat{y}_i - y_i|)^2} \tag{4.4}$$

$$\text{MAPE} = \frac{1}{n}\sum_{i=1}^{n}(|\frac{\hat{y}_i - y_i}{y_i}|)\times 100\% \tag{4.5}$$

$$\text{SDofAPE} = \sqrt{\frac{1}{n}\sum_{i=1}^{n}(|\frac{\hat{y}_i - y_i}{y_i}| - \frac{1}{n}\sum_{i=1}^{n}|\frac{\hat{y}_i - y_i}{y_i}|)^2}\times 100\% \tag{4.6}$$

Table 4.3 shows the test results of the models developed by the seven algorithms. The data-driven model (see Eq.(4.2)) developed by the NNE algorithm provided the best test result among the seven algorithms. (See Table 4.3) Thus, NNE algorithm was selected to develop the data-driven power generation model (see Eq.(4.2)). Figure 4.1 illustrates the results provided by the NNE algorithm for the first 100 test points.

Table 4.3 Test results of seven data-driven models

Algorithm	MAE	SD of AE	MAPE	SD of APE
NNE	5.2040	4.9492	0.0084	0.0194
NN	5.6784	7.2280	0.0093	0.0293
BT	38.6601	39.9745	0.0635	0.2236
RF	205.5020	188.1148	0.2209	0.4707
SVM	27.3313	17.5824	0.0509	0.0639
CART	237.0131	190.9273	0.2347	0.1290
*k*NN	12.6050	14.7446	0.0239	0.1119

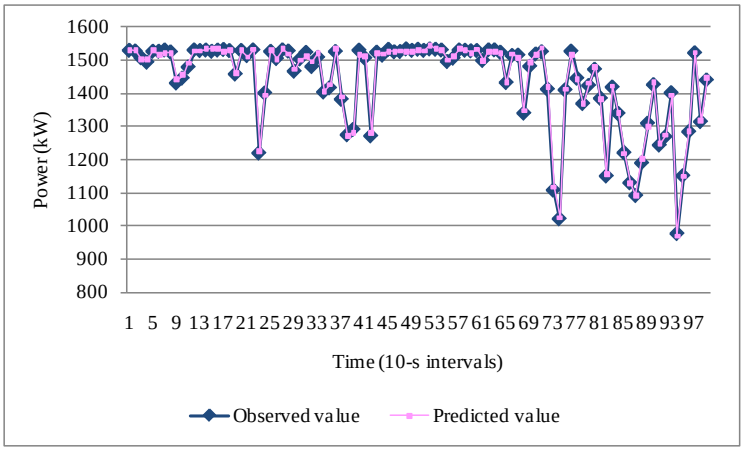

Figure 4.1 Predicted and observed power for the first 100 test points

The power ramp rate (PRR) can be computed from equation (4.7). As the sample time of the data in this study is 10 s, the unit of PRR is kW/10 s.

$$PRR_t = \frac{P_t - P_{t-T}}{T} \tag{4.7}$$

where *PRR* is the power ramp rate; notation for the other parameters can be obtained from Table 4.2.

4.3 Power Generation Constraints

Power optimization must be performed with realistic constraints. In previous publications (Kusiak *et al.* 2009a; Kusiak and Zheng 2010), Betz' law was used to form unrealistic constraints. In the instance addressed in (Kusiak *et al.* 2009a), the boundary calculated by Betz' law for power generated by a wind turbine was $\min\{2.625v^3, 1600\}$. This indicates that the wind turbine could potentially reach its maximum capacity for a wind speed of 10 m/s, which is not the case.

A more effective and feasible constraint for regulating power optimization should be investigated. In this research, the concept of a control chart was used to develop the new constraint for power optimization. A power-monitoring scheme based on the concept of a control chart was studied in (Kusiak *et al.* 2009e). In (Kusiak *et al.* 2009e), principle component analysis (PCA) was used for preprocessing of 10-min data. A nonlinear parametric approach, integrating a logistic function and evolutionary computation, was applied to determine the power curve model. To build control charts, the power curve models were treated as centerlines, and they were used as the basis for establishing the upper and lower control limits. In this research, the upper control limit used to regulate the maximum generated power served as a constraint for power optimization.

In this study, data-mining algorithms rather than the logistic function of (Kusiak *et al.* 2009e) were used to develop the power curve model based on higher frequency, 10-s data. The performance of the power curve models derived by the seven data-mining algorithms of Section 4.2 was tested. The best performing algorithm was selected. The upper control limit of the control chart for monitoring generated power is expressed in (4.8) – (4.10).

$$P_D = f_2(\upsilon) + \mu_r + c(\sigma_r / \sqrt{m}) \tag{4.8}$$

$$\mu_r = [\sum_{i=1}^{n} | \hat{y}_i - y_i |] / n \tag{4.9}$$

$$\sigma_r = \sqrt{[\sum_{i=1}^{n} (| \hat{y}_i - y_i | - \mu_t)^2] / (n-1)} \tag{4.10}$$

where P_D is the maximum power calculated based on the control chart-based boundary, c is the constant to control the sensitivity of the control chart, μ_r is the average of absolute residuals between predicted and observed power based on the training dataset, σ_r is the standard deviation of the absolute residuals, m is the sampling data points in the control chart, $f_2(\cdot)$ is the model trained by data-mining algorithms discussed in Section 4.2, $\hat{y}_i$ is the predicted value of power in the training dataset, y_i is the observed power, and n is the total number of points in the training dataset.

Table 4.4 illustrates the performance of seven data-mining algorithms in fitting the power curve. Since the NN algorithm had the best performance, it was selected to learn the function, $f_2(\cdot)$, which represents the upper control limit of the control chart. Figure 4.2 shows the results of the first 100 test points in predicting power by using wind speed only.

Table 4.4 Test results for data-mining algorithms fitting power curves

Algorithm	MAE	SD of AE	MAPE	SD of APE
NNE	64.1443	70.1687	0.1147	0.5630
NN	64.0627	70.0847	0.1146	0.5606
BT	83.7407	71.5324	0.1451	0.5923
RF	249.0231	201.4617	0.2615	0.4235
SVM	131.9324	94.8365	0.2203	0.5592
CART	240.5598	204.1513	0.2461	0.4342
*k*NN	65.9877	72.3457	0.1164	0.5628

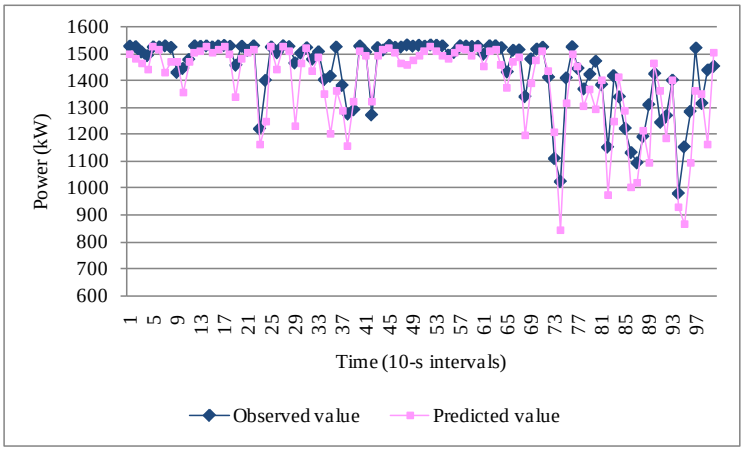

Figure 4.2 The observed power and predicted power based on only wind speed for first 100 test points

Figure 4.3 demonstrates the Betz' law boundary and the control chart-based boundary with the constant, $c = 3$. (The variable c controls the sensitivity of the control chart and in the statistical quality control it is usually set to 3.) In Figure 4.3, the scattered points represent the industrial data, the lowest curve is the power curve fitted by the NN algorithm, the curve in the middle represents the upper control limit of the control chart, and the highest curve depicts the Betz' law boundary. Although the upper control limit makes a more reasonable constraint for power optimization than the Betz' law boundary, it is not entirely satisfactory because it violates the theoretical maximum value of the generated power. This violation occurs when the wind speed is lower than a particular value, the cross point of Betz' law boundary and upper control limit of the control chart. This cross point is not fixed, and it is impacted by the constant, *c*. (See (4.8).) A likely reason that the upper control limit violates the theoretical maximum is the use of erroneous wind speed data (at low wind speeds) that were included from the analysis. Thus, in order to construct a reasonable constraint, the upper control limit of the control chart and the Betz' law boundary must be combined.

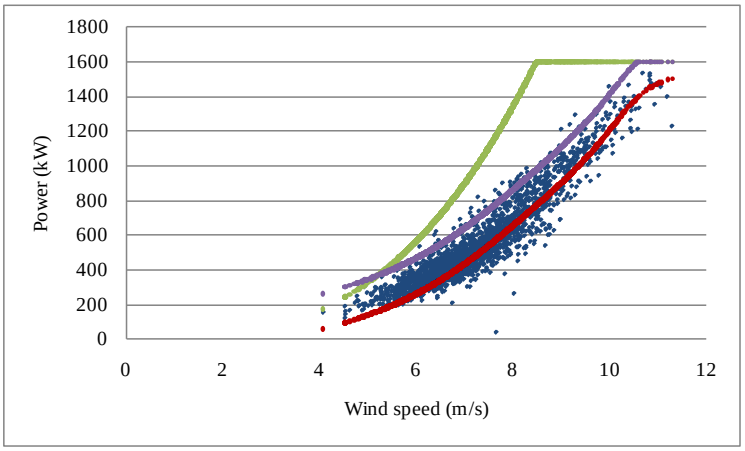

Figure 4.3 Betz' law and the control chart based boundaries

Equations for the combined boundary for power optimization are presented below (4.11):

$$P_c = \begin{cases} \frac{1}{2}\rho\pi R^2 C_p(\cdot)v^3 & \text{if } v < v_o \\ f_2(v) + \mu_r + c(\sigma_r / \sqrt{m}) & \text{if } v > v_o \end{cases} \tag{4.11}$$

where P_c is the maximum power in the combined constraint, and v_o is the wind condition at which the control chart boundary starts to be infeasible and the function to calculate the constraint should switch.

The fact that the maximum amount of power generated by the wind turbine is 1600 kW should also be considered in the new boundary. Then, the new boundary for power optimization is expressed as (4.12):

$$P_t \le \min\{1600, \frac{1}{2}\rho\pi R^2 C_p(\cdot)v^3 I_{[0,v_o)}(v) + [f_2(v) + \mu_r + c(\sigma_r / \sqrt{m})] I_{[v_o,+\infty)}(v)\} \tag{4.12}$$

where $I(\cdot)$ is the indicator function.

The value of v_o is variable. It is impacted by several factors, such as the change of the fitted power curve and the change of c in estimating the upper control limit for the control chart. The most effective way of computing the value of v_o is based on Figure 4.2.

To estimate the exact value of v_o, the power coefficient, $C_p(\cdot)$, is assumed to be constant. It is obvious in (4.13) that the value of v_o can be obtained when the two functions in (4.11), $0.5\rho\pi R^2 C_p(\cdot)v^3$ and $f_2(v)+\mu_r+c(\sigma_r/\sqrt{m})$, are equal. The right side of (4.13) is obtained by substituting μ_r and $c(\sigma_r/\sqrt{m})$ of (4.8) by (4.9) and (4.10).

$$\frac{1}{2}\rho\pi R^2 C_p(\cdot)v_o^{\,3} = f_2(v_o)+[\sum_{i=1}^{n}|\hat{y}_i - y_i|]/n + c(\sqrt{[\sum_{i=1}^{n}(|\hat{y}_i - y_i| - \mu_t)^2]/(n-1)}/\sqrt{m}) \tag{4.13}$$

The two parts in (4.13), $[\sum_{i=1}^{n}|\hat{y}_i - y_i|]/n + c(\sqrt{[\sum_{i=1}^{n}(|\hat{y}_i - y_i| - \mu_t)^2]/(n-1)}/\sqrt{m})$ and $0.5\rho\pi R^2 C_p(\cdot)$, can be considered as two constants. Eq. (4.13) can be simplified and expressed as (4.14):

$$C_1 v_o^{\,3} = f_2(v_o)+C_2 \tag{4.14}$$

where C_1 is equivalent to $0.5\rho\pi R^2 C_p(\cdot)$, and C_2 is $[\sum_{i=1}^{n}|\hat{y}_i - y_i|]/n + c(\sqrt{[\sum_{i=1}^{n}(|\hat{y}_i - y_i| - \mu_t)^2]/(n-1)}/\sqrt{m})$.

Simultaneously, (4.14) can be further re-written as (4.15):

$$C_1 v_o^{\,3} - f_2(v_o) = C_2 \tag{4.15}$$

Next, since the term, $C_1 v_o^{\,3} - f_2(v_o)$, can be replaced as another function of v_o, $f'_2(v_o)$, then the wind speed, v_o, can be estimated based on Eq. (4.16):

$$v_o = f'^{-1}_2(C_2) \tag{4.16}$$

The $f'^{-1}_2(C_2)$ can be specifically addressed when $f_2(\cdot)$ is parametric.

4.4 Modeling Formulation

In the optimization of generated power, two additional constraints must be considered in addition to the constraint for the maximum power. The two constraints are set for limiting the ranges of the generator torque and the blade pitch angle, which are controlled. In the industrial data, the minimum and maximum values of generator torque are 0 and 100, respectively. The minimum blade pitch angle is -0.57°, and the maximum value is 90°. Thus, the two constraints for generator torque and blade pitch angle are formulated in (4.17) and (4.18):

$$\max\{0, \tau_t - 50\} \le \tau_t^* \le \min\{100, \tau_t + 50\} \tag{4.17}$$

$$\max\{-0.57, \beta_t - 10\} \le \beta_t^* \le \min\{90.61, \beta_t + 10\} \tag{4.18}$$

where τ^* means the computed generator torque for wind turbine operation, β^* is the computed blade pitch angle, τ presents the measured generator torque and β is the measured blade pitch angle.

Two objectives were considered in the optimization model. The first objective was to maximize the power generated by the wind turbine. The second objective was to minimize the absolute value of power ramp rate. Since the maximal generated power is 1600 kW, the first objective then can be equivalently translated to minimize the value of difference between 1600 kW and the generated power. To optimize the two objectives simultaneously, a linear combination of the two objectives was utilized by assigning a weight to each objective. Then, the objective function of this bi-objective model can be expressed as (4.19):

$$O = w_1 |1600 - P_t| + w_2 |PRR_t| \tag{4.19}$$

The optimization model in (4.20) includes two objectives, the generated power and power ramp rate (See (4.2) and (4.7).). The model also includes three constraints (See (4.12), (4.17), and (4.18)).

$$\begin{aligned}
&\underset{\tau_t^*, \beta_t^*}{\text{Minimize}} \ O = w_1 |1600 - P_t| + w_2 |PRR_t| \\
&\text{subject to} \\
&P_t = f_1(\tau_t^*, \tau_{t-T}, \beta_t^*, \beta_{t-T}, v_t, v_{t-T}, d_t, d_{t-T}) \\
&PRR_t = \frac{P_t - P_{t-T}}{T} \\
&\max\{-0.57, \beta_t - 10\} \le \beta_t^* \le \min\{90.61, \beta_t + 10\} \\
&\max\{0, \tau_t - 50\} \le \tau_t^* \le \min\{100, \tau_t + 50\} \\
&P_t \le \min\{1600, \frac{1}{2}\rho\pi R^2 C_p(\cdot) v^3 I_{[0, v_o)}(v) + [f_2(v) + \mu_r + c(\sigma_r / \sqrt{m})] I_{[v_o, +\infty)}(v)\}
\end{aligned} \tag{4.20}$$

where c = 3, μ_r = 48, σ_r = 53, m = 1, and the term $0.5\rho\pi R^2 C_p(\cdot) = 2.625$. The values of μ_r and σ_r are calculated based on (4.9) and (4.10), respectively. The estimation procedure of $0.5\rho\pi R^2 C_p(\cdot)$ can be referred to [14].

4.5 Artificial Immune Network Algorithm

The optimization model (4.20) is complex. The model can be solved with a novel computational intelligence scheme, the artificial immune network algorithm (de Castro and Timmis 2002a; b).

The concept of an artificial immune system (AIS) was inspired by the principles and processes of the human immune system. The theory used in AIS mimics the biological functions in the human immune system, and this simulation transforms to a new computational approach that exploits the adaptive and memory mechanisms of the immune system. The AIS was developed in the mid-1980s. Farmer *et al.* (1986) and Bersini *et al.* (1990) were the first researchers to publish their work on immune networks. In the following years, research related to AISs gradually expanded, and various AIS algorithms were developed and applied in different fields. Two versions of the clonal selection principle were derived by de Castro and Von Zuben (2002) and applied to machine learning, pattern recognition, and multi-model optimization. Timmis *et al.* (2000) presented the application of an immune network model of AIS in data analysis. Dasgupta (1998) developed a multi-agent decision support system by examining the recognition and response mechanisms of the immune system. Forrest *et al.* (1993) combined a genetic algorithm and an immune system algorithm to study the pattern recognition process.

Among the various computational algorithms belong to the artificial immune system category, one famous algorithm, the artificial immune network algorithm (aiNet) (de Castro and J. Timmis 2002a; b), was selected to solve the optimization model (4.20). The steps of the aiNet algorithm used in this research are provided below:

Step 1. Population initialization: Randomly generate an initial population of size N of the network antibodies.

Step 2. Clonal expansion: Create a clone of size n for each antibody. The antibodies contained in the clone are the exact copies of their parent antibody.

Step 3. Local search: Search until the stopping criterion, $\overline{f}_i - \overline{f}_{i-1} \le \zeta$, is met.

Step 3.1. Determine the fitness of each parent antibody and normalize the fitness values.

Step 3.2. Mutate each antibody of every clone based on the fitness value of the parent antibody. The equations for antibody mutation can be addressed as $\tau' = \tau + (1/a_1)\exp(-f^*)N(0,1)$ and $\beta' = \beta + (1/a_2)\exp(-f^*)N(0,1)$ where $\overline{f}$ is the average fitness value of a clone, i is the iteration index, ζ is the threshold to determine the convergence of local search, a is the constant to control the decay of the inverse exponential function, f^*means the fitness value of the parent antibody, $N(0,1)$ is a standard normal distribution, and ε determines how many parent antibodies could remain in each iteration.

Step 3.3. Compare the parent antibody and the antibody that has the highest fitness in the clone. If the fitness value of the antibody in the clone is better than the parent antibody's fitness value, replace the parent antibody by this antibody in the clone.

Step 3.4. Compute the average fitness of each clone.

Step 4. Network interactions and suppression: Compare the fitness values of the parent network antibodies and eliminate parent network antibodies whose fitness values are less than the threshold ε.

Step 5. Diversity: Introduce a number of new randomly generated antibodies into the network, which is the parent antibody set.

Step 6. Go back to Step 2 until the number of iterations has been reached.

In the aiNet algorithm, two types of search, i.e., local search and global search, are illustrated to obtain the best solution for the optimization model (4.20). The local search identifies potential solutions around the parent antibody by clonal expansion and antibody mutation. It is controlled by the threshold, ζ , which is the difference between

the average fitness of antibodies in the clone. In the local search, once an antibody in the clone has a fitness value better than the fitness of the corresponding parent antibody, it replaces the parent antibody. The global search allows the aiNet algorithm to determine the best solutions among parent antibodies. The memory mechanism of the aiNet algorithm is handled by the network interactions and the suppression step. In the suppression step, the fitness values of the parent antibodies are examined, and only a portion of the parent antibodies survive and remain in the next iteration.

To implement the aiNet algorithm, values of some parameters must be determined. In this research, ζ is set to 0.05, $a_1 = 2$, $a_2 = 10$, and ε is set to 1.2 times the global fitness value in each iteration. Besides these parameters, the ratio of the size of parent antibodies to the size of the clone antibodies must be determined. An experiment was designed to compare four ratios. Ratio 1 includes 10 parent antibodies and 10 clone antibodies, ratio 2 contains 10 parents and 20 clone antibodies, ratio 3 includes 10 parent antibodies and 30 clone antibodies, and ration 4 includes 10 parent antibodies and 40 clone antibodies. To run this experiment, the weights of the two objectives were both as 0.5, and one observation was selected from the industrial dataset to make the comparison. Table 4.5 shows partial information from the selected observation.

Table 4.5 Information of selected observation

Date	Time	P_t	v_t	…	τ_t	d_t	d_{t-T}
10/30/2009	5:43:40 AM	1528	11.05	…	100.03	-9.8	-1.6

To compare the four ratios, the aiNet algorithm was run for 1500 iterations for one ratio at a time. The results of the experiment are presented in Table 4.6. As shown in Table 4.6, ratio 3 leads to faster convergence of the algorithm than ratios 1 and 2. Although the convergence speeds of ratios 3 and 4 are the same, ratio 3 involved a

smaller clone size than ratio 4. This is indicative of the smaller computational cost of ratio 3. Thus, ratio 3 was selected.

Table 4.6 Selection of the ratio of the parent size to clone size of antibodies

Ratio	Parent/Clone Size	Convergence (No. of Iterations)
1	10P/10C	12
2	10P/20C	10
3	10P/30C	9
4	10P/40C	9

Figure 4.4 demonstrates the convergence of the aiNet algorithm in solving the optimization problem based on the selected observation with ratio 3. In Figure 4.4, the vertical axis presents the standardized global fitness, and the horizontal axis shows the number of iterations. It can be seen that the standardized global fitness gradually drops from the initial iteration and then converges from the ninth iteration.

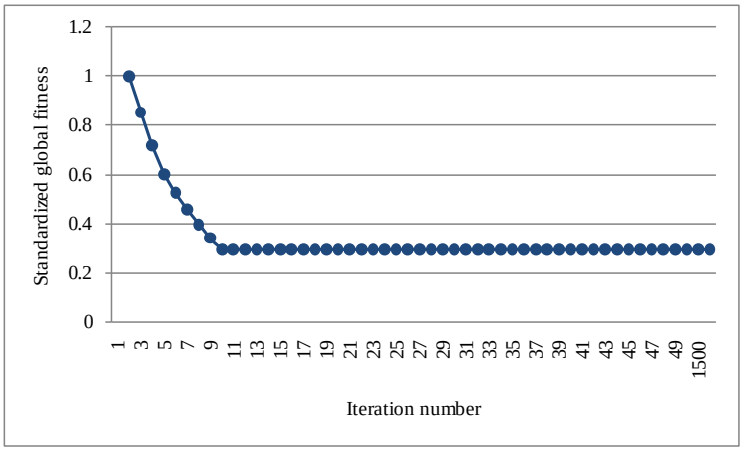

Figure 4.4 Convergence of the aiNet algorithm

Table 4.7 shows the optimization results of the single observation presented in Table 4.5. As illustrated in Table 4.7, the gain of the generated power was 0.2%, and the reduction of power ramp rate was 84% (from 2.1 to 0.33).

Table 4.7 Summary of optimization result
for the selected observation

Solution (τ^*, β^*)	Original Power	Computed Power	Gain	Original PRR	Computed PRR	Gain
99.80,8.36	1528	1530.43	0.002	2.1	0.33	-0.84

4.6 Industrial Case Studies

Three industrial case studies were considered to demonstrate optimization for the generated power and the power ramp rate (PRR). In Case 1, the model maximizes the generated power only, which means $w_1 = 1$ and $w_2 = 0$. In Case 2, the two objectives are treated as being equally important, thus $w_1 = w_2 = 0.5$. In Case 3, the model minimizes PRR only, which means $w_1 = 0$ and $w_2 = 1$. To generate optimization results in the implementation of the continuous optimization, the values of $\tau_{t-\mathrm{T}}$, $\beta_{t-\mathrm{T}}$, and $P_{t-\mathrm{T}}$ at time t are equal to the values of τ_t^*, β_t^*, and P_t computed at time t – T.

To reduce the computational cost of the aiNet algorithm, the number of iterations N (Section 4.5) must be determined. Based on the experiment discussed in Section 4.5, the best ratio of parent size and clone size indicates that the aiNet can converge within 20 iterations. To assure that the aiNet algorithm will converge, a more conservative value of $N = 100$ was selected.

Thirty observations from the test dataset from 6:32:20 A.M. on 10/30/2009 to 6:37:20 A.M. on 10/30/2009 (discussed in Section 4.2) are used in Section 4.6.

4.6.1 Case 1 Results

In Case 1, by assigning $w_1 = 1$ and $w_2 = 0$, the bi-objective optimization model reduces to a single-objective, power optimization model. This case demonstrates that the power generation efficiency can be further improved with improved control of the generator torque and blade pitch angle. Figures 4.5 – 4.8 present the computed and original (measured) values of power, PRR, generator torque, and blade pitch angle, respectively. In the four figures, the horizontal axis represents the time in 10-s intervals, and the vertical axis shows the value of the parameter of interest. Figure 4.5 illustrates improvements in power generation. Generally, the computed power values are larger than the original power value. (See Figure 4.5) To achieve this power gain, the generator torque and the blade pitch angle must vary as indicated in Figures 4.7 and 4.8. The chart in Figure 4.6 indicates that the PRR increases when the wind turbine is controlled to optimize only the generated power.

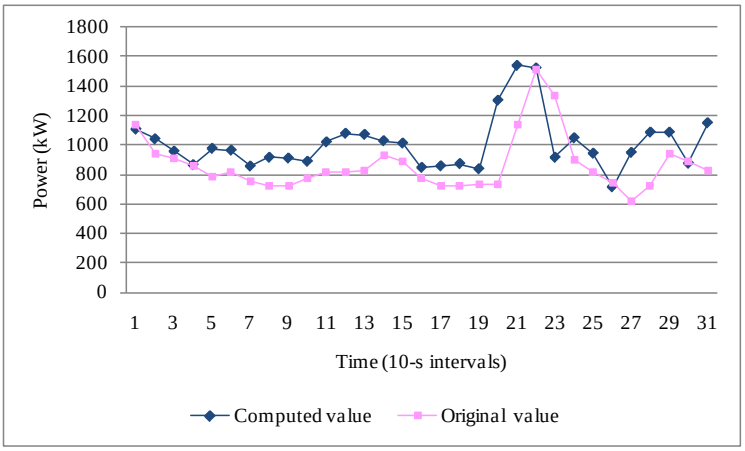

Figure 4.5 Computed and original value of the power in Case 1

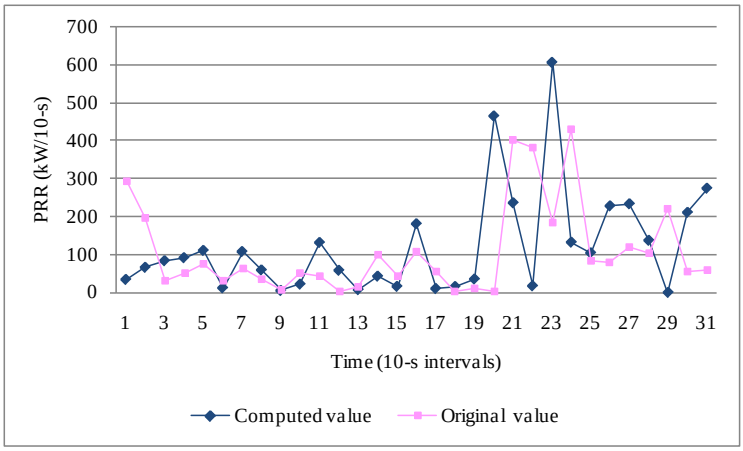

Figure 4.6 Computed and original value of the PRR in Case 1

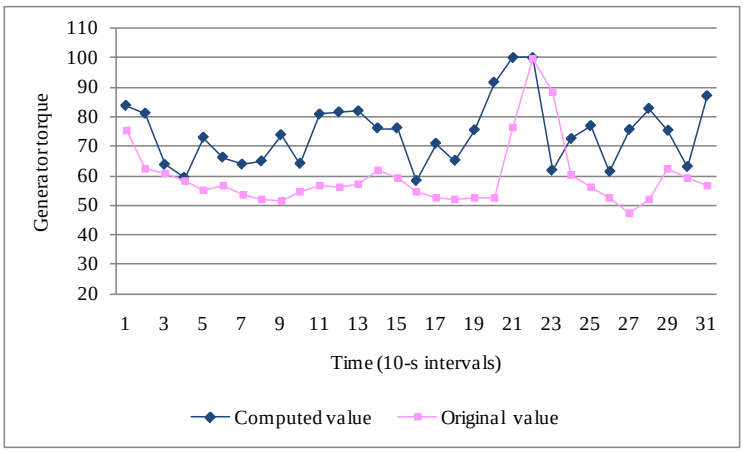

Figure 4.7 Computed and original value of the generator torque in Case 1

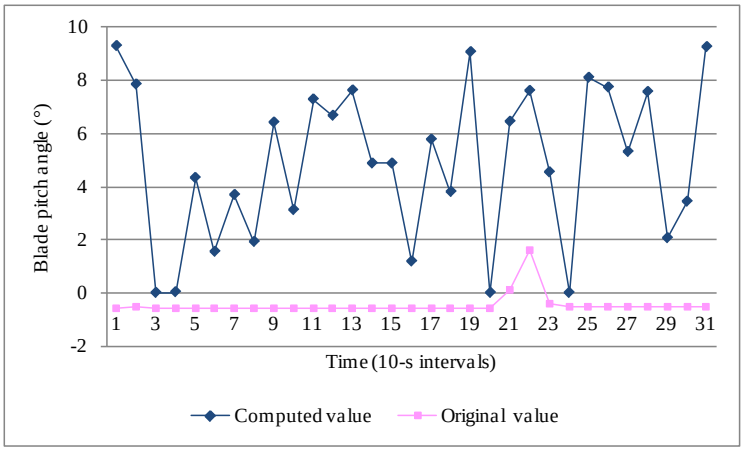

Figure 4.8 Computed and original value of the blade pitch angle in Case 1

4.6.2 Case 2 Results

In Case 2, the optimization model with $w_1 = w_2 = 0.5$ demonstrated a scenario in which power maximization and PRR minimization are considered to be equally important. Figures 4.9– 4.12 present the computed and original (measured) values of power, PRR, and the corresponding settings of the generator torque and the blade pitch angle. For the computed settings of generator torque and blade pitch angle, the gain in the generated power is shown in Figure 4.9. Although the computed and original (measured) values of PRR cannot be easily compared visually based on Figure 4.10, the summary of results in Table 4.8 indicates a reduction of PRR. To achieve the wind turbine performance shown in Figures 4.9 and 4.10, the generator torque of wind turbine and the blade pitch angle must be updated, as shown in Figure 4.11 and 4.12.

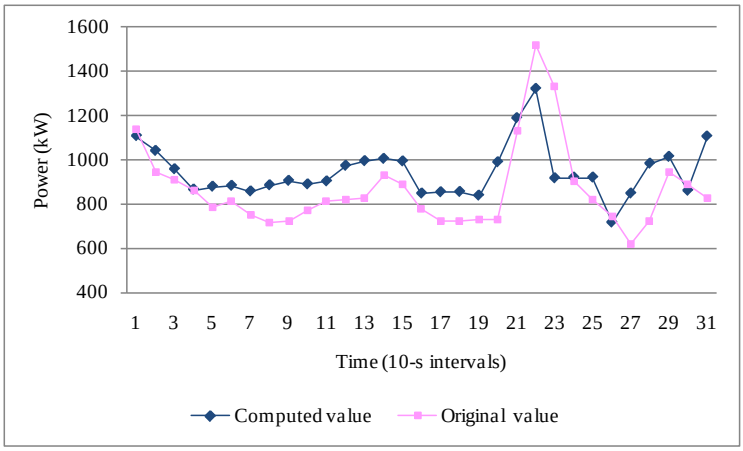

Figure 4.9 Computed and original values of the power in Case 2

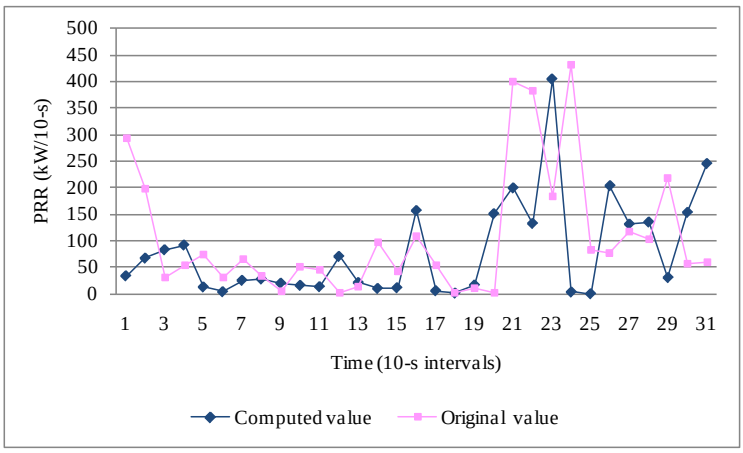

Figure 4.10 Computed and original values of the PRR in Case 2

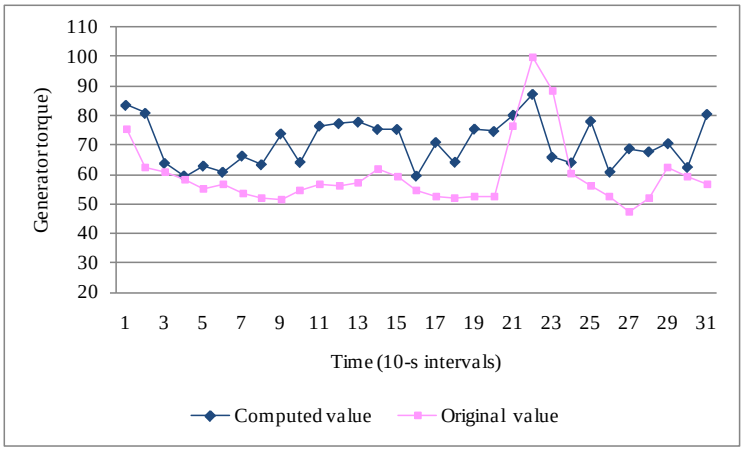

Figure 4.11 Computed and original values of the generator torque in Case 2

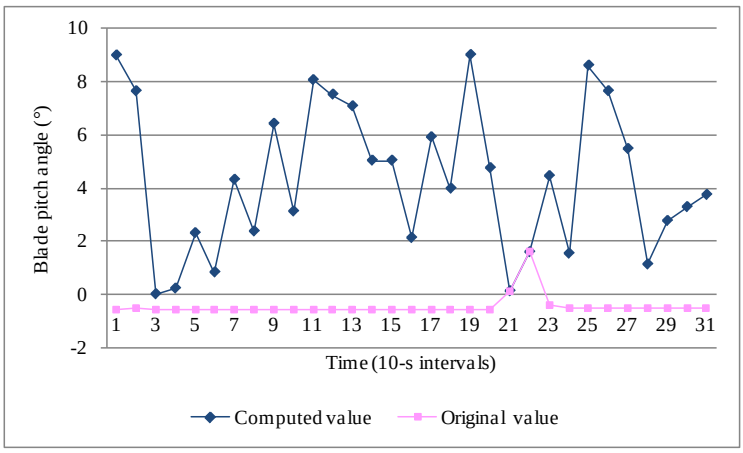

Figure 4.12 Computed and original values of the blade pitch angle in Case 2

4.6.3 Case 3 Results

In Case 3, minimization of PRR with the weight value $w_1 = 0$ and $w_2 = 1$ was considered, i.e., PRR was minimized without considering the actual power generated. Figure 4.13 illustrates the computed and original (measured) power values. The computed power curve is smoother than the original power curve. Figure 4.14, which compares the computed and the original (measured) values of the power ramp rate (PRR),

shows that PRR was reduced significantly. Figures 4.15 and 4.16 demonstrate the computed and original settings of generator torque and blade pitch angle.

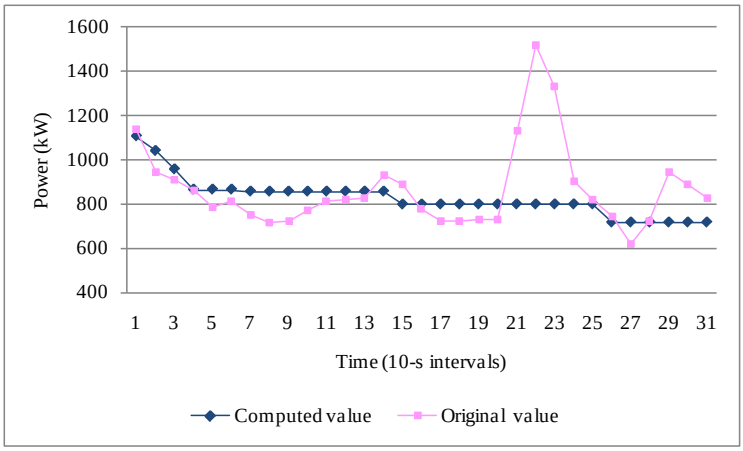

Figure 4.13 Computed and original values of the power in Case 3

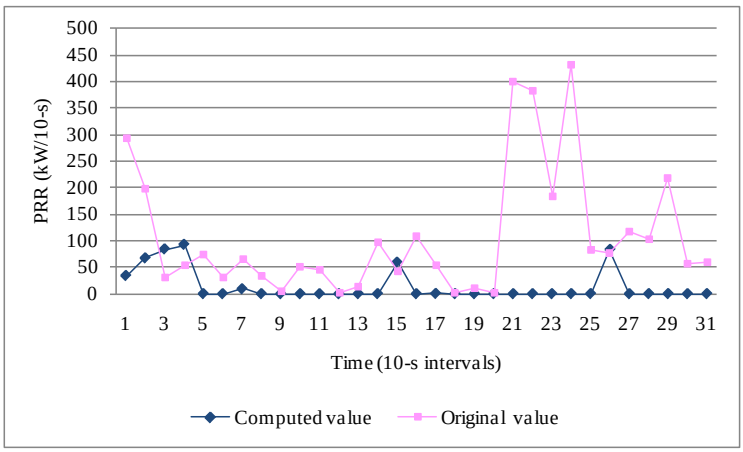

Figure 4.14 Computed and original values of the PRR in Case 3

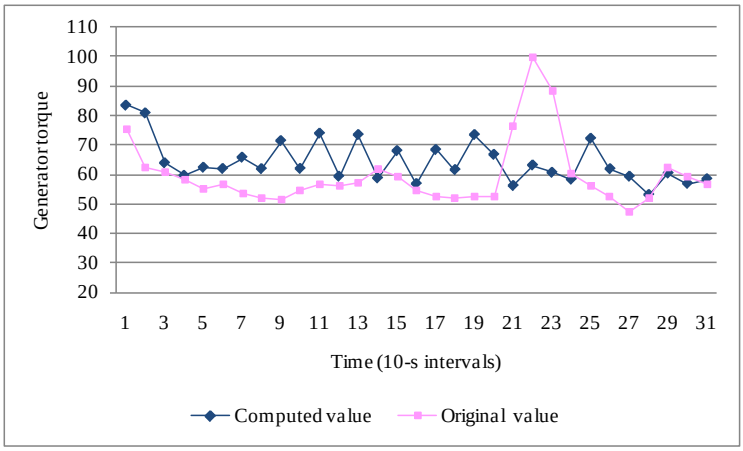

Figure 4.15 Computed and original values of the generator torque in Case 3

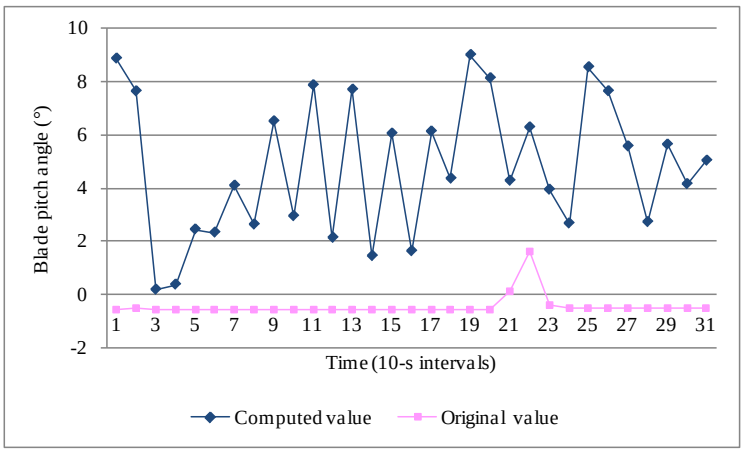

Figure 4.16 Computed and original value of the blade pitch angle in Case 3

4.6.4 Summary of Optimization Results

In this section, the results produced by continuous optimization for the three cases are summarized. (See Table 4.8) The first column of Table 4.8 shows the parameters used to compare wind turbine performance before and after optimization. Other columns show the values of parameters for the three different cases. The results for Case 1 show an improvement in power generation (The power gain is around 16%). This power gain comes at the cost PRR, which increased by almost 13%. In Case 2, the gain in generated

power is about 9% and PRR was reduced by about 25%. In Case 3, the PRR value decreased from 107 kW/10 s to 14 kW/10 s, a significant reduction of approximately 87%. To achieve smooth operation of the power train, the generated power was reduced by almost 5%.

Table 4.8 Summary of continuous optimization

Parameter	Case 1 ($w_1 = 1$, $w_2 = 0$)	Case 2 ($w_1 = 0.5$, $w_2 = 0.5$)	Case 3 ($w_1 = 0$, $w_2 = 1$)
Computed mean power (kW)	1006.59	943.86	825.26
Original mean power (kW)	865.37	865.37	865.37
Power Gain (%)	16.32%	9.07%	-4.63%
Computed mean PRR (kW/10-s)	120.59	80.06	13.86
Original mean PRR (kW/10-s)	107.07	107.07	107.07
PRR Reduction (%)	-12.63%	25.23%	87.06%

4.7 Sensitivity Analysis in the Presence of Constraints

The optimization results discussed in Section 4.6 are produced based on model (4.20) constrained by the power optimization boundary (see (4.12)) with the value c arbitrarily fixed at 3. In this section, the optimization model (4.20) with the shifting power optimization boundary is considered. The boundary is shifted by assigning setting the value of c to 4, 5, and 6. As discussed in Section 4.3, the power optimization boundary is composed of two parts, the Betz' law constraint and the upper control limit of the control chart (see (4.12)). In this study, only the upper control limit part of the power optimization boundary will be shifted as the Betz' law constraint implies the theoretical maximum and it cannot be moved. Figure 4.17 illustrates different power optimization boundaries, where, UCL1 is the power optimization boundary with $c = 3$. UCL2 to UCL4 represent the power optimization boundaries for $c = 4$, 5, and 6.

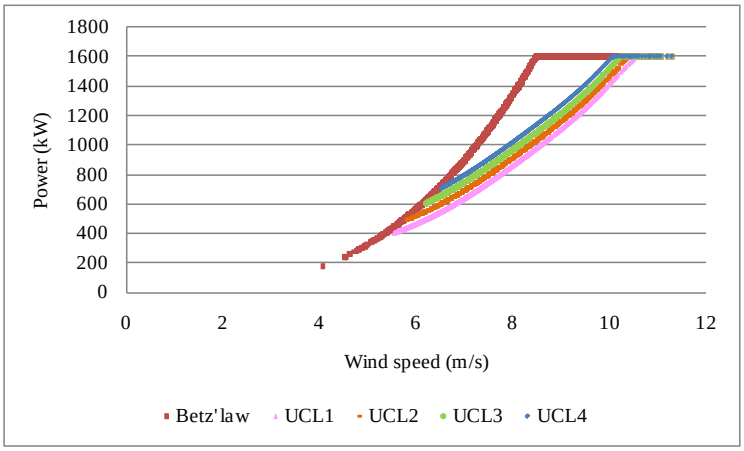

Figure 4.17 Five power optimization boundaries

The value of parameter v_0 in (4.12) change with parameter c. For example, when c increases to 4, v_0 becomes 5.8 m/s. Table 4.9 provides the computed power and PRR optimization results different values of parameter c obtained for three different cases (same as in Section 4.6) by solving model (4.20). As shown in Table 4.9, the wind turbine performance improves as the value of c increases from 3 to 4 and 5. Both the power gain and PRR are improved. This is due to fact that the power boundary allows more room for optimization. However, these improvements are not monotonically increasing. For c = 6, the computed PRR in Case 2 is 78 kW/10-s, i.e., it is larger than the computed PRR (69 kW/10-s) with c = 5 in the same case (Table 4.9). This indicates the limit for improvement of both the power gain and the PRR. Power gain can be accomplished at the cost of increased PRR.

Table 4.9 Summary of sensitivity analysis

Parameter	Case 1 (w_1=1, w_2=0)	Gain	Case 2 (w_1=0.5, w_2=0.5)	Gain	Case 3 (w_1=0, w_2=1)	Gain
Computed Power (c=4)	1023.18	0.18	984.56	0.14	870.59	0.01
Computed PRR (c=4)	129.94	0.21	82.25	-0.23	19.42	-0.82
Computed Power (c=5)	1075.15	0.24	1012.16	0.17	928.96	0.07
Computed PRR (c=5)	113.39	0.06	69.34	-0.35	10.55	-0.90
Computed Power (c=6)	1126.14	0.30	1067.01	0.23	975.29	0.13
Computed PRR (c=6)	111.52	0.04	78.43	-0.27	8.81	-0.92

4.8 Summary

In this chapter, an optimization model for maximizing the generated power and minimizing the power ramp rate of a wind turbine was developed. The function deriving the power generation process of a wind turbine was identified with data-mining algorithms. A new constraint used to regulate the maximum generated power was developed based on the Betz' law and process control. Data-mining algorithms derived the centerline function describing the power curve that was applied to build a control chart. The bi-objective function was transformed in a single objective model by assigning weights to the objectives. The optimization model was established by integrating the objective function and constraints.

An artificial immune network algorithm was applied to solve the challenging optimization model. Two types of search techniques, local and global search, were included in the network algorithm. Local search was applied to obtain the best solution among the antibodies contained in the clone of each parent antibody. In the global search the parent antibodies were compared and the best one was selected. The convergence of local search was controlled by the change of average fitness of the clone. The stopping

criterion of the algorithm was the number of iterations. To improve performance of the artificial immune network algorithm, an experiment was conducted to select the best combination of the parent antibody and the clone antibody size. This is similar to the elite set concept of evolutionary computation. In this way, the artificial immune system algorithm was able to eliminate some dominated solutions (parent antibodies) and introduce new parent antibodies to the antibodies network (parent population).

Industrial data was used to demonstrate performance of the optimization model in three scenarios. The model generated power and the power ramp rate (PRR) were compared to their measured values. The computed set point values of the generator torque and the blade pitch angle have increased the power and reduced the PRR. The model allows for considering other optimization scenarios where greater gains in one objective could be accomplished at the expense of the other one.

In wind farm operated turbines, control objectives may vary due to factors such as, grid requirement, wind conditions, and wind turbine maintenance policies. Such industrial requirements can be easily accommodated by the model by dynamic modification of the weights attached to the control objectives.

CAPTER 5

SCHEDULING A WIND FARM

5.1 Introduction

This chapter presents a model for scheduling wind turbines of a wind farm. A particle swarm optimization algorithm with a small world network structure is introduced for solving this model. The solution generated by the algorithm defines operational status of wind turbines for a scheduling horizon selected by a decision maker. Different operational scenarios are constructed based on time series data of electricity price, grid demand, and wind speed. The computational results provide insights into management of wind farm.

5.2 Model for Scheduling Wind Turbines

A model for wind turbine scheduling is developed. The model minimizes the cost function defined in the next section subject to various constraints.

5.2.1 Objective Function

Quantifying the total cost of running a wind farm is complex and wind industry does not have a widely accepted standard. In this study, the cost of running a wind farm is simply depicted as three major components: power shortage cost, wind turbine operations and maintenance cost, and wind turbine start-up cost.

Power shortage occurs when the supply of power from a wind farm does not meet the grid demand as expressed in (5.1):

$$\Delta P_t = \max\{0, D_t - \sum_{i=1}^{I} P_{i,t} s_{i,t}\} \tag{5.1}$$

In (5.1), ΔP_t, is always nonnegative because power shortage only occurs when the grid demand is greater than the energy generated by all turbines.

The power shortage cost can be further categorized into the opportunity cost of power shortage (Definition 5.1) and the compensation cost (Definition 5.2).

Definition 5.1. *Once power shortage occurs, the opportunity cost equals the benefits of selling the amount equivalent to the power shortage, i.e., the product of the electricity price and the power shortage at a given time window.*

The total opportunity cost of power shortage over the scheduling time horizon is expressed in (5.2).

$$C_{ps} = \sum_{t=1}^{T} B_t \Delta P_t \tag{5.2}$$

Definition 5.2. *The compensation cost is the penalty paid to compensate for the amount of power shortage.*

The wind farm can compensate the power shortage by activating an alternative power generation resource or purchasing power from other utilities. The total compensation is expressed in (5.3).

$$C_{pc} = \sum_{t=1}^{T} p_t \Delta P_t \tag{5.3}$$

where p_t is the penalty cost per power unit.

The operations and maintenance (O&M) cost of all wind turbines in a farm is formulated in (5.4):

$$C_{om} = \sum_{t=1}^{T} \sum_{i=1}^{I} c P_{i,t} s_{i,t} \tag{5.4}$$

where c is the cost in generating a unit of power.

The O&M cost is then determined as a function of the generated power and on/off decision variable.

The last major component is the start-up cost of wind turbines. The start-up cost refers to the energy consumed by wind turbines during the start-up process. Activating a wind turbine requires a certain amount of electricity from the grid as stated in (5.5).

$$C_{start} = \sum_{t=1}^{T}\sum_{i=1}^{I} B_t K_{i,t} s_{i,t}(1 - s_{i,t-1}) \tag{5.5}$$

By considering (5.2) – (5.5), the total operating cost of a wind farm is expressed in (5.6).

$$TC = \sum_{t=1}^{T} B_t \Delta P_t + \sum_{t=1}^{T} p_t \Delta P_t + \sum_{t=1}^{T}\sum_{i=1}^{I} cP_{i,t} s_{i,t} + \sum_{t=1}^{T}\sum_{i=1}^{I} B_t K_{i,t} s_{i,t}(1 - s_{i,t}) \tag{5.6}$$

It is obvious that the first two components of the total cost are not considered when the grid demand is met (i.e., $\Delta P_t = 0$). However, satisfying the grid demand increases both the O&M and the start-up costs. To minimize *TC* in (5.6) it is necessary to turn off some wind turbines once the grid demand is met. The goal is to turn on the minimum number of wind turbines meeting the grid demand.

5.2.2 Constraints

The scheduling model built in this chapter calls for constraints. A wind turbine operates, if and only if, the wind speed is between the specified cut-in and cut-out wind speed. Therefore, the wind speed condition in (5.7) is needed.

$$v_{ci} < v_t < v_{co} \tag{5.7}$$

Another constraint is related to the performance of wind turbines expressed by power curves. A power curve describes a mapping between wind speeds and wind energy produced by a wind turbine. Various functions have been investigated in the literature to model power curves. Boukhezzar *et al.* (2009) developed a power-curve function to design a non-linear controller for optimizing the power of the DFIG (Doubly Fed Induction Generator). The power curve was simply expressed as a product of a constant, a power coefficient function, and wind speed cube. Ustüntas and Sahin (2008) investigated a new approach, cluster center fuzzy logic, to model the power curve of a wind turbine. Kusiak *et al.* (2009d) utilized the logistic function to model the power curve in and developed a wind turbine monitoring method.

In this study, a power curve modeled with the logistic function presented in Kusiak *et al.* (2009d) is employed (see (5.8)).

$$P_{i,t} = f_i(v_t, \theta_i) = \theta_{1,i} \frac{1+\theta_{2,i} e^{-v_t/\theta_{4,i}}}{1+\theta_{3,i} e^{-v_t/\theta_{4,i}}},\ \theta_i = (\theta_{1,i}, \theta_{2,i}, \theta_{3,i}, \theta_{4,i}) \tag{5.8}$$

The expression (5.8) can be transformed into (5.9) by considering the cut-in and cut-out wind speeds.

$$P_{i,t} = f_i(v_t, \theta_i) = \theta_{1,i} \frac{1+\theta_{2,i} e^{-v_t/\theta_{4,i}}}{1+\theta_{3,i} e^{-v_t/\theta_{4,i}}} I_{(v_{ci}, v_{co})}(v_t), \theta_i = (\theta_{1,i}, \theta_{2,i}, \theta_{3,i}, \theta_{4,i}) \tag{5.9}$$

As the generated power cannot exceed the maximum capacity of a wind turbine, the power generation constraint is expressed in (5.10).

$$P_{i,t} \le P_C \tag{5.10}$$

5.2.3 Scheduling Model Formulation

The objective function and constraints discussed in Section 5.2.1 and 5.2.2 lead to the wind farm scheduling model in (5.11).

$$\begin{aligned} &\text{Min } TC \\ &\text{subject to} \\ &P_{i,t} \le P_C \\ &s_{i,t} \in \{0,1\} \end{aligned} \tag{5.11}$$

The solution of the model (5.11) is a schedule represented by variable $s_{i,t}$.

The model expressed in (5.11) is generic. It can be extended by incorporating different objectives and additional constraints, such as curtailment of wind power and maintenance activities.

5.3 Particle Swarm Small World Optimization Algorithm

Solving model (5.11) is challenging as the number of decision variables $s_{i,t}$ increases with the number of wind turbines and the length of scheduling horizon. For example, assume the scheduling horizon is 24 h, the number of binary decision variables

increases from 240 to 480 when the number of wind turbines increases from 10 to 20. Similarly, assume the number of wind turbines is 10, the number of binary decision variables changes from 240 to 480 if the scheduling horizon is extended from 24 h to 48 h. A Particle Swarm Small World Optimization (PSSWO) is applied to solve model (11) due to its complexity.

The PSSWO algorithm is inspired by two streams of research: Particle Swarm Optimization (PSO) discussed in Kennedy and Eberhart (1995) and Small World Theory reported in Milgram (1967).

The development of PSO was simulated by the social behavior of bird flocks and fish schools. The survey paper by AlRashidi and El-Hawary (2009) addressed eight advantages of PSO that are summarized as follows:

1) Ease of implementation: Less tuned parameters, simple logic operations in search and derivative free property.
2) Ability of escaping local optima: The stochastic nature of the search function, low sensitivity to the form of an objective function, and slight dependence on population initialization.
3) Compatibility: Ease of integration with other algorithms.

The PSO algorithm has been widely applied. Park *et al.* (2005) applied PSO to solve economic dispatch problem with a non-smooth cost function. Park *et al.* (2008) improved PSO algorithm to handle more complex economic dispatch problems with non-convex cost functions. Kusiak and Zhang (2011) developed an adaptive PSO by integrating fuzzy logic to optimize performance of wind turbine systems. Kusiak and Li (2010) applied a modified PSO algorithm to optimize a heating, ventilating and air conditioning system. Seo *et al.* (2006) studied PSO in electromagnetic applications.

Although the original PSO algorithm has performed well in many applications, a drawback is that its search trajectory is uncontrollable (de Castro, 2002; Lee and Park, 2006; Saxena and Vora, 2008). This drawback can be handled by balancing the

exploration and exploitation in the PSO algorithm. Numerous techniques have been developed to improve performance of PSO. Clerc and Kennedy (2001) studied convergence and the search trajectories of PSO. The ability of PSO to find an optimal solution was improved by controlling particle's velocities. Liu *et al.* (2007) combined PSO with the memetic algorithm to enhance its performance. Ratnaweera *et al.* (2004) presented a study of improving PSO by controlling local search and convergence to global optima. To control the local search and convergence, a mutation operator and re-initialization of particles' velocities were added to PSO.

In this research, PSO is integrated with the small world theory to balance the exploration and exploitation. Although the original small world experiment conducted by Milgram (1967) aimed at examining the mean length of path between two unknown people in a social network, the research was then extended. March (1991) applied it to organizational learning and discussed the myopia of learning. Watts and Strogatz (1998) studied the collective dynamics of small world networks based on various structures of networks. Fang *et al.* (2010) argued that the semi-isolated subgroups may help the balance of exploration and exploitation, and the simulation results supported the argument. This semi-isolated network structure then was utilized in the proposed PSSWO to assist the balance of exploration and exploitation in search.

In the PSSWO algorithm discussed in this chapter, particles are organized into semi-isolated, equal-size groups. Each group in the swarm presents a tribe. In each tribe, the best position of particles is treated as the tribe's best.

Definition 5.3. *Assume* x_{hm} *presents a particle in a tribe and* $\hat{g}_m$ *presents the tribe's best, the* $\hat{g}_m$ *equals to* x_{hm}*, if* $f(x_{hm}) \leq f(\hat{g}_m)$ *and* $f(x_{hm})$ *attain minimum in the tribe.*

The network structure can vary with the level of connections between groups. Tribes without connections to others are isolated subgroups. The semi-isolated structure is a network structure that individuals in the network are highly clustered while there are

some connections between the groups. The network becomes a random network, if individuals in the network are randomly connected to others.

Figure 1 illustrates the semi-isolated structure of PSSWO algorithm. The network structure is established through the communication between tribes. After each flight, a random size of particles in a tribe is selected to communicate with one of the other tribe's bests. **Definition 5.4** is concerned with the communication process.

Definition 5.4. *Assume S_m presents the set of randomly selected particles in a tribe and $\hat{g}_q$ presents another tribe's best. If $f(\hat{g}_q) \le f(x_{hm})$ and $x_{hm} \in S_m$, the local best of x_{hm} will be updated by* (5.12).

$$\hat{x}_{hm} = \alpha \hat{x}_{hm} + (1-\alpha)\hat{g}_q \tag{5.12}$$

where $\alpha \sim$ U[0,1] and the size of S_m is determined by the product of a random number $\rho \sim$ U[0,1] and the size of tribe m. Both α and ρ impact the semi-isolated network structure.

Assume the number of tribes in a swarm is N_t, the number of particles in each tribe is N_p, j represents the index of iterations for implementing PSSWO algorithm and ψ is the dimension of search space, then the PSSWO algorithm is expressed next (see also Fig. 5.1).

Step 1. Initialize N_t tribes of particles, N_p particles for each tribe, the position of each particle, $x_{hm}^j \in R^\psi$, and the associated velocity, $v_{hm}^j \in R^\psi$, where, h = 1,2,…,N_p, m = 1,2,…,N_t and j = 0.

Step 2. Initialize the local best $\hat{x}_{hm}^j$ for each particle by $\hat{x}_{hm}^j \leftarrow x_{hm}^j$ in each tribe, and estimate the initial tribe's best $\hat{g}_m^j$ by $\hat{g}_m^j \leftarrow \arg\min(f(x_{hm}^j))$, where h = 1,2,…,N_p and j = 0.

Step 3. Repeat until the stopping criterion is satisfied

For each tribe $1 \le m \le N_t$ and for each particle $1 \le h \le N_p$

Step 3.1. Create random vectors r_1^j and $r_2^j \in R^\psi$ where $r_1^j, r_2^j \sim U[0,1]$.

Step 3.2. Update the velocities of particles by $v_{hm}^{j} \leftarrow \omega v_{hm}^{j} + c_1 r_1^{j}(\hat{x}_{hm}^{j} - x_{hm}^{j}) + c_2 r_2^{j}(\hat{g}_{m}^{j} - x_{hm}^{j})$ and update the particle positions by $x_{hm}^{j} \leftarrow x_{hm}^{j} + v_{hm}^{j}$.

Step 3.3. Update the local best by $\hat{x}_{hm}^{j} \leftarrow x_{hm}^{j}$ if $f(x_{hm}^{j}) \le f(\hat{x}_{hm}^{j})$.

Step 3.4. Update the tribe's best by $\hat{g}_{m}^{j} \leftarrow x_{hm}^{j}$ if $f(x_{hm}^{j}) \le f(\hat{g}_{m}^{j})$.

Step 3.5. Determine the value of ρ by $\rho \sim U[0,1]$

Step 3.6. Communication: Assume S_m presents a set of selected particles from each tribe, then $\hat{x}_{hm}^{j} \leftarrow \alpha \hat{x}_{hm}^{j} + (1-\alpha)\hat{g}_{q}^{j}$, $x_{hm}^{j} \in S_m$ if $f(\hat{g}_{q}^{j}) \le f(x_{hm}^{j})$, $q \neq m$.

Step 3.7. Update the global best by $g_{b}^{j} \leftarrow \hat{g}_{m}^{j}$ if $f(\hat{g}_{m}^{j})$ has the lowest value

Step 4. Terminate the algorithm when the stopping criterion (number of iterations in this chapter) is satisfied.

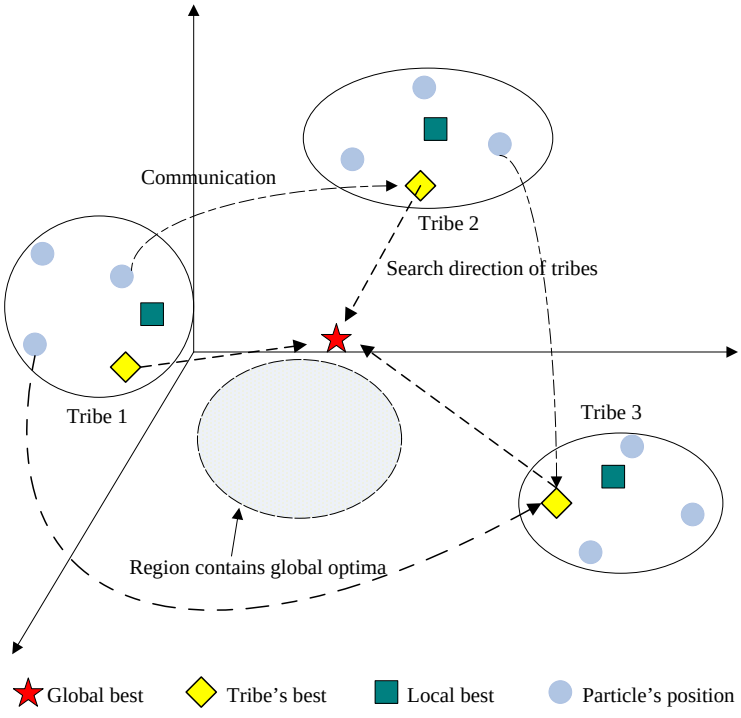

Figure 5.1 Structure of the PSSWO algorithm

To implement the PSSWO, some parameters need to be determined. Based on Shi and Eberhart (1998), the inertia weight ω is set to 0.5 because their experiments have shown that the inertia weight less than 0.8 improved convergence. The c_1 and c_2 are both set to 2 as suggested by Shi and Eberhart (1998).

5.4 Description of Simulation Experiments

In this section, two simulation experiments, Experiment 1 and Experiment 2, are conducted to investigate the wind farm scheduling model in different operating scenarios.

5.4.1 Scheduling Model Formulation

In this chapter, the wind turbine schedules are determined using eight scenarios constructed based on three parameters: wind speed, electricity price, and grid demand (see Table 5.1). These three parameters are categorized into two levels, high and low.

Table 5.1 Scheduling scenarios

Scenario No.	Description
Scenario 1	High electricity price, High grid demand, High wind speed
Scenario 2	High electricity price, High grid demand, Low wind speed
Scenario 3	High electricity price, Low grid demand, High wind speed
Scenario 4	High electricity price, Low grid demand, Low wind speed
Scenario 5	Low electricity price, High grid demand, High wind speed
Scenario 6	Low electricity price, High grid demand, Low wind speed
Scenario 7	Low electricity price, Low grid demand, High wind speed
Scenario 8	Low electricity price, Low grid demand, Low wind speed

In this research hourly average wind speed data of a wind farm is used. Weibull distribution is employed to simulate the 24 h wind speed for scheduling. Table 5.2 presents the five combinations of scale and shape parameters of the Weibull distribution used to describe wind speeds in five different areas in Taiwan (Yeh and Wang, 2008).

Table 5.2 Scale and shape parameters of the Weibull distribution

Combination	**Scale (λ)**	**Shape (k)**
Combination 1	11.01	1.96
Combination 2	10.66	1.92
Combination 3	11.91	1.77
Combination 4	11.09	1.61
Combination 5	10.42	2.05

In this study, the scale and shape parameters of Weibull distribution in Combination 4 is selected to generate wind speed data. Two sets of wind speed data are then generated based on Weibull distribution. Then, before categorization, two sets of generated wind speed data need to be examined to make sure they are significantly different. Categorizing two data sets that were almost identical would be meaningless.

A *t*-test is utilized to determine whether two data sets are significantly different. Table 5.3 illustrates the mean and standard deviation of two data sets. It is obvious that the mean of data set 1 and mean of data set 2 are not equal (*t*-test also confirms this difference). This indicates that the two sets of data are different. Figure 5.2 shows the run-chart of data set 1 and data set 2. Next, based on Table 5.3, we can conclude that data set 1 of wind speed data presents a high wind speed condition and data set 2 describes a low wind speed condition.

Table 5.3 Summary of two sets of wind speed data

Data Set	**No. of Data Points**	**Mean (m/h)**	**St. Dev.**
Data set 1	24	10.85	6.13
Data set 2	24	7.25	5.22

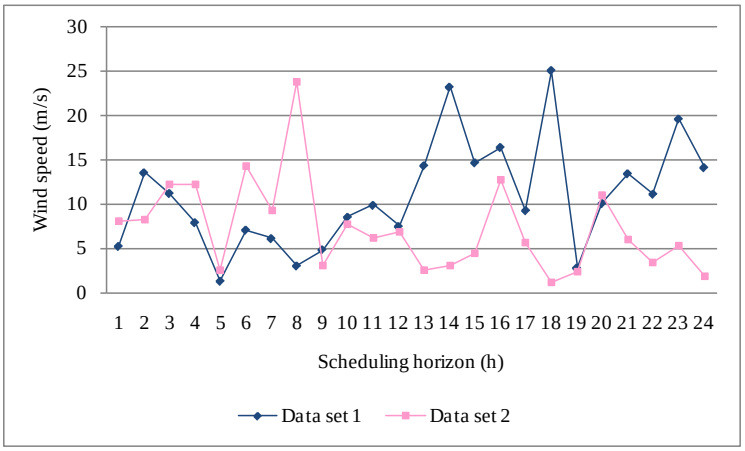

Figure 5.2 Two sets of wind speed data

The website of European Energy Exchange (EEX) offers real-time European Electricity Index (ELIX) describes the hourly electricity price. Two sets of ELIX data are collected to represent different conditions of electricity price for wind farm scheduling. The data set 1 contains hourly ELIX data on October 29th 2010 and the data set 2 includes the hourly ELIX data on October 31st 2010. Table 5.4 summarizes these two data sets. The *t*-test is utilized here to evaluate the difference between the means of two data sets.

Figure 5.3 shows the electricity price of data set 1 and 2.

Table 5.4 Summary of two sets of electricity price data

Data set	**No. of Data Points**	**Mean (Eur/MWh)**	**St. Dev.**
Data set 1	24	52.8	10.1
Data set 2	24	43.46	6.94

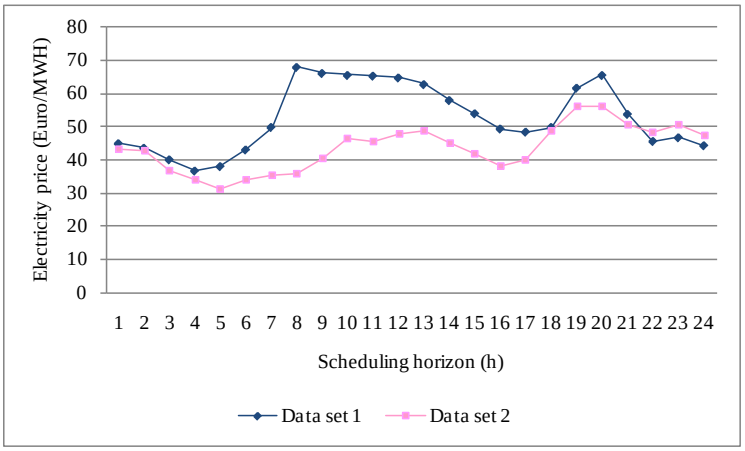

Figure 5.3 Two sets of electricity price data

The hourly grid demand data are derived based on national grid demand data from the website of National Grid. The website offers data of electricity demand in United Kingdom (UK) at 30 min intervals. Then 30-minute demand data are transformed into to the hourly demand. In this chapter, the wind farm is assumed to satisfy 1/3000 of national grid demand. Data set 1 is the demand data on July 1st 2010 and data set 2 is the demand data on July 3rd 2010. Table 5.5 shows the summary of two sets. The *t*-test is applied to determine if there two demand data sets are different.

The means of two samples are significantly different. Based on the summary in Table 5.5, data average demand for data set 1 is higher than that of data set 2. Figure 5.4 depicts the two sets.

Table 5.5 Summary of two sets of grid demand data

Data Set	**No. of Data Points**	**Mean (MW)**	**St. Dev.**
Data set 1	24	11.28	2.13
Data set 2	24	9.67	1.41

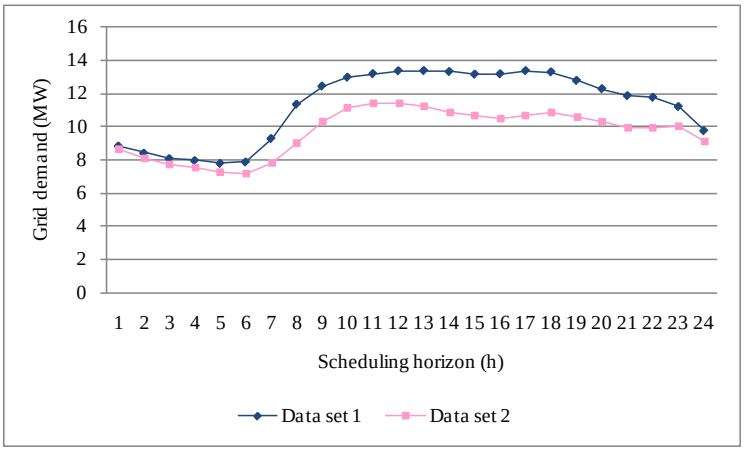

Figure 5.4 Two sets of grid demand data

5.4.2 Experiment 1

In Experiment 1, the schedules are developed for a wind farm based on the 8 scenarios. The wind turbines are categorized into two groups with all turbines identical within each group. In this experiment, wind turbines in Group 1 are assumed to be less efficient than wind turbines in Group 2. **Definition 5.5** expresses the condition that wind turbines in one group have higher efficiency than the turbines in another group.

Definition 5.5. *If a wind turbine of Group 2 generates more power than a wind turbine of Group 1 under any wind speed conditions, the turbine in Group 2 is assumed to have a better performing power curve. This definition is formularized in* (5.13).

$$\theta_{1,G2}\frac{1+\theta_{2,G2}e^{-v_t/\theta_{4,G2}}}{1+\theta_{3,G2}e^{-v_t/\theta_{4,G2}}}I_{(v_{ci},v_{co})}(v_t) > \theta_{1,G1}\frac{1+\theta_{2,G1}e^{-v_t/\theta_{4,G1}}}{1+\theta_{3,G1}e^{-v_t/\theta_{4,G1}}}I_{(v_{ci},v_{co})}(v_t) \qquad (5.13)$$

To ensure that a wind turbine of Group 2 has a more efficient power curve than a wind turbine of Group 1, a lower value of $\theta_{4,G2}$ than $\theta_{4,G1}$. Figure 5 introduces one example of power curves of wind turbines in Group 1 and Group 2. To construct a power curve, the values of vector θ need to be provided. Kusiak *et al.* (2009e) applied logistic function to model power curves and suggested θ={103.33, 20.53, 1190.73, 1.14}. The logistic function needs to be scaled to reflect the power curve of a 1.5 MW wind turbine.

For the power curve in Figure 5.5, $\theta_{4,G1}$ follows the value of 1.14 suggeated in Kusiak *et al.* (2009e). The value of $\theta_{4,G2}$ is arbitrarily set to 1.05.

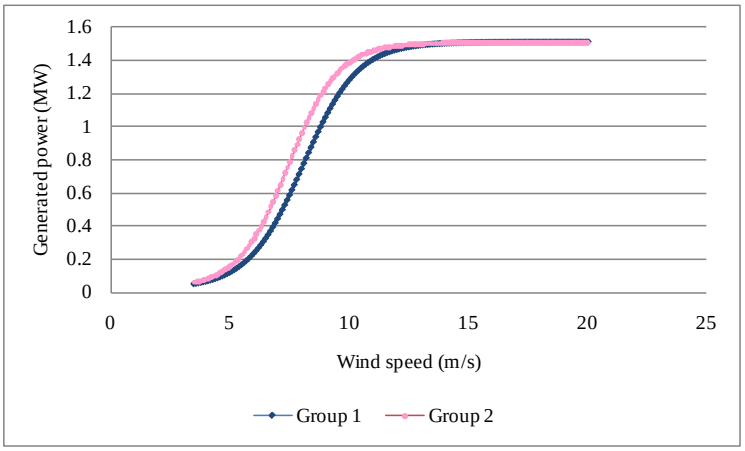

Figure 5.5 Power curve models in Group 1 and Group 2

Another interesting question to investigate is the ratio of wind turbines between Group 1 and Group 2. In this experiment, five ratios (i.e., the number of turbines in Group 1 divided by the number of turbines in Group 2), Ratio 1 = (100%/0), Ratio 2 = (70%/30%), Ratio 3 = (50%/50%), Ratio 4 = (30%/70%), Ratio 5 = (0/100%), are used to conduct sensitivity analysis of the schedule for this wind farm. For simplicity, the total number of wind turbines in the wind farm is assumed to be 10 for. As the wind turbines in each group are assumed to be identical, the scheduling model in (5.11) is expressed in (5.14).

$$
\begin{aligned}
&\text{Min } TC \\
&\text{s.t.} \\
&TC = \sum_{t=1}^{T} B_t \Delta P_t + \sum_{t=1}^{T} p_t \Delta P_t + \sum_{i=1}^{T} c_t P_t (X_{G1,t} + X_{G2,t}) \\
&\qquad + \sum_{i=1}^{T} B_t K_t \,|\, (X_{G1,t} + X_{G2,t}) - (X_{G1,t-1} + X_{G2,t-1}) \,| I_{(0,+\infty)}((X_{G1,t} + X_{G2,t}) - (X_{G1,t-1} + X_{G2,t-1})) \\
&\Delta P_t = \max\{0, D_t - (P_{G1,t} X_{G1,t} + P_{G2,t} X_{G2,t})\} \qquad (5.14) \\
&P_{\beta,t} = f_\beta(\upsilon_t, \theta_\beta) = \theta_{1,\beta} \frac{1 + \theta_{2,\beta} e^{-v_t/\theta_{4,\beta}}}{1 + \theta_{3,\beta} e^{-v_t/\theta_{4,\beta}}} I_{(v_{ci}, v_{co})}(v_t), \;\; \theta_\beta = (\theta_{1,\beta}, \theta_{2,\beta}, \theta_{3,\beta}, \theta_{4,\beta}) \text{ and } \beta = G1 \text{ or } G2 \\
&P_{I_t,t} \le P_C \\
&X_{G1,t} + X_{G2,t} \le I \\
&X_{G1,0} = X_{G2,0} = 0
\end{aligned}
$$

where $X_{G1,t}$ and $X_{G2,t}$ denote the number of wind turbines in each group at time t and I is the total number of wind turbines.

The binary programming problem described of (5.11) is transformed into an integer programming model (5.14) which can be solved by the proposed PSSWO. Note that the number of decision variables is significantly reduced, from 240 binary variables to 48 variables.

Table 5.6 presents electricity prices and two series of grid demand utilized in Experiment 1. Table 5.7 includes the high wind speed data and the corresponding power generated by a single wind turbine in Group 1 or Group 2. Table 5.8 addresses the similar information as Table 5.7 except that the level of wind speed in Table 5.8 is low.

Table 5.6 Electricity price and the grid demand data over the scheduling horizon

Scheduling Horizon	1	2	3	4	5	6	7	8	9	10	11	12
High B_t	44.94	43.56	40.06	36.66	38.01	43.04	49.85	68.00	66.17	65.58	65.37	64.82
Low B_t	43.02	42.81	36.54	33.91	31.27	33.72	35.11	35.60	40.58	46.27	45.46	47.93
High D_t	8.84	8.41	8.08	7.96	7.80	7.88	9.28	11.34	12.43	12.96	13.17	13.34
Low D_t	8.62	8.08	7.74	7.57	7.28	7.17	7.84	9.01	10.33	11.15	11.36	11.37
Scheduling Horizon	**13**	**14**	**15**	**16**	**17**	**18**	**19**	**20**	**21**	**22**	**23**	**24**
High B_t	62.80	57.99	53.99	49.38	48.43	49.85	61.72	65.56	53.81	45.61	46.73	44.32
Low B_t	48.48	45.04	41.74	38.24	40.08	48.56	56.06	56.27	50.70	48.15	50.35	47.17
High D_t	13.36	13.30	13.14	13.16	13.35	13.28	12.77	12.27	11.85	11.76	11.20	9.76
Low D_t	11.21	10.89	10.63	10.51	10.62	10.85	10.61	10.30	9.95	9.89	9.98	9.08

Table 5.7 High wind speed data and the generated power over the scheduling horizon

Scheduling horizon	1	2	3	4	5	6	7	8	9	10	11	12
High v_t	5.24	13.55	11.22	7.92	1.31	7.08	6.12	3.04	4.86	8.53	9.88	7.49
$P_{G1,t}$	0.14	1.49	1.42	0.72	0	0.46	0.25	0	0.11	0.91	1.25	0.58
$P_{G2,t}$	0.20	1.50	1.47	0.94	0	0.65	0.37	0	0.15	1.13	1.38	0.79
Scheduling horizon	**13**	**14**	**15**	**16**	**17**	**18**	**19**	**20**	**21**	**22**	**23**	**24**
High v_t	14.35	23.22	14.68	16.42	9.28	25.10	2.80	10.08	13.44	11.14	19.61	14.13
$P_{G1,t}$	1.50	1.50	1.50	1.50	1.12	0	0	1.29	1.49	1.41	1.50	1.50
$P_{G2,t}$	1.50	1.50	1.50	1.50	1.29	0	0	1.40	1.50	1.46	1.50	1.50

Table 5.8 Low wind speed data and the generated power over the scheduling horizon

Scheduling Horizon	1	2	3	4	5	6	7	8	9	10	11	12
Low v_t	8.12	8.20	12.29	12.25	2.60	14.27	9.28	23.79	3.03	7.77	6.21	6.89
$P_{G1,t}$	0.78	0.81	1.47	1.47	0	1.50	1.12	1.50	0	0.67	0.27	0.41
$P_{G2,t}$	1.01	1.03	1.49	1.49	0	1.50	1.29	1.50	0	0.89	0.39	0.59
Scheduling Horizon	**13**	**14**	**15**	**16**	**17**	**18**	**19**	**20**	**21**	**22**	**23**	**24**
Low v_t	2.58	2.98	4.34	12.73	5.65	1.12	2.33	10.99	6.00	3.38	5.22	1.91
$P_{G1,t}$	0	0	0.08	1.48	0.18	0	0	1.40	0.23	0	0.14	0
$P_{G2,t}$	0	0	0.11	1.50	0.27	0	0	1.46	0.34	0	0.20	0

5.4.3 Experiment 2

The wind farm in Experiment 2, is realistic as the total number of wind turbines is 10 and the power curve of each wind turbine is unique. To generate different power curves, a normal distribution with the mean 1.14 and the standard deviation 0.114 is utilized to produce 10 random values of $\theta_{4,i}$. Figure 5.6 illustrates the power curves of 10 wind turbines, with T1 to T10 representing the wind turbine No. 1 to No. 10.

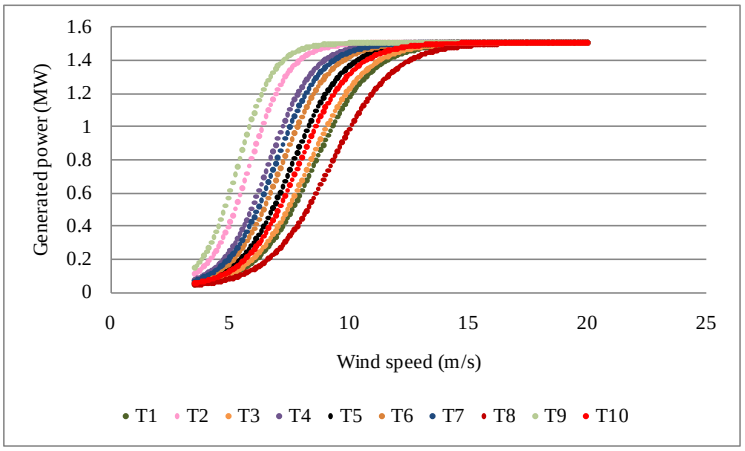

Figure 5.6 Power curve models of wind turbines

Solving (5.11) directly is computationally expensive since there are 240 binary decision variables. In addition, solving (5.11) (a binary programming formulation) with the proposed PSSWO is not feasible. In this study, binary string variables are transformed into duty-cycle based variables (Pappala *et al*. 2009, and Erlich (2008)) to reduce the model complexity as illustrated in Figure 5.7.

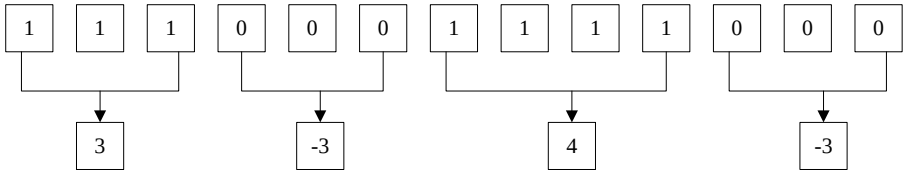

Figure 5.7 Transformation of a binary string into duty-cycle based variable

The electricity price and grid demand data used in Experiment 2 are the same as in Table 5.6. Table 5.9 and 5.10 presented the high wind speed data and the corresponding generated power of each wind turbine of a wind farm. Table 5.11 and 5.12 presented data similar to the ones of Table 5.9 and 5.10 for low wind speed.

Table 5.9 High wind speed and the generated power over the first half of the scheduling horizon

Scheduling Horizon	1	2	3	4	5	6	7	8	9	10	11	12
High v_t	5.24	13.55	11.22	7.92	1.31	7.08	6.12	3.04	4.86	8.53	9.88	7.49
$P_{1,t}$	0.12	1.48	1.37	0.59	0	0.37	0.21	0	0.09	0.78	1.15	0.47
$P_{2,t}$	0.52	1.50	1.50	1.40	0	1.25	0.91	0	0.38	1.45	1.49	1.34
$P_{3,t}$	0.13	1.49	1.39	0.65	0	0.42	0.23	0	0.10	0.84	1.20	0.52
$P_{4,t}$	0.31	1.50	1.49	1.22	0	0.96	0.58	0	0.23	1.34	1.46	1.10
$P_{5,t}$	0.18	1.50	1.46	0.88	0	0.60	0.33	0	0.13	1.07	1.35	0.74
$P_{6,t}$	0.22	1.50	1.48	1.03	0	0.74	0.42	0	0.16	1.20	1.41	0.89
$P_{7,t}$	0.26	1.50	1.49	1.13	0	0.85	0.49	0	0.19	1.28	1.44	0.99
$P_{8,t}$	0.09	1.45	1.25	0.43	0	0.27	0.15	0	0.08	0.58	0.95	0.34
$P_{9,t}$	0.73	1.50	1.50	1.46	0	1.38	1.13	0	0.55	1.48	1.50	1.43
$P_{10,t}$	0.15	1.50	1.44	0.79	0	0.52	0.28	0	0.12	0.98	1.30	0.64

Table 5.10 High wind speed and the generated power over the second half of the scheduling horizon

Scheduling Horizon	13	14	15	16	17	18	19	20	21	22	23	24
High v_t	14.35	23.22	14.68	16.42	9.28	25.10	2.80	10.08	13.44	11.14	19.61	14.13
$P_{1,t}$	1.49	1.50	1.50	1.50	1.00	0	0	1.19	1.48	1.36	1.50	1.49
$P_{2,t}$	1.50	1.50	1.50	1.50	1.48	0	0	1.50	1.50	1.50	1.50	1.50
$P_{3,t}$	1.50	1.50	1.50	1.50	1.06	0	0	1.24	1.49	1.39	1.50	1.49
$P_{4,t}$	1.50	1.50	1.50	1.50	1.43	0	0	1.47	1.50	1.49	1.50	1.50
$P_{5,t}$	1.50	1.50	1.50	1.50	1.25	0	0	1.37	1.50	1.45	1.50	1.50
$P_{6,t}$	1.50	1.50	1.50	1.50	1.34	0	0	1.43	1.50	1.48	1.50	1.50
$P_{7,t}$	1.50	1.50	1.50	1.50	1.39	0	0	1.45	1.50	1.49	1.50	1.50
$P_{8,t}$	1.48	1.50	1.48	1.50	0.79	0	0	1.01	1.45	1.23	1.50	1.47
$P_{9,t}$	1.50	1.50	1.50	1.50	1.50	0	0	1.50	1.50	1.50	1.50	1.50
$P_{10,t}$	1.50	1.50	1.50	1.50	1.18	0	0	1.33	1.50	1.43	1.50	1.50

Table 5.11 Low wind speed and the generated power over the first half of the scheduling horizon

Scheduling Horizon	1	2	3	4	5	6	7	8	9	10	11	12
Low v_t	8.12	8.20	12.29	12.25	2.60	14.27	9.28	23.79	3.03	7.77	6.21	6.89
$P_{1,t}$	0.65	0.67	1.44	1.44	0	1.49	1.00	1.50	0	0.55	0.22	0.33
$P_{2,t}$	1.42	1.43	1.50	1.50	0	1.50	1.48	1.50	0	1.38	0.94	1.19
$P_{3,t}$	0.71	0.74	1.46	1.46	0	1.50	1.06	1.50	0	0.60	0.24	0.37
$P_{4,t}$	1.27	1.28	1.50	1.50	0	1.50	1.43	1.50	0	1.18	0.62	0.89
$P_{5,t}$	0.95	0.97	1.49	1.49	0	1.50	1.25	1.50	0	0.83	0.35	0.54
$P_{6,t}$	1.10	1.12	1.50	1.50	0	1.50	1.34	1.50	0	0.98	0.44	0.67
$P_{7,t}$	1.19	1.21	1.50	1.50	0	1.50	1.39	1.50	0	1.09	0.52	0.77
$P_{8,t}$	0.47	0.49	1.38	1.38	0	1.48	0.79	1.50	0	0.39	0.16	0.24
$P_{9,t}$	1.47	1.47	1.50	1.50	0	1.50	1.50	1.50	0	1.45	1.16	1.34
$P_{10,t}$	0.85	0.88	1.48	1.48	0	1.50	1.18	1.50	0	0.73	0.30	0.46

Table 5.12 Low wind speed and the generated power over the second half of the scheduling horizon

Scheduling Horizon	13	14	15	16	17	18	19	20	21	22	23	24
Low v_t	2.58	2.98	4.34	12.73	5.65	1.12	2.33	10.99	6.00	3.38	5.22	1.91
$P_{1,t}$	0	0	0.07	1.46	0.15	0	0	1.34	0.19	0	0.12	0.00
$P_{2,t}$	0	0	0.24	1.50	0.70	0	0	1.50	0.85	0	0.51	0.00
$P_{3,t}$	0	0	0.07	1.47	0.17	0	0	1.37	0.21	0	0.13	0.00
$P_{4,t}$	0	0	0.15	1.50	0.42	0	0	1.49	0.54	0	0.30	0.00
$P_{5,t}$	0	0	0.09	1.49	0.24	0	0	1.45	0.30	0	0.17	0.00
$P_{6,t}$	0	0	0.11	1.50	0.30	0	0	1.47	0.38	0	0.22	0.00
$P_{7,t}$	0	0	0.13	1.50	0.35	0	0	1.48	0.45	0	0.25	0.00
$P_{8,t}$	0	0	0.06	1.41	0.12	0	0	1.21	0.14	0	0.09	0.00
$P_{9,t}$	0	0	0.34	1.50	0.93	0	0	1.50	1.08	0	0.72	0.00
$P_{10,t}$	0	0	0.09	1.49	0.20	0	0	1.42	0.26	0	0.15	0.00

5.5 Simulation Results

To solve the wind farm scheduling model, the values of parameters, p_t, c_t and K, need to be determined. Parameter p_t is arbitrarily set to 0.8. c_t is conservatively set to 50 Eur/MWh according to "www.wind-energy-the-facts.org". The parameter K is set to 0.06 MW based on the advice of wind farm managers. A more accurate model of estimating these three parameters need to be investigated in the future research.

5.5.1 Simulation Results of Experiment 1

To reduce computational cost, a stopping criterion, the number of iterations, needs to be determined. The convergence of the PSSWO algorithm is examined by solving (5.14) for Scenario 1. Figure 5.8 shows the convergence of the PSSWO algorithm attaining minimum at 50th iteration. However, this number of iterations (stopping criterion) may not hold for all scheduling scenarios. Therefore, a more conservative stopping criterion, 100 iterations, is adopted.

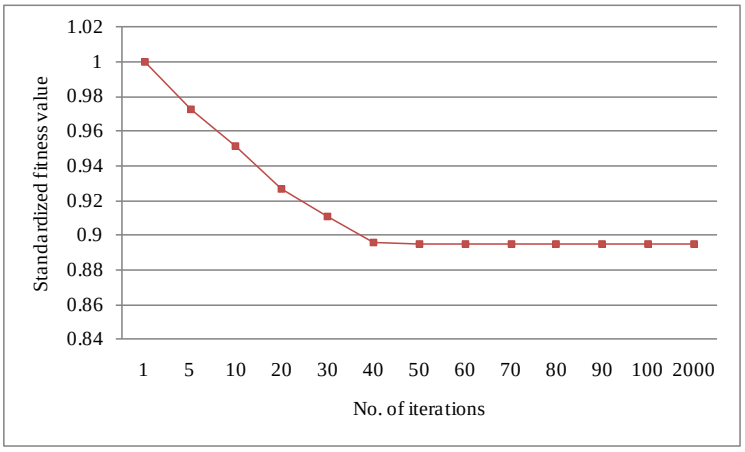

Figure 5.8 Convergence of PSSWO algorithm in Experiment 1

Sample simulation results of Experiment 1 are illustrated in Table 5.13, where the first column lists the scheduling scenarios. The index of scheduling time period is

addressed in the first and tenth row. The entries (separated by a comma) in Table 5.13 are the computed schedules at each time period.

The PSSWO does not guarantee global optimality. To evaluate the quality of the solutions, a comparative analysis is performed based on a baseline schedule. In the baseline schedule all wind turbines are activated once the measured wind speed is between the cut-in and the cut-out values. Table 5.14 includes the costs of operating a wind farm with the baseline schedule and the computed schedules. It is obvious that the computed schedules outperform the baseline schedule as indicated by the increasing trend of the total cost gain from ratio 1 to ratio 5 is shown in Table 5.14, which indicates that the wind farm performs better.

The data in Table 5.15 illustrate the total cost gain for the computed schedules for 5 ratios. A metric, *Gain*, is utilized to evaluate the gain of total cost reduction.

$$Gain = \frac{TC_b - TC_c}{TC_b} \times 100\% \tag{5.15}$$

As shown in Table 5.15, on average, 10% of total cost can be reduced through the computed schedules. The potential benefits of scheduling have been validated.

The schedules in Table 5.13 reveal that the efficient wind turbines do not need always run. The reason is that wind turbines balance the power shortage cost, operations and maintenance cost, and start-up cost.

Table 5.13 Scheduling results for Ratio 2

Scheduling Horizon	1	2	3	4	5	6	7	8	9	10	11	12
Scenario 1	7,3	4,2	6,0	7,3	0,0	7,3	7,2	0,0	7,3	7,3	7,3	7,3
Scenario 2	7,3	5,3	4,1	4,1	0,0	2,3	5,3	7,1	0,0	7,3	7,3	7,3
Scenario 3	7,2	3,2	4,1	7,2	0,0	5,3	7,3	0,0	7,3	7,3	7,2	7,3
Scenario 4	7,1	6,3	4,1	4,1	0,0	2,3	5,2	5,1	0,0	7,3	7,3	7,1
Scenario 5	7,0	4,1	5,0	6,0	0,0	7,1	7,1	0,0	7,3	7,1	7,3	7,2
Scenario 6	7,3	6,3	2,3	2,3	0,0	2,3	6,2	6,1	0,0	7,3	7,3	7,3
Scenario 7	7,3	3,2	4,1	6,1	0,0	5,2	7,3	0,0	7,3	7,2	6,3	7,2
Scenario 8	7,2	6,3	4,1	3,2	0,0	2,2	4,2	5,1	0,0	7,3	7,3	7,2
Scheduling Horizon	**13**	**14**	**15**	**16**	**17**	**18**	**19**	**20**	**21**	**22**	**23**	**24**
Scenario 1	7,2	7,2	7,2	7,1	7,3	0,0	0,0	7,3	7,1	7,1	7,0	4,2
Scenario 2	0,0	0,0	7,1	7,2	7,3	0,0	0,0	6,3	7,3	0,0	7,3	0,0
Scenario 3	5,2	6,1	4,3	5,2	6,3	0,0	0,0	6,2	6,1	5,2	5,1	5,1
Scenario 4	0,0	0,0	6,1	6,1	7,2	0,0	0,0	5,2	7,3	0,0	7,2	0,0
Scenario 5	7,2	7,1	7,1	7,1	7,3	0,0	0,0	6,3	7,1	6,2	5,2	5,1
Scenario 6	0,0	0,0	7,0	7,2	7,3	0,0	0,0	7,2	7,3	0,0	7,3	0,0
Scenario 7	4,3	5,2	6,1	5,2	6,3	0,0	0,0	5,3	7,0	6,1	6,1	5,1
Scenario 8	0,0	0,0	7,0	6,1	7,3	0,0	0,0	4,3	7,3	0,0	7,1	0,0

Table 5.14 Comparison between baseline and computed schedules

Scenario	Ratio 1		Ratio 2		Ratio 3		Ratio 4		Ratio 5	
	TC_b	TC_c	TC_b	TC_c	TC_b	TC_c	TC_b	TC_c	TC_b	TC_c
Scenario 1	19941.02	18415.31	19800.18	18301.01	19725.12	18149.27	19683.45	18067.27	19628.1	17906.37
Scenario 2	23323.15	21957.93	23222.78	21849.95	23178.92	21760.88	23165.32	21690.52	23144.91	21529.92
Scenario 3	17981.29	15445.18	17942.06	15365.79	17933.6	15372.68	17925.14	15290.27	17918.49	15095.57
Scenario 4	20407.74	18515.14	20333.47	18528.54	20306.97	18370.68	20293.37	18345.22	20272.97	18049.37
Scenario 5	17793.48	16272.39	17738.81	16378.57	17719.79	16200.89	17726.23	16071.08	17740.89	16002.81
Scenario 6	20602.82	19193.54	20559.5	19114.34	20553.15	19122.16	20575.77	19096.65	20609.69	18939.71
Scenario 7	16330.9	13763.94	16356.31	13806.17	16389.61	13780.49	16422.92	13750.65	16477.13	13597.21
Scenario 8	18205.75	16293.77	18188.09	16260.34	18198.36	16156.28	18220.97	16119.16	18254.9	16018.6

Table 5.15 The cost gain for Experiment 1

Scenario	$Gain_1$	$Gain_2$	$Gain_3$	$Gain_4$	$Gain_5$
Scenario 1	0.08	0.08	0.08	0.08	0.09
Scenario 2	0.06	0.06	0.06	0.06	0.07
Scenario 3	0.14	0.14	0.14	0.15	0.16
Scenario 4	0.09	0.09	0.10	0.10	0.11
Scenario 5	0.09	0.08	0.09	0.09	0.10
Scenario 6	0.07	0.07	0.07	0.07	0.08
Scenario 7	0.16	0.16	0.16	0.16	0.17
Scenario 8	0.11	0.11	0.11	0.12	0.12
Average	0.10	0.10	0.10	0.10	0.11

5.5.2 Simulation Results of Experiment 2

The stopping criterion of PSSWO algorithm in Experiment 2 is determined in a similar way. Figure 5.9 shows that the PSSWO definitely converges within 150th iterations. The stopping criterion of the PSSWO algorithm in Experiment 2 is conservatively set to 300.

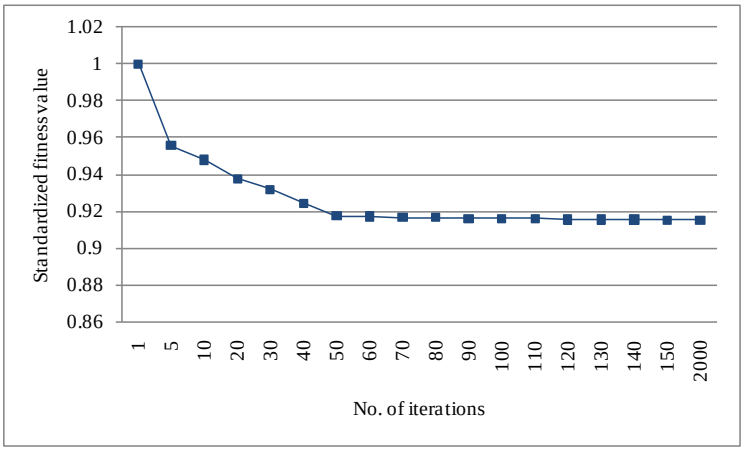

Figure 5.9 Convergence of the PSSWO algorithm in Experiment 2

Table 5.16 illustrates one sample of the scheduling strategies interpreted by duty-cycle based variables. Table 5.17 presents the baseline schedule of wind turbines under high and low wind speed conditions.

In this experiment, the comparative analysis of total costs between baseline schedule and computed schedules is performed. Table 5.18 discusses the gain in terms of cost reduction. As presented in Table 5.18, the average gain is 10%. These results reveal that even though the power curves of wind turbines are different, the model can produce appropriate schedules to minimize the total costs of running the wind farm. At the same, the produced schedules outperform the baseline schedule.

Table 5.16 Wind turbine schedule in Scenario 1 of Experiment 2

Turbine Index	1	2	3	4	5	6	7	8	9	10	11	12	13	14	15
Turbine 1	4	-1	2	-1	9	-7	0	0	0	0	0	0	0	0	0
Turbine 2	4	-1	2	-1	4	-4	1	-2	3	-2	0	0	0	0	0
Turbine 3	4	-1	2	-1	9	-2	5	0	0	0	0	0	0	0	0
Turbine 4	1	-2	1	-1	2	-1	9	-2	5	0	0	0	0	0	0
Turbine 5	-5	2	-1	9	-2	1	-4	0	0	0	0	0	0	0	0
Turbine 6	-5	2	-1	9	-2	5	0	0	0	0	0	0	0	0	0
Turbine 7	4	-1	2	-1	9	-2	5	0	0	0	0	0	0	0	0
Turbine 8	4	-1	2	-1	9	-2	5	0	0	0	0	0	0	0	0
Turbine 9	4	-1	2	-1	9	-2	5	0	0	0	0	0	0	0	0
Turbine 10	4	-1	2	-1	9	-2	4	-1	0	0	0	0	0	0	0

Table 5.17 Baseline schedule

Wind Speed	1	2	3	4	5	6	7	8	9	10	11	12
High wind speed	4	-1	2	-1	9	-2	5	0	0	0	0	0
Low wind speed	4	-1	3	-1	3	-2	3	-2	2	-1	1	-1

Table 5.18 Cost reduction for Experiment 2

	TC_b	TC_c	Gain
Scenario 1	19399.10	17756.54	0.08
Scenario 2	22775.85	21121.55	0.07
Scenario 3	17657.43	15042.15	0.15
Scenario 4	19903.90	17716.81	0.11
Scenario 5	17594.80	16045.10	0.09
Scenario 6	20352.17	18660.32	0.08
Scenario 7	16304.70	13582.13	0.17
Scenario 8	17997.38	15754.51	0.12
Average			0.11

5.5.3 PSSWO versus PSO

To assess performance of the PSSWO algorithm, a canonical PSO is implemented with 2000 iterations to solve the models in Scenario 1 for the two experiments. Performance of the two algorithms is compared in Table 5.19.

Table 5.19 Comparison of PSO and PSSWO algorithms

Algorithm	No. of Conv. Iterations in Exp. 1	Best Fitness in Exp. 1	No. of Conv. Iterations in Exp. 2	Best Fitness in Exp. 2
PSO	37	18513.36	50	17802.54
PSSWO	50	18415.31	150	17756.54

As shown in Table 5.19, the PSO converges faster than the PSSWO algorithm. However, the PSSWO produced a better quality solution while PSO was trapped in local optima. The semi-isolated network structure indeed improves the performance of the canonical PSO.

5.6 Summary

A model for scheduling wind turbines was presented. The total cost of operating a wind farm was minimized. The optimized cost included the power shortage cost,

operational and maintenance cost, and start-up cost. Each schedule represents the operational status of wind turbines over a scheduling horizon.

To solve the model formulated in this chapter, a PSSWO algorithm was developed by integrating the traditional PSO with the small world network structure. A swarm of particles was divided into tribes with each tribe having its own search trajectory. A communication mechanism was introduced to exchange information among the semi-isolated tribes. The goal of the communication was to balance the exploration and exploitation of the search process by introducing diversity.

Two experiments were designed to analyze the optimized schedules produced by the models. Experiment 1 represented a simple wind farm structure with wind turbines having two types of power curves, efficient and less efficient. In Experiment 2, a wind farm contained 10 wind turbines each with a different power curve. To evaluate the quality of the computed schedules, a baseline schedule was used. The comparative analysis indicated that the cost of operating a wind farm was reduced by the computed schedules over the baseline schedule. Moreover, the computed schedules indicated that the wind turbines with more efficient power curves were not always run due to a tradeoff between the power shortage cost, operations and maintenance cost, and the start-up cost. As the gains in the cost reduction were estimated based on the actual data, the proposed model has a potential to be used in practice.

CAPTER 6

SCHEDULING A WIND FARM WITH DATA DRIVEN STOCHASTIC OPTIMIZATION

6.1 Introduction

Environmental concerns and sustainable living call for renewable energy solutions. Wind energy, one of the most important renewable energy sources, has experienced a rapid growth in the past decade. As a new research area, wind energy has posed numerous research questions and power generation efficiency of wind turbines has been one of them. Improvement of wind turbine efficiency is generally achieved in two ways, wind turbine control and wind turbine condition monitoring. Boukhezzar and Siguerdidjane (2009) designed a non-linear controller for optimizing the power of the DFIG (double-fed induction generator). Wang and Chang (2004) investigated a maximum power extraction algorithm to improve the performance of wind turbine systems. Munteanu *et al.* (2005) designed two control loops to optimize power in low frequency and high frequency scenarios. Senjyu *et al.* (2006) studied the impact of limited activation of blade pitch angle on the power output. Watson *et al.* (2010) applied a wavelet method to monitor the power output of wind turbines. Besnard and Bertling (2010) proposed a Markov Chain based method to optimize the condition-based maintenance strategies for degraded components. Although the published research on wind turbine efficiency is valuable, it predominantly focuses on local solutions as wind farms usually include numerous wind turbines and improving the efficiency of wind turbines is not equivalent to the optimization of the entire wind farm.

Optimization of a wind farm requires answers of two questions, the number of operational wind turbines and the control settings of the operational wind turbines. The stochastic nature of the wind, electric power demand, and the electricity price makes scheduling wind farm challenging. In the studies on scheduling energy systems published

to date a wind farm is usually considered as a single power generator in the energy system. Pappala *et al.* (2009) presented a stochastic optimization model of wind-thermal system. Javier *et al.* (2008) discussed a stochastic joint optimization of a hybrid system of a wind farm and pumps. Lee (2007) published a study of scheduling a number of wind turbines and thermal units optimizing spinning reserves of this hybrid-energy system. In (Pappala *et al.* 2009) and (Javier *et al.* 2008), the wind farm is considered as a single power generation unit. In (Lee 2007), although a number of wind turbines is considered, the wind power is represented by the power curve and the wind speed is assumed to be known.

In the research presented in this chapter, individual wind turbines are scheduled in the presence of uncertain wind speed. The decisions to the number of operational wind turbines (on/off) and the turbine control are both considered in scheduling. In reality, performance of wind turbines of the same type is not identical. The heterogeneity of wind turbines is considered by models developed with data mining algorithms. A base model and a stochastic optimization model are developed for scheduling a wind farm. A novel computational intelligence algorithm, the migrated particle swarm optimization, is introduced to solve the wind farm scheduling models.

6.2 Base Model

In this section, a base model for scheduling a wind farm is developed. The model minimizes the cost of operating a wind farm over a pre-determined time horizon subject to equality and inequality constraints. The schedule minimizing the cost of operating a wind farm is described by decision and control variables defined in **Definition 6.1** and **Definition 6.2**.

Definition 6.1. *The decision variable is a vector* $\boldsymbol{s}_t = [s_{1,t}, s_{2,t}..., s_{I,t}]$, $s_{i,t} \in \{0,1\}$ *and* $i = 1, 2, 3, \ldots, I$, *determining the operational status (on/off) of wind turbines in the wind farm at time window t.*

Definition 6.2. *The control variables is represented as a 2-tuple* ($\boldsymbol{\tau}_t$, $\boldsymbol{\beta}_t$). *In this 2-tuple,* $\boldsymbol{\tau}_t = [\tau_{1,t}, \tau_{2,t}, \ldots, \tau_{I,t}]$ *and* $\boldsymbol{\beta}_t = [\beta_{1,t}, \beta_{2,t}, \ldots, \beta_{I,t}]$, $\tau_{i,t}, \beta_{i,t} \in \mathbb{R}^I$ *and* $i = 1, 2, 3, \ldots, I$, *are two vectors represent the settings of the generator torque and the blade pitch angle of wind turbines at time window t.*

The wind farm schedules are developed based on three types of data, the power commitment, the electricity price, and the wind speed. In this chapter, the power commitment and the electricity price are assumed to be known while considering uncertain wind speed. The objective function, constraints, and the model are formulated next.

6.2.1 Objective Function of the Base Model

The objective of the wind farm scheduling base model is to minimize the cost of operating a wind farm, *TC*, over a fixed time horizon. This cost includes the power shortage cost, operations and maintenance (O&M) cost, and the idle turbine cost.

The power shortage occurs when the power generation capacity of a wind farm cannot meet the power commitment at time window *t* (see (6.1)).

$$\Delta P_t = \max\{0, D_t - \sum_{i=1}^{I} P_{i,t} s_{i,t}\} \tag{6.1}$$

The power shortage cost is expressed as the opportunity and the compensation cost due to power shortage. The opportunity cost and the compensation cost are defined next.

Definition 6.3. *The opportunity cost reflects the potential revenue of selling the amount of electric power equivalent to the power shortage, i.e., the product of the electricity price and the electric power shortage at a given time window.*

Definition 6.4. *The compensation cost is the penalty paid to compensate for the amount of power shortage.*

The opportunity cost and compensation cost due to power shortage at time *t* are expressed in Eqs. (6.2) and (6.3).

$$C_{oc} = B_t \Delta P_t \tag{6.2}$$

$$C_{cc} = p_t \Delta P_t \tag{6.3}$$

The O&M (operations and maintenance) cost includes the cost attributed to operations and maintenance of wind turbines is expressed in (6.4).

$$C_{om} = \sum_{i=1}^{I} cP_{i,t} s_{i,t} \tag{6.4}$$

The last component of the total cost is the idle turbine cost. The idle turbine cost describes the cost of energy consumed by idle wind turbines to support the electronics. The total idle turbine cost at *t* is formulated in (6.5).

$$C_{ic} = \sum_{i=1}^{I} B_t K_{i,t} (1 - s_{i,t}) \tag{6.5}$$

Based on (6.2) – (6.5), the total cost of operating a wind farm over a scheduling time horizon *T* is expressed in (6.6). It involves the power shortage cost, O&M cost, and the idle turbine cost over *T*.

$$TC = \sum_{t=1}^{T} B_t \Delta P_t + \sum_{t=1}^{T} p_t \Delta P_t + \sum_{t=1}^{T} \sum_{i=1}^{I} cP_{i,t} s_{i,t} + \sum_{t=1}^{T} \sum_{i=1}^{I} B_t K_{i,t} (1 - s_{i,t}) \tag{6.6}$$

6.2.2 Constraints of the Base Model

In this section the four types of constraints discussed in Section 6.2.2.1, 6.2.2.2, 6.2.2.3, and 6.2.2.4 are introduced.

6.2.2.1 Wind Turbine Power Generation Model

In the base scheduling model the power generated in a wind farm at time *t* equals the sum of power generated by wind turbines at this wind farm. To accurately predict the generated power of each wind turbine, a wind turbine power generation model needs to be established. The power generation models of wind turbines are usually not identical.

The published research has focused on the development of a general wind power generation model. Kang (2007) applied a fuzzy set approach to develop a wind power prediction model. Bhowmik *et al.* (1999) designed a variable speed generation controller which employed a wind speed estimation-based maximum power point tracker and a heuristic-model-based maximum efficiency point tracker to optimize the energy captured for the doubly-fed wind power generator. Calderaro *et al.* (2008) developed a fuzzy clustering method integrated with a genetic algorithm to maximize the wind power generation. Wind power generation process models in (Kang 2007; Bhowmik *et al.* 1999; Calderaro *et al.* 2008) were general and the heterogeneity of wind turbines was not studied. The general model was suitable for the study of a single machine system. However, the heterogeneity of wind turbines has to be considered as the power generation efficiency can impact scheduling strategies.

The Supervisory Control and Data Acquisition (SCADA) systems allow for continuous collection of wind turbine data. Such data can be used to model wind turbines. Data driven approaches for developing wind power generation models have been discussed in (Kusiak *et al.* 2009a; Kusiak and Zhang 2011; Kusiak and Zheng 2010). In this chapter, a Neural Network algorithm (Siegelmann and Sontag 1994; Liu 2011; Smith 1993) is utilized to model wind turbines.

A group of five 1.5 MW wind turbines (numbered here as 1 – 5) installed in a commercial wind farm has been selected for analysis. The SCADA data from 09/02/2011 to 2/28/2011 is selected to form five datasets for developing Neural Network models. The sampling interval of the collected SCADA data is 10-min. The 10-min SCADA data is averaged to 30-min data to match the length of scheduling time window.

Based on (Kusiak *et al.* 2009a), the generator torque, blade pitch angle, and wind speed are considered to predict the generated power in this chapter. The wind power generation model is formulated as (6.7).

$$P_{i,t} = f_i(\tau_{i,t}, \beta_{i,t}, \hat{\upsilon}_t) I_{(\upsilon_{ci}, \upsilon_{co})}(\hat{\upsilon}_t) \tag{6.7}$$

The indicator function *I* in (6.7) indicates that the wind turbine is only operated when wind speed is in the cut-in and cut-out region.

To develop the power generation model, each of the five datasets is split to two subsets, training dataset and test dataset, by 4/5 and 1/5. The training dataset is used to develop a power generation model validated with the test dataset. Table 1 shows the test results of the power generation model of turbine No. 1 – 5. Four metrics (6.8 – 6.11), the mean absolute error (MAE), the standard deviation of absolute error (SD of AE), the mean absolute percentage error (MAPE), and the standard deviation of absolute percentage error (SD of APE) are applied for assessing quality of the data driven models.

$$\text{MAE} = \frac{1}{n}\sum_{k=1}^{n} | \hat{y}_k - y_k | \tag{6.8}$$

$$\text{SDofAE} = \sqrt{\frac{1}{n}\sum_{k=1}^{n}(| \hat{y}_k - y_k | - \frac{1}{n}\sum_{k=1}^{n} | \hat{y}_k - y_k |)^2} \tag{6.9}$$

$$\text{MAPE} = \frac{1}{n}\sum_{k=1}^{n}(| \frac{\hat{y}_k - y_k}{y_k} |) \times 100\% \tag{6.10}$$

$$\text{SDofAPE} = \sqrt{\frac{1}{n}\sum_{k=1}^{n}(| \frac{\hat{y}_k - y_k}{y_k} | - \frac{1}{n}\sum_{k=1}^{n} | \frac{\hat{y}_k - y_k}{y_k} |)^2} \times 100\% \tag{6.11}$$

where n is the number of data points in test datasets, y_i is the observed value, and $\hat{y}_i$ is the predicted value.

As shown in Table 6.1, the MAPE of five data driven power generation models is about 5% which corresponds to the accuracy of power prediction of 95%.

Table 6.1 Test results of the power generation models

Turbine No.	MAE (kW)	SD of AE (kW)	MAPE (%)	SD of APE (%)
1	11.55	10.91	4.00	9.00
2	9.72	8.87	4.00	8.00
3	14.39	10.29	6.00	14.00
4	6.85	6.17	4.00	11.00
5	11.91	11.63	5.00	11.00

Figure 6.1 – 6.5 show the first 100 predictions by the NN power generation models of wind turbines 1 – 5.

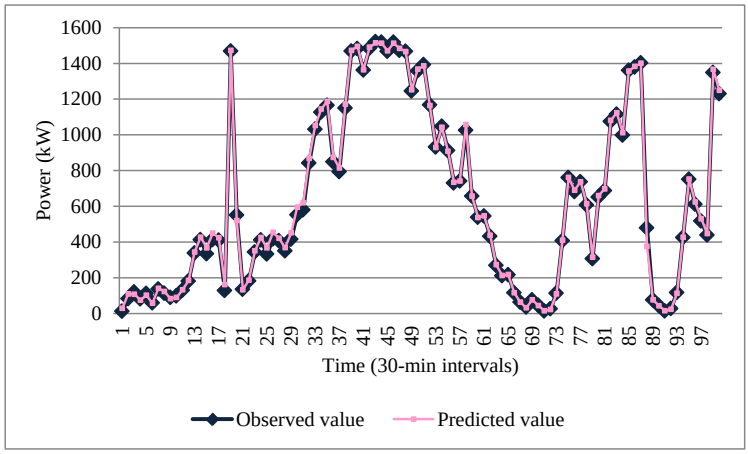

Figure 6.1 Observed v.s. predicted power values of turbine 1

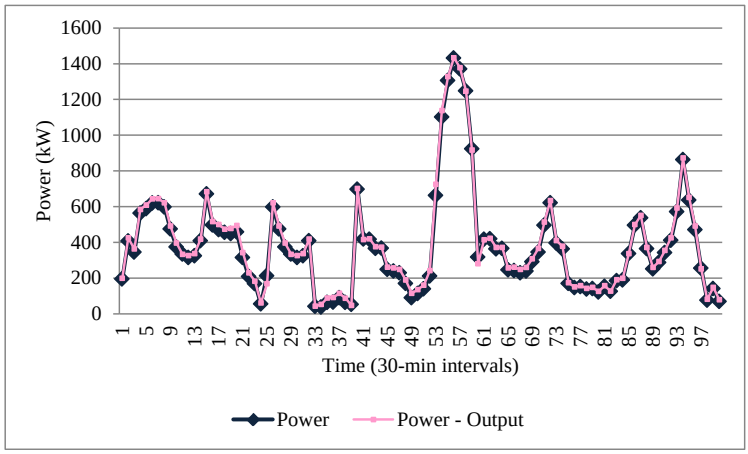

Figure 6.2 Observed v.s. predicted power values of turbine 2

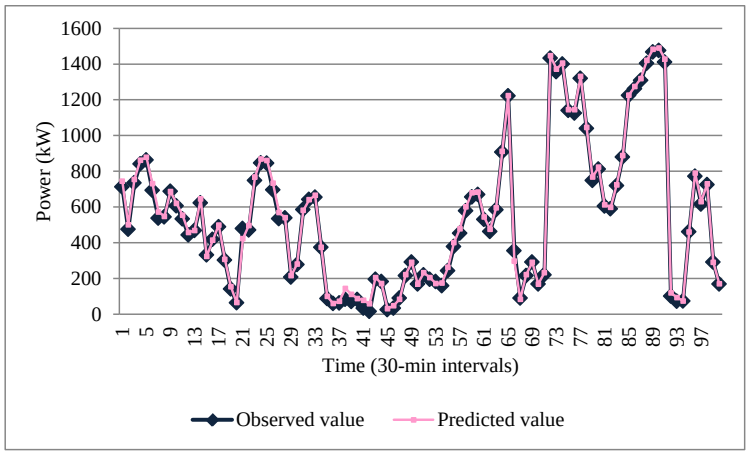

Figure 6.3 Observed v.s. predicted power values of turbine 3

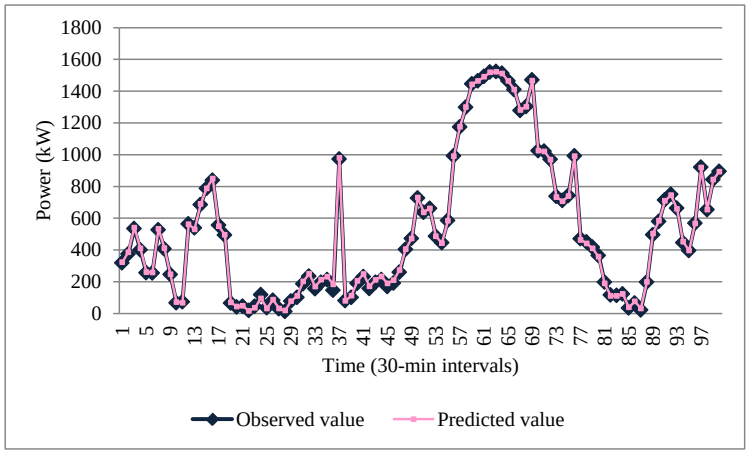

Figure 6.4 Observed v.s. predicted power values of turbine 4

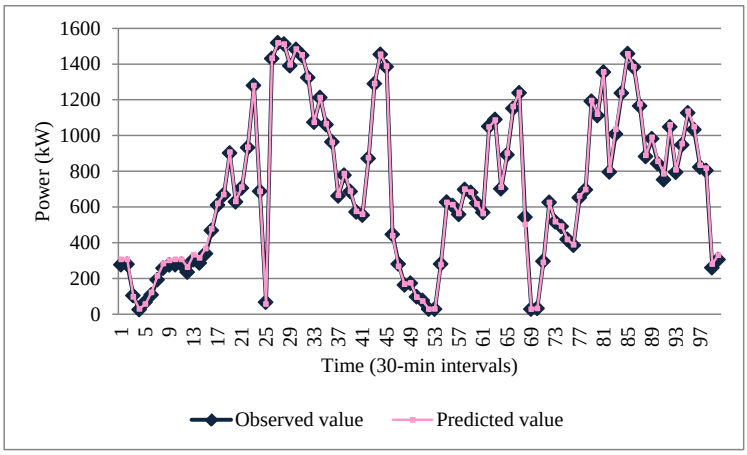

Figure 6.5 Observed v.s. predicted power values of turbine 5

6.2.2.2 Power Generation Constraint

The power generated by a turbine should not exceed its maximum power generation capacity. According to (Kusiak *et al.* 2009a), these two rules can be expressed as a constraint in (6.11)

$$P_{i,t} \le \min\{1.5, (2.625\hat{\upsilon}_t^3)/1000\} \tag{6.11}$$

where 1.5 denotes the maximum power generation capacity (1.5 MW) and $2.625\hat{\upsilon}_t^3/1000$ is the power generation constraint derived from Betz' law.

6.2.2.3 Constraints of Decision and Control Variables

In the base model, the decision variable is binary and the control variables are expressed as real numbers. The theoretical range of the generator torque is [0%, 100%] and the range of blade pitch angle is [-360^o, 360^o]. However, since not all values of the two control variables are reflected in the datasets, constraints need to be developed. The maximum and minimum of generator torque and blade pitch angle present in the datasets then are used to develop constraints of the control variables for each wind turbine. The two constraints are expressed in (6.12 – 6.14).

$$s_{i,t} \in \{0,1\} \tag{6.12}$$

$$\tau_{1,t} \in [1.5, 100.78], \tau_{2,t} \in [1.23, 100.63], \tau_{3,t} \in [1.14, 100.68], \\ \tau_{4,t} \in [1.55, 100.63], \tau_{5,t} \in [1.8, 100.62] \quad (6.13)$$

$$\beta_{1,t} \in [-0.07, 76.14], \beta_{2,t} \in [-0.07, 76.12], \beta_{3,t} \in [-0.07, 84.23], \\ \beta_{4,t} \in [-0.08, 80.51], \beta_{5,t} \in [0.04, 359.6] \quad (6.14)$$

6.2.2.4 The Wind Speed Prediction Model

The average wind speed in the wind farm is not known. To predict the turbine generated power based on (6.7), the average wind speed needs to be provided. A model is introduced in this section to predict wind speed at time window *t* based on its past states. The wind speed data of the five wind turbines discussed in Section 6.2.2.1 is first averaged and then the time series of the wind speed is derived. As in Section 6.2.2.1, the wind speed data is split into training and test datasets for developing models.

Eight past states of wind speed, v_{t-Q}, v_{t-2Q}, …, v_{t-7Q}, and v_{t-8Q}, are considered to form a pool of parameters to predict wind speed at *t*. A parameter selection method, wrapper search with genetic algorithm (Witten and Frank 2005; Kohavi and John 1997), is applied to select the important parameters in the pool. The parameters, v_{t-Q}, v_{t-2Q}, v_{t-3Q}, v_{t-4Q}, and v_{t-7Q}, are considered as important based on the wrapper search with v_{t-Q} being the most important amount the five parameters. The wind speed prediction model is formulated in (6.15).

$$\hat{v}_t = f(v_{t-Q}, v_{t-2Q}, v_{t-3Q}, \ldots, v_{t-7Q}) \quad (6.15)$$

A Neural Network algorithm is applied to learn the model $f(\bullet)$ of (6.15) using a training dataset. The trained model is then validated by the test dataset. Table 6.2 shows the test accuracy of wind speed prediction model. Figure 6.6 represents prediction results of the first 100 points of the test dataset.

Table 6.2 Accuracy of the wind speed prediction model

MAE (m/s)	SD of AE (m/s)	MAPE (%)	SD of APE (%)
0.38	0.51	7.00	13.00

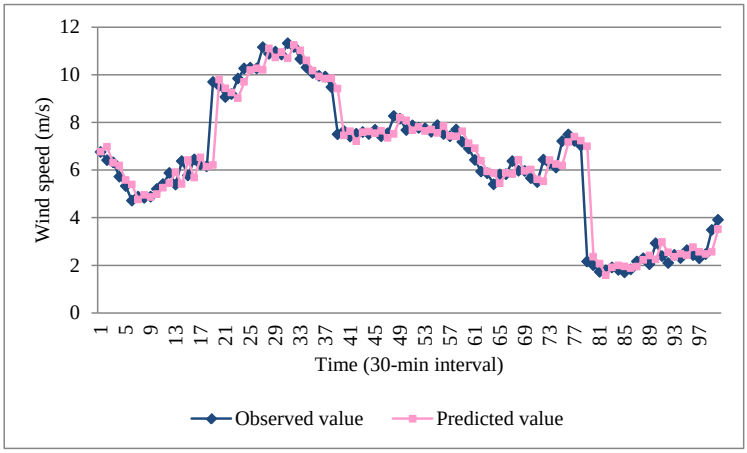

Figure 6.6 The first 100 observed and predicted values of the wind speed

6.2.3 Formulation of the Base Model

The base model of scheduling a wind farm can is presented in (6.16) by integrating the objective function and constraints discussed in Section 6.2.1 and 6.2.2.

$$
\begin{aligned}
&\min_{s,\tau,\beta} TC \\
&\text{s.t.} \\
&TC = \sum_{t=1}^{T} B_t \Delta P_t + \sum_{t=1}^{T} p_t \Delta P_t + \sum_{t=1}^{T}\sum_{i=1}^{I} c P_{i,t} s_{i,t} + \sum_{t=1}^{T}\sum_{i=1}^{I} B_t K_{i,t}(1-s_{i,t}) \\
&\Delta P_t = \max\{0, D_t - \sum_{i=1}^{I} P_{i,t} s_{i,t}\} \\
&P_{i,t} = f(\tau_{i,t}, \beta_{i,t}, \hat{\upsilon}_t) I_{(\upsilon_{ci},\upsilon_{co})}(\hat{\upsilon}_t) \\
&P_{i,t} \le \min\{1500, 2.625\hat{\upsilon}_t^3\} \\
&\hat{\upsilon}_t = f(\upsilon_{t-\mathrm{Q}}, \upsilon_{t-2\mathrm{Q}}, \upsilon_{t-3\mathrm{Q}}, \ldots, \upsilon_{t-7\mathrm{Q}}) \\
&s_{i,t} \in \{0,1\} \\
&\tau_{1,t} \in [1.5, 100.78], \tau_{2,t} \in [1.23, 100.63], \tau_{3,t} \in [1.14, 100.68], \\
&\tau_{4,t} \in [1.55, 100.63], \tau_{5,t} \in [1.8, 100.62] \\
&\beta_{1,t} \in [-0.07, 76.14], \beta_{2,t} \in [-0.07, 76.12], \beta_{3,t} \in [-0.07, 84.23], \\
&\beta_{4,t} \in [-0.08, 80.51], \beta_{5,t} \in [0.04, 359.6]
\end{aligned}
\tag{6.16}
$$

6.3 Stochastic Optimization Model

In this section, a single-stage stochastic optimization model is introduced. The uncertainty of wind speed is modeled by a set of wind speed scenarios. The stochastic optimization model provides a deterministic solution when the power commitment and the electricity price are determined.

6.3.1 Wind Speed Scenarios

Since the highest wind speed recorded in the world is 113 m/s (World Meteorological Organization, Accessed 2011), the range of wind speed can be restricted to [0 m/s, 113 m/s]. However, the wind turbines considered in this research are only operated between the cut-in speed of 4 m/s and cut-out speed of 24 m/s. Moreover, the generated power reaches its maximum for the wind speed between the rated wind speed of 12 m/s and cut-out wind speed. Eight wind speed scenarios are developed by discretizing the wind speed in the eight intervals (6.17).

$$\begin{aligned}&\partial_1 \in (0,4), \partial_2 \in [4,6), \partial_3 \in [6,8), \partial_4 \in [8,10),\\ &\partial_5 \in [10,12), \partial_6 \in [12,14), \partial_7 \in [14,24), \partial_8 \in [24,113)\end{aligned} \tag{6.17}$$

It has been observed in (6.15) that the parameter υ_{t-Q} is statistically more significant than that other wind speed data used to estimate the wind speed at *t*. Therefore, the assumption presented next is made.

Assumption 6.1. *Given a set of wind speed scenarios,* $\{\partial_1, \partial_2, \partial_3, \ldots, \partial_8\}$*, the probability that the wind speed value changes in the future scenario depends only on wind speed value in the present scenario rather than the sequence of scenarios preceding the present scenario.*

The **Assumption 6.1** is represented in (6.18).

$$\Pr(\upsilon_{t+Q} \in \partial_h \,|\, \upsilon_t \in \partial_h, \upsilon_{t-Q} \in \partial_h, \ldots, \upsilon_{t-8Q} \in \partial_h) = \Pr(\upsilon_{t+Q} \in \partial_h \,|\, \upsilon_t \in \partial_h) \tag{6.18}$$

where h = 1, 2, 3, …, 8.

Then the conditional probabilities of all wind speed scenarios constitute a transition matrix A presented in (6.19).

$$A=\begin{bmatrix} \Pr(\upsilon_{t+Q}\in\partial_1\,|\,\upsilon_t\in\partial_1),\ldots,\Pr(\upsilon_{t+Q}\in\partial_8\,|\,\upsilon_t\in\partial_1) \\ \vdots \quad ,\ddots, \quad \vdots \\ \Pr(\upsilon_{t+Q}\in\partial_1\,|\,\upsilon_t\in\partial_8),\ldots,\Pr(\upsilon_{t+Q}\in\partial_8\,|\,\upsilon_t\in\partial_8) \end{bmatrix} \tag{6.19}$$

The average wind speed data discussed in Section 6.2.2.4 and an additional wind speed dataset, 30-min wind speed data in year 2008, are integrated as a dataset for estimating the probability in (6.19). Eq. (6.20) is applied to calculate the probability in (6.19) based on this dataset.

$$\Pr(\upsilon_{t+Q}\in\partial_h\,|\,\upsilon_t\in\partial_h)=\frac{\Pr(\upsilon_{t+Q}\in\partial_h\bigcap\upsilon_t\in\partial_h)}{\Pr(\upsilon_t\in\partial_h)}=\frac{N_{\upsilon_{t+Q}\in\partial_h\bigcap\upsilon_t\in\partial_h}}{N_{\upsilon_t\in\partial_h}} \tag{6.20}$$

where h = 1, 2, 3, …, 8.

The estimated matrix A is shown in Table 6.3. Since the wind speed above 24 m/s is rarely observed in the dataset, scenario 8 of wind speed is excluded in A. The wind speed at time t is observable and therefore the wind speed scenario at time t denoted as ∂' can be determined. Then, the probability of wind speed scenarios at t + Q are obtained from Table 6.3.

Table 6.3 The estimated matrix A

Pr	$\upsilon_{t+Q}\in\partial_1$	$\upsilon_{t+Q}\in\partial_2$	$\upsilon_{t+Q}\in\partial_3$	$\upsilon_{t+Q}\in\partial_4$	$\upsilon_{t+Q}\in\partial_5$	$\upsilon_{t+Q}\in\partial_6$	$\upsilon_{t+Q}\in\partial_7$
$\upsilon_t\in\partial_1$	0.8547	0.1220	0.0166	0.0048	0.0016	0.0003	0.0000
$\upsilon_t\in\partial_2$	0.1219	0.6944	0.1669	0.0128	0.0032	0.0006	0.0003
$\upsilon_t\in\partial_3$	0.0128	0.1379	0.7144	0.1247	0.0083	0.0015	0.0004
$\upsilon_t\in\partial_4$	0.0061	0.0153	0.1973	0.6659	0.1089	0.0056	0.0009
$\upsilon_t\in\partial_5$	0.0022	0.0062	0.0208	0.2132	0.6583	0.0929	0.0062
$\upsilon_t\in\partial_6$	0.0011	0.0015	0.0114	0.0197	0.2292	0.6455	0.0917
$\upsilon_t\in\partial_7$	0.0017	0.0008	0.0059	0.0093	0.0271	0.2120	0.7430

6.3.2 Objective Function of the Stochastic Optimization Model

In the single-stage stochastic optimization model, the wind speed at present time is described as scenarios with conditional probability rather than an estimated value discussed in Section 6.2.2.4. The objective of the stochastic optimization model is to minimize the expected cost of operating a wind farm over a scheduling horizon. For the wind speed scenario at present time ∂_h, $\partial_h \in \partial$, the objective function of the stochastic optimization model is formulated in (6.21).

$$TC = \sum_{t=1}^{T} \sum_{\partial_h \in \partial} \Pr(\upsilon_t \in \partial_h \,|\, \upsilon_{t-\mathrm{Q}} \in \partial') \cdot (C_{oc,\partial_h} + C_{cc,\partial_h} + C_{om,\partial_h} + C_{ic,\partial_h}) \tag{6.21}$$

In (6.21), the opportunity cost, compensation cost, O&M cost, and the idle turbine cost in each wind speed scenario need to be estimated based on the expected power shortage.

Definition 6.5. *Expected power shortage in the wind speed scenario ∂_h equals the difference between the electric power commitment and the expectation of generated power in the wind speed scenario ∂_h and it is expressed in* (6.22).

$$\Delta P_t = \max\{0, D_t - \sum_{i=1}^{I} E_{\partial_h}(P_{i,t}) s_{i,t}\} \tag{6.22}$$

As discussed in Section 6.3.1, each wind speed scenario presents an interval of wind speed. Therefore, the expected generated power in wind speed scenario ∂_h can be calculated from (6.23).

$$E_{\partial_h}(P_{i,t}) = \int_{\upsilon_t \in \partial_h} P_{i,t} f_{\upsilon_t \in \partial_h}(\upsilon_t) d\upsilon_t = \int_{\upsilon_t \in \partial_h} f(\tau_{i,t}, \beta_{i,t}, \upsilon_t) f_{\upsilon_t \in \partial_h}(\upsilon_t) d\upsilon_t \tag{6.23}$$

However, since the wind power generation model in (6.23) is nonparametric, its integration is challenging. To calculate the expected generated power, an approximation method is applied. In the approximation method, the wind speed interval of each scenario

is divided to many sub-intervals and the mean value of wind speed in each sub-interval is computed. Then, the expected generated power is expressed in (6.24).

$$E(P_{i,t}) = \int_{\upsilon_t \in \partial_h} f(\tau_{i,t}, \beta_{i,t}, \upsilon_t) f_{\upsilon_t \in \partial_h}(\upsilon_t) d\upsilon_t \approx \sum_{\partial_S \in \partial_h} f(\tau_{i,t}, \beta_{i,t}, \overline{\upsilon}_{\partial_S}) \Pr(\overline{\upsilon}_{\partial_S}) \quad (6.24)$$

where ∂_s is the sub-interval of scenario ∂_h and $\overline{\upsilon}_{\partial_S}$ is the mean value of ∂_s.

6.3.3 Formulation of the Stochastic Optimization Model

The constraints discussed in Section 6.2.2.2 and 6.2.2.3 are integrated with the objective function in Section 6.3.2 to form the stochastic optimization model for scheduling a wind farm. The decision and control variables in the stochastic optimization model are the same as in the base model. The stochastic optimization model is presented in (6.25).

$$\begin{aligned}
&\min_{s,\tau,\beta} TC \\
&\text{s.t.} \\
&TC = \sum_{t=1}^{T} \sum_{\partial_h \in \partial} \Pr(\upsilon_t \in \partial_h \,|\, \upsilon_{t-Q} \in \partial') \cdot (B_t \Delta P_t + p_t \Delta P_t + \sum_{i=1}^{I} cE_{\partial_h}(P_{i,t}) s_{i,t} + \sum_{i=1}^{I} B_t K_{i,t}(1 - s_{i,t})) \\
&\Delta P_t = \max\{0, D_t - \sum_{i=1}^{I} E_{\partial_h}(P_{i,t}) s_{i,t}\} \\
&E(P_{i,t}) = (\sum_{\partial_S \in \partial_h} f(\tau_{i,t}, \beta_{i,t}, \overline{\upsilon}_{\partial_S}) \Pr(\overline{\upsilon}_{\partial_S})) \cdot I_{(\upsilon_{ci}, \upsilon_{co})}(\overline{\upsilon}_{\partial_S}) \\
&f(\tau_{i,t}, \beta_{i,t}, \overline{\upsilon}_{\partial_S}) \le \min\{1500, 2.625(\overline{\upsilon}_{\partial_S})^3\} \\
&s_{i,t} \in \{0,1\} \\
&\tau_{1,t} \in [1.5, 100.78], \tau_{2,t} \in [1.23, 100.63], \tau_{3,t} \in [1.14, 100.68], \\
&\tau_{4,t} \in [1.55, 100.63], \tau_{5,t} \in [1.8, 100.62] \\
&\beta_{1,t} \in [-0.07, 76.14], \beta_{2,t} \in [-0.07, 76.12], \beta_{3,t} \in [-0.07, 84.23], \\
&\beta_{4,t} \in [-0.08, 80.51], \beta_{5,t} \in [0.04, 359.6]
\end{aligned} \quad (6.25)$$

6.4 Migrated Particle Swarm Optimization Algorithm

Both of the base model and stochastic optimization model discussed in Section 6.2 and 6.3 involve binary decision variables and real value control variables. Solving mixed-integer programming models, especially mixed-integer nonlinear programming problems (MINLP) is challenging. Traditional solution approaches for solving MINLP,

such as Outer Approximation (OA) methods (Duran and Grossmann 1986), Branch-and-Bound (Gupta and Ravindran 1985), Extended Cutting Plane algorithm (Westerlund and Petersson 1995), and Generalized Bender's Decomposition (Geoffrion 1972), have been discussed in the literature. The traditional solution approaches guarantee global optimality when convexity is observed. In addition, the traditional solution approaches (Duran and Grossmann 1986; Gupta and Ravindran 1985; Westerlund and Petersson 1995; Geoffrion 1972) do not perform well for large-scale MINLPs. Lastly, an explicit formulation of the MINLP is required by the traditional solution approaches.

In this chapter, the wind power generation model is derived by NN algorithm which is non-parametric. Since the traditional solution approaches are difficult to apply for solving such a model, a migrated particle swarm optimization algorithm (MPSO) is developed. The MPSO algorithm is inspired by the concepts of particle swarm optimization (PSO) (Kennedy and Eberhart 1995; Clerc and Kennedy 2002) and genetic algorithms (GA) (Fraser 1957). Figure 6.7 shows the structure of the migrated particle swarm optimization algorithm.

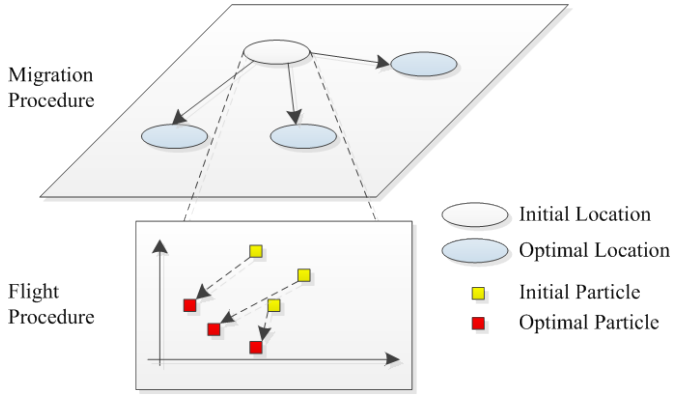

Figure 6.7 Structure of the migrated particle swarm optimization algorithm

A wind turbine is controlled only when its operational status is 'on'. **Observation 6.1** describes a relationship between the decision and control variables.

Observation 6.1. *The control variables, τ and β, impact the objective function only if the decision variable s is* 1. *If s* =0, *the control variables are considered to be independent to the objective function.*

Observation 6.1 is reflected in the MPSO algorithm in Figure 6.7. A migration procedure is applied to explore decisions for the operating wind turbines. Based on the explored decisions, the flight procedure is utilized to search the optimal settings of control variables. The detailed steps of the MPSO algorithm are presented next.

The migrated particle swarm optimization algorithm

Step 1. Initialization of swarm locations: Initialize *b* locations for distributing particle swarms with each location representing a binary part of a solution.

Step 2. Flight procedure of particles in each location

For each location l, $l = 1, 2, 3, ..., b$

Step 2.1. Initialize the positions of a population of particles with population size, m.

Step 2.2. Initialize the local best of each particle in the population and the global best.

Step 2.3. Update the velocity of particles by

$$v_l^j \leftarrow \omega v_l^j + c_1 r_1^j (\hat{x}_l^j - x_l^j) + c_2 r_2^j (\hat{g}^j - x_l^j).$$

Step 2.4. Update the position of particles by $x_l^j \leftarrow x_l^j + v_l^j$.

Step 2.5. Update the local best $\hat{x}_l^j \leftarrow x_l^j$ if $fit(x_l^j) \le fit(\hat{x}_l^j)$.

Step 2.6. Update the global best $\hat{g}_l^j \leftarrow x_l^j$ if $fit(x_l^j) \le fit(\hat{g}^j)$.

Step 2.7. Compute the fitness value

Step 2.8. Stop the flight procedure if the stopping criterion is met. Otherwise, repeat Steps 2.3 – 2.7.

Step 3. Compare the fitness value of solutions and preserve the best one as the best solution in the search.

Step 4. Migration procedure of swarms

Step 4.1. Apply a genetic operator to develop a new set of swarm locations with size *b* by crossover and mutation of the locations in last iteration.

Step 4.1.1. Crossover: Randomly select a single point in the string (binary part of the solution). Exchange the part of string before the selected point of one location in last iteration and the best location.

Step 4.1.2. Mutation: Randomly select a single point in the string and mutate the value of it between 0 and 1.

Step 4.2. Employ the flight procedure in Step 2 to search the real value part of the solution.

Step 4.3. Select the best solution in this migration, update the best solution in the search if the best solution in this migration is better than the best solution in the last iteration.

Step 4.4. Stop the algorithm if the stopping criterion is met. Otherwise, go back to Step.4.1.

To implement the MPSO, the settings of some parameters need to be determined. The parameters, ω, c_1 and c_2, in the flight procedure are set to 0.5, 2, and 2 according to (Kennedy and Eberhart 1995). The parameters, r_1 and r_2, are generated from $U(0,1)$. The size of swarm locations, *b*, is set to 5 and the size of particles, *m*, is set to 10.

6.5 Case Study

In this section, wind farm scheduling is considered using a sample of five 1.5 MW class wind turbines. The values of the power commitment and electricity prices in this case study come from the websites of the National Grid UK and European Energy Exchange. In this case study, *T* is set to 12 and Q is set to 30-min. Thus, 12 data points of power commitment and electricity price from 1/15/2011 9:30:00 PM to 1/16/2011

3:00:00 AM are selected. The power commitment data is produced by rescaling the demand data recorded by the National Grid UK to a level close to the generation capacity of a 7.5 MW wind farm. The sampling interval for the electricity price data in EEX is 1 hour and the 30-min electricity price is derived based on the 1 hour EEX data. Table 6.4 illustrates the wind speed data at t – Q, electric power demand data at t, and electricity price at t.

Table 6.4 The data used in the case study

Scheduling time window (30-min)	1	2	3	4	5	6	7	8	9	10	11	12
t – Q wind Speed (m/s)	6.9	7.0	6.8	6.4	6.3	5.7	5.3	4.7	4.9	4.8	4.9	5.2
Electric power demand (MW)	6.0	5.8	5.6	5.4	5.3	5.4	5.3	5.2	5.0	4.9	4.8	4.8
Electricity price (USD/MW)	23.4	26.4	29.3	25.1	20.8	16.7	12.6	11.1	9.56	8.3	7.1	6.8

6.5.1 Convergence of the MPSO

The convergence of the migration procedure and the flight procedure has been assessed to determine the stopping criterion for the MPSO algorithm. The time window t = 1 of the scheduling horizon is utilized to examine the convergence of two procedures.

To assess the convergence of the flight procedure of MPSO, the value of all decision variables, $s_{i,t}$, is set to 1. It presents a most computationally expensive case in the flight procedure because the number of control variables need to be searched in the flight procedure is the maximum based on Observation 6.1. The stopping criterion of this most computationally expensive case is also applied to other cases that not all $s_{i,t}$ is 1. The stopping criterion is set at 1500 iterations of the flight procedure. Figure 6.8 and 6.9 illustrate the convergence of the flight procedure. As shown in Figure 6.8 and 6.9, the

flight procedure converges in 20 iterations. Thus, the stopping criterion of the flight procedure is set 20.

Figure 6.8 Convergence of the flight procedure for the base model

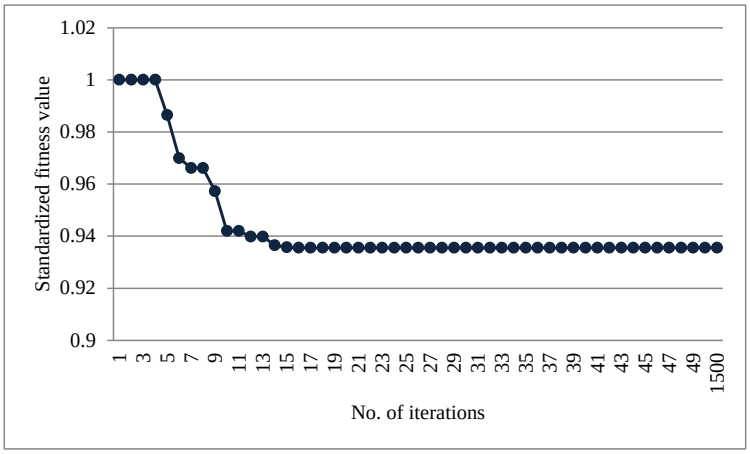

Figure 6.9 Convergence of the flight procedure for the stochastic optimization model

The stopping criterion of the migration procedure is studied based on the stopping criterion of the flight procedure. As the number of combinations of decision variables in this study is $2^5 = 32$, the number of iterations of the migration procedure is set to 100. Figure 6.10 and 6.11 demonstrate that convergence of the migration procedure in for the base and stochastic optimization models.

Figure 6.10 Convergence of the migration procedure for the base model

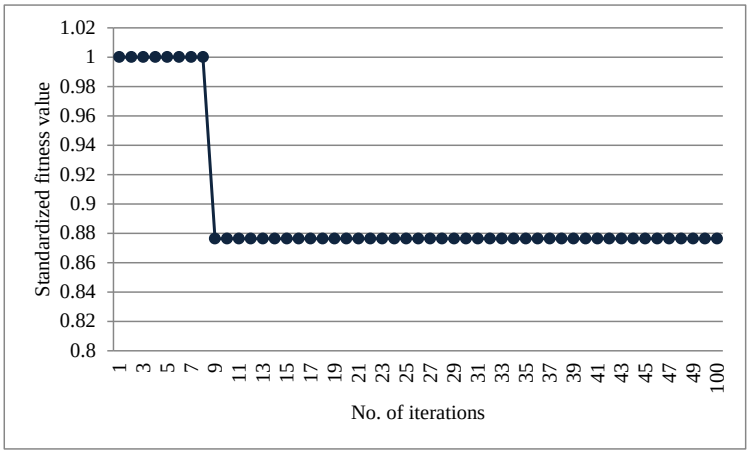

Figure 6.11 Convergence of the migration procedure for the stochastic optimization model

As shown in Figure 6.10 and 6.11, the migration procedure converges within 15 iterations. Thus, the stopping criterion of migration procedure is set to 15.

6.5.2 Solution of the Scheduling Models

In the stochastic optimization model, each wind speed scenario is equally divided into 10 intervals to compute the expected generated power in (6.24). Table 6.5 illustrates all values of $\overline{\upsilon}_{\partial_s}$ and the corresponding probabilities. The range of wind speed in scenario

7 discussed in Section 6.3.1 is between 14 m/s and 24 m/s. Since no evidence of wind speed higher than 19 m/s is recorded, the range of wind speed in scenario 7 divided into 10 intervals is further restricted to [14 m/s, 19 m/s] as shown in Table 6.5.

Table 6.5 Probability of wind speeds in each sub-interval

Sce. 2	$\{\overline{\upsilon}_{\partial_S} \mid \partial_S \in \partial_2\}$	4.1	4.3	4.5	4.7	4.9	5.1	5.3	5.5	5.7	5.9
	Pr	0.08	0.08	0.09	0.09	0.1	0.1	0.11	0.12	0.12	0.12
Sce. 3	$\{\overline{\upsilon}_{\partial_S} \mid \partial_S \in \partial_3\}$	6.1	6.3	6.5	6.7	6.9	7.1	7.3	7.5	7.7	7.9
	Pr	0.10	0.10	0.10	0.10	0.10	0.10	0.10	0.1	0.1	0.1
Sce. 4	$\{\overline{\upsilon}_{\partial_S} \mid \partial_S \in \partial_4\}$	8.1	8.3	8.5	8.7	8.9	9.1	9.3	9.5	9.7	9.9
	Pr	0.13	0.13	0.12	0.12	0.10	0.09	0.09	0.08	0.07	0.07
Sce. 5	$\{\overline{\upsilon}_{\partial_S} \mid \partial_S \in \partial_5\}$	10.1	10.3	10.5	10.7	10.9	11.1	11.3	11.5	11.7	11.9
	Pr	0.13	0.12	0.12	0.11	0.10	0.1	0.09	0.08	0.07	0.07
Sce. 6	$\{\overline{\upsilon}_{\partial_S} \mid \partial_S \in \partial_6\}$	12.1	12.3	12.5	12.7	12.9	13.1	13.3	13.5	13.7	13.9
	Pr	0.15	0.13	0.12	0.10	0.10	0.1	0.09	0.08	0.07	0.07
Sce. 7	$\{\overline{\upsilon}_{\partial_S} \mid \partial_S \in \partial_7\}$	14.25	14.75	15.25	15.75	16.25	16.75	17.25	17.75	18.25	18.75
	Pr	0.26	0.21	0.12	0.12	0.10	0.05	0.02	0.05	0.04	0.03

The wind farm scheduling strategies generated from the base and the stochastic optimization model are shown in Table 6.6 and 6.7, respectively. The columns with headings, Solution Part 1, Solution Part 2, and Solution Part 3, in Table 6.6 and 6.7 describe the settings of the decision variable and the two control variables, generator torque and blade pitch angle. As shown in Table 6.6 and 6.7, the decisions to operate a wind turbine suggested by the base and the stochastic optimization models are identical. The difference of the two solutions is mainly reflected in the settings of generator torque and blade pitch angle. The settings of generator torque and blade pitch angle offered by the base model are slightly different from the settings recommended by the stochastic optimization model.

Table 6.6 Schedules provided by the base model

Scheduling Time Window	Solution Part 1 $\{s_1, s_2, s_3, s_4, s_5\}$	Solution Part 2 $\{\tau_1, \tau_2, \tau_3, \tau_4, \tau_5\}$	Solution Part 3 $\{\beta_1, \beta_2, \beta_3, \beta_4, \beta_5\}$
1	1,1,1,1,1	53.09,53.63,70.02,61.56,81.72	75.78,52.30,16.05,5.42,97.81
2	1,1,1,1,1	54.35,48.90,68.90,56.09,81.60	73.95,50.56,14.54,5.82,94.91
3	1,1,1,1,1	68.03,64.26,70.50,62.42,86.63	35.25,47.69,11.07,7.61,67.51
4	1,1,1,1,1	45.62,38.19,65.71,56.49,83.10	68.47,58.92,18.90,-0.07,94.06
5	1,1,1,1,1	40.07,48.70,64.59,63.10,81.55	68.41,60.91,14.17,2.38,65.55
6	1,1,1,1,1	35.82,38.36,63.60,100.02,82.97	67.22,59.77,18.43,1.29,294.77
7	1,1,1,1,1	42.28,44.99,61.56,85.33,82.86	67.89,59.28,17.61,1.98,214.87
8	1,1,1,1,1	35.82,38.36,63.60,100.02,83.00	67.22,59.77,18.43,1.29,294.77
9	1,1,1,1,1	1.50,1.23,41.03,1.55,1.80	-0.07,0.02,31.52,27.00,4.90
10	0,1,1,1,0	0,1.49,1.14,1.55,0	0,0.06,-0.07,26.94,0
11	0,0,1,1,0	0,0,1.14,1.55,0	0,0,-0.07,26.92,0
12	0,0,1,1,0	0,0,1.14,1.55,0	0,0,-0.07,26.77,0

Table 6.7 Schedules provided by the stochastic optimization model

Scheduling Time Window	Solution Part 1 $\{s_1, s_2, s_3, s_4, s_5\}$	Solution Part 2 $\{\tau_1, \tau_2, \tau_3, \tau_4, \tau_5\}$	Solution Part 3 $\{\beta_1, \beta_2, \beta_3, \beta_4, \beta_5\}$
1	1,1,1,1,1	59.51,63.72,62.69,63.58,69.42	56.67,54.67,23.34,17.16,92.00
2	1,1,1,1,1	62.97,67.71,76.06,65.44,93.76	27.38,42.74,8.83,8.81,31.81
3	1,1,1,1,1	61.60,64.47,63.20,69.66,71.04	54.42,56.20,23.43,19.52,93.77
4	1,1,1,1,1	64.15,44.78,55.01,82.95,77.95	64.68,56.27,22.12,0.52,105.51
5	1,1,1,1,1	40.79,40.01,74.76,58.21,55.17	75.34,68.28,14.72,0.24,101.84
6	1,1,1,1,1	40.32,45.34,61.73,84.84,82.86	68.05,59.29,17.63,1.99,212.21
7	1,1,1,1,1	42.39,45.11,61.57,85.34,82.86	67.91,59.27,17.60,1.98,214.97
8	1,1,1,1,1	35.82,38.36,63.60,100.02,82.97	67.22,59.77,18.43,1.29,294.77
9	1,1,1,1,1	1.51,1.25,53.10,1.55,1.83	-0.07,10.28,32.92,26.45,1.09
10	0,1,1,1,0	0,1.56,1.14,1.55,0	0,0.07,-0.07,26.63,0
11	0,0,1,1,0	0,0,1.14,1.55,0	0,0,-0.07,26.57,0
12	0,0,1,1,0	0,0,1.14,1.55,0	0,0,-0.07,26.57,0

Table 6.4, 6.6 and 6.7 offer some insights into the scheduling strategies generated by the two models. As shown in Table 6.4, the electric power commitment is close to the wind farm maximum power generation capacity at the beginning and it gradually decreases over time. The decisions to operate wind turbines in Table 6.6 and 6.7 show a similar pattern. The solutions suggest operating all wind turbines at the wind farm for some time and shutting down some wind turbines towards the end of the scheduling horizon. This strategy encourages the wind farm to generate an amount of power that matches the power commitment. If the power commitment is close to the maximum power generation capacity of the wind farm, all wind turbines are to be operated. If the power commitment is much lower than the wind farm maximum power generation capacity, operating all wind turbines is not necessary.

6.5.3 Solution Quality

The quality of solutions generated by the two models is evaluated in this section. The solutions of the base and the stochastic optimization model are compared with the best schedule and the baseline schedule. A desirable solution should be better than the baseline schedule and be close or equal to the best schedule. The best schedule and the baseline schedule are defined in **Definition 6.6** and **6.7**.

Definition 6.6. *The best schedule is a schedule obtained by solving model (6.16) under perfect information (known wind speed) over a scheduling horizon.*

Definition 6.7. *The baseline schedule is a schedule obtained by solving model (6.16) over a scheduling horizon with wind speed predicted by (6.15) and all* $s_{i,t} = 1$ *provided that the constraint,* $\upsilon_{ci} \le \hat{\upsilon}_t \le \upsilon_{co}$ *, is met. The baseline schedule describes a schedule that all wind turbines will be operational if* $\upsilon_{ci} \le \hat{\upsilon}_t \le \upsilon_{co}$ *.*

Table 6.8 and 6.9 present the best schedule and the baseline schedule for operating the wind farm.

Table 6.8 The best schedules

Scheduling Time Window	Solution Part 1 $\{s_1, s_2, s_3, s_4, s_5\}$	Solution Part 2 $\{\tau_1, \tau_2, \tau_3, \tau_4, \tau_5\}$	Solution Part 3 $\{\beta_1, \beta_2, \beta_3, \beta_4, \beta_5\}$
1	1,1,1,1,1	58.58,47.36,64.88,69.32,81.75	66.71,54.43,11.54,3.63,95.28
2	1,1,1,1,1	53.00,51.21,66.08,56.08,80.71	76.14,50.63,13.55,4.41,98.47
3	1,1,1,1,1	44.23,41.82,64.92,65.52,81.80	68.35,53.04,13.42,1.15,108.44
4	1,1,1,1,1	44.36,37.24,64.67,99.53,81.24	68.45,61.34,12.26,2.34,127.02
5	1,1,1,1,1	35.82,38.36,63.60,100.02,82.97	67.22,59.77,18.43,1.29,294.77
6	1,1,1,1,1	35.82,38.36,63.60,100.02,82.97	67.22,59.77,18.43,1.29,294.77
7	1,1,1,1,1	35.82,38.36,63.60,100.02,82.97	67.22,59.77,18.43,1.29,294.77
8	1,1,1,1,1	19.94,22.06,68.40,75.47,82.76	70.67,58.87,16.92,2.04,161.30
9	1,1,1,1,1	1.52,1.23,1.14,1.56,1.81	0.03,1.02,26.39,26.14,0.31
10	0,1,1,1,0	0,1.45,1.14,1.55,0	0,0.03,-0.07,26.71,0
11	0,0,1,1,0	0,0,1.14,1.55,0	0,0,-0.07,26.82,0
12	0,0,1,1,0	0,0,1.14,1.55,0	0,0,-0.07,26.63,0

Table 6.9 The baseline schedules

Scheduling Time Window	Solution Part 1 $\{s_1, s_2, s_3, s_4, s_5\}$	Solution Part 2 $\{\tau_1, \tau_2, \tau_3, \tau_4, \tau_5\}$	Solution Part 3 $\{\beta_1, \beta_2, \beta_3, \beta_4, \beta_5\}$
1	1,1,1,1,1	52.85,53.87,70.09,62.01,81.73	75.79,52.44,16.16,5.33,98.19
2	1,1,1,1,1	54.35,48.90,68.90,56.09,81.60	73.95,50.56,14.54,5.82,94.91
3	1,1,1,1,1	68.03,64.26,70.50,62.42,86.63	35.25,47.69,11.07,7.61,67.51
4	1,1,1,1,1	43.35,44.53,64.97,65.23,83.71	66.80,58.67,19.50,0.06,98.05
5	1,1,1,1,1	36.89,46.16,66.79,75.75,80.65	70.64,63.07,10.99,1.59,69.57
6	1,1,1,1,1	35.82,38.36,63.60,100.02,82.97	67.22,59.77,18.43,1.29,294.77
7	1,1,1,1,1	42.39,45.11,61.57,85.34,82.86	67.91,59.27,17.60,1.98,214.97
8	1,1,1,1,1	35.82,38.36,63.60,100.02,82.97	67.22,59.77,18.43,1.29,294.77
9	1,1,1,1,1	1.50,1.23,43.91,1.55,1.82	-0.06,5.55,28.30,26.65,2.05
10	1,1,1,1,1	1.53,1.27,44.71,1.55,1.81	-0.07,0.14,25.91,28.06,0.26
11	1,1,1,1,1	1.50,1.23,47.73,1.55,1.80	-0.07,11.51,30.46,26.78,0.22
12	1,1,1,1,1	1.50,1.23,50.78,1.55,1.80	-0.07,6.66,26.91,26.73,0.08

The base model schedule (BMS), the stochastic model schedule (SMS), the best schedule (BES), and the baseline schedule (BS) are compared. Table 6.10 describes total cost of running a wind farm according to these solutions.

Table 6.10 Comparative analysis of different scheduling strategies

Scheduling Time Window	BES	BMS	SMS	BS
1	198.93	198.93	199.99	198.93
2	210.95	210.95	210.95	210.95
3	242.03	242.03	242.03	242.03
4	212.65	212.65	212.65	212.65
5	207.18	207.18	207.18	207.18
6	189.62	189.62	189.62	189.62
7	157.80	157.8	157.8	157.8
8	138.90	138.9	138.9	138.9
9	120.66	120.68	120.68	120.68
10	101.92	101.92	101.92	103.08
11	85.40	85.4	85.4	88.26
12	80.25	80.25	80.25	83.77
Total	1946.29	1946.31	1947.37	1953.85

The data in Table 6.10 indicates that the BES, BMS, SMS, and BS costs are similar because these four schedules are produced by model (6.16) and (6.25). However, the cost of BS is slightly higher than the cost of BES, BMS and SMS. This indicates that by selection of wind turbines to be operational may reduce the cost of operating a wind farm. Since the total costs of the four schedules in Table 6.10 are expressed in small numbers, it is difficult to directly determine the quality of the solutions. A solution index (*SI*) (see **Definition 6.8**) is proposed to evaluate the quality of the solutions generated from model (6.16) and (6.25).

Definition 6.8. *Given the total cost of the best schedule (BES), the baseline schedule (BS), and the solution (MS) obtained by solving model (6.16) or (6.25) denoted as* TC_{BES}, TC_{BS}, *and* TC_{MS}, *respectively, the solution index SI is defined in (6.26).*

$$SI = \frac{TC_{\mathrm{MS}} - TC_{\mathrm{BES}}}{TC_{\mathrm{BS}} - TC_{\mathrm{BES}}} \tag{6.26}$$

where $TC_{\mathrm{BS}} > TC_{\mathrm{BES}}$ and $TC_{\mathrm{MS}} > TC_{\mathrm{BES}}$.

The value of *SI* between 0 and 1 indicates a good quality wind farm schedule. A value of *SI* = 0 indicates that the computed schedule based on the optimization model (6.16) and (6.25) is the same as the best schedule. A value of *SI* = 1 indicates that the computed schedule is similar to the baseline schedule. If *SI* is larger than 1, the quality of a schedule is considered as poor. In this study, *SI* = 0.0026 for BMS and the *SI* = 0.1429 for SMS. The quality of both schedules is acceptable while BMS is slightly better than SMS. However, the SMS has an advantage over BMS. The SMS is a deterministic solution based on wind speed scenarios for the case when the electricity price and electric power commitment are known. Once the wind farm operator gets to know the electricity price and the electric power commitment, the SMS can be applied to run the wind farm based on the wind speed at $t - Q$.

6.6 Summary

A new scheduling study of a wind farm that considered uncertainty of wind speed over a scheduling horizon was presented in this chapter. The goal of scheduling of a wind farm was to minimize the total cost of operating a wind farm over the scheduling horizon. The total cost included the power shortage cost, operations and maintenance cost, and idle turbine cost. The wind farm schedule was formed based on two types of variables, the decision variable and control variables. The decision variable captured the operational status of wind turbines (the on/off status). The control variables, generator torque and blade pitch angle, were applied to determine the power generation of wind turbines.

Two models, the base model and the stochastic optimization to schedule a wind farm were developed. In the base model, the wind speed was predicted by a data-driven model. In the stochastic model, the uncertainty of the wind speed was modeled with wind speed scenarios. The wind turbine power generation model used in the base model and stochastic model was implemented as a neural network. Solving the base and stochastic

optimization models was challenging. A migrated particle swarm optimization was developed to solve the two models.

A comparative analysis was performed to evaluate the quality of schedules produced by the base and the stochastic optimization models. A best schedule and a baseline schedule were introduced as reference schedules for schedule quality evaluation. The cost of the base model schedule and the stochastic model schedule was close to the cost of the best schedule. In the future research, the proposed model will be extended by considering uncertainty of the electricity price and the power commitment. Additional constraints, such as balancing the runtime of wind turbines will be introduced.

CHAPTER 7

CONCLUSION

A data-mining framework for optimization of wind turbines performance was introduced. The framework included construction and optimization of data-driven models. Data-mining algorithms were applied to identify accurate wind turbine models from the SCADA collected data. Once the accuracy of data-driven models was validated, optimization algorithms were utilized to compute the optimal solutions. Since data-driven models are not explicit, evolutionary computation algorithms, such as evolutionary strategy, particle swarm optimization and artificial immune systems, were considered. Although the global optimal solution was not always guaranteed by evolutionary computation algorithms, the computed solutions improved performance of wind turbines and wind farms.

Seven data mining algorithms, Neural Network, Neural Network Ensemble, Support Vector Machine, Boosting Tree, Random Forests, Classification and Regression Tree and k Nearest Neighbors, were applied to the development of data driven models. Modeling a single wind turbine and a wind farm were both discussed in this dissertation. In the single wind turbine research, data mining algorithms were utilized to model the performance of a single wind turbine. To study the wind farm optimization, data driven single wind turbine models then were integrated together to construct a wind farm model.

This dissertation aimed to solve four main wind industry challenges. The first challenge was that the delay caused by the feedback loops of wind turbine control systems degraded the wind turbine performance. A solution to the system delay was offerd in the form of a model predictive control approach. The second challenge came from the optimization of wind turbine performance in multiple objectives. The multiple objectives were transformed to a single objective by linear combination in the optimization. The weights of objectives needed to be determined. Therefore, developing a scheme could automatically assign values to the weights of objectives was desired. The

third challenge was the boundary of wind power optimization. A more realistic power optimization constraint rather than Betz's law based constraint was needed in wind industry. Investigation of scheduling a wind farm was the last challenge. As wind industry is emerging, limited research related to wind farm scheduling has been performed.

An anticipatory control model for optimizing performance of wind turbines was developed in Chapter 2. It was set to accomplish three goals, increasing the power extracted from the wind, and mitigating vibration of the drive-train system and the tower. By considering these goals, the power generation model, drive-train acceleration model, tower acceleration model and the time-series wind speed prediction model were derived to establish this optimization model. To solve the constructed optimization model, a particle swarm optimization algorithm was applied.

Chapter 3 presented the adaptive control of a wind turbine to maximize power generation and minimize the torque ramp rate. Data-mining algorithms were utilized to generate non-parametric models of wind turbine power generation and the wind power prediction model. An integrated model with a linear combination of weighted objectives was created. The weights associated with the objectives were estimated based on the predicted power and demand. The demand was generated from two simulation models. A novel optimization approach, the particle swarm fuzzy algorithm (PSFA), was developed to solve the model developed in this chapter.

Although a bi-objective optimization problem was discussed to maximize the generated power and minimize the power ramp rate, the main contribution of Chapter 4 was to develop a new power optimization constraint by combining Betz' law and statistical quality control theory.

In Chapter 5, a model for scheduling wind turbines was presented to study the minimization of the total cost of operating a wind farm. The optimized cost included the power shortage cost, operational and maintenance cost, and start-up cost. Each schedule

represents the operational status of wind turbines over a scheduling horizon. In Chapter 6, scheduling a wind farm in the presence of uncertain wind speed conditions was presented. Two scheduling models, the base model and the stochastic optimization model, were developed by integration of mathematical programming and data mining. A migrated particle swarm optimization algorithm was developed for solving the two scheduling models.

In the single wind turbine study, one challenge of the future research was the wind speed signal sensed by anemometer mounted at the back of wind turbine nacelle. Due to the location of the wind speed sensor, the measured data could not describe the wind speed conditions at the front of wind turbine rotor. Control of wind turbines based on the current wind speed data impaired the performance of wind turbine. Therefore, a more advanced wind speed sensors, such as laser sensors, needed to be mounted on wind turbines to improve the wind turbine control.

In the further research on wind farm scheduling, the wake loss effect needed to be considered. Since the wind speed would be decayed after passing a wind turbine, the wake loss effect could significantly impact the scheduling strategies of a wind farm. To consider the wake loss effect, the wind direction data was needed. The wind farm scheduling model could also be extended by considering the uncertainty of electric power demand and electricity prices.

REFERENCES

[1] A. Abdelli, B. Sareni and X. Roboam, "Optimization of a small passive wind turbine generator with multiobjective genetic algorithms", *International Journal of Applied Electromagnetics and Mechanics*, Vol. 26, No. 3-4, pp. 175-182, 2007.

[2] M.A. Abido,"Optimal design of power-system stabilizers using particle swarm optimization," *IEEE Transactions on Energy Conversion*, Vol. 17, No. 3, pp. 406-413, 2002.

[3] A. A. Al-Haddad, E. Enaya and M.A. Fahim, "Performance of a thermodynamic water pump," *Applied Thermal Engineering*, Vol. 16, No. 4, pp. 321 – 334, 1996.

[4] M. R. AlRashidi and M. E. El-Hawary, "A Survey of Particle Swarm Optimization Applications in Electric Power Systems", *IEEE Transactions on Evolutionary Computation*, Vol. 13, No. 4, pp. 913 – 918, 2009.

[5] B. Barán, C. Von Lücken and A. Sotelo, "Multi-objective pump scheduling optimisation using evolutionary strategies," *Advances in Engineering Software*, Vol. 36, No. 1, pp. 39 – 47, 2005.

[6] T. G. Barbounis, J. B. Theocharis, and P. S. Dokopoulosy, "Long-term Wind Speed and Power Forecasting Using Local Recurrent Neural Network Models", *IEEE Transactions on Energy Conversion*, Vol.21, No.1, pp.273-284, 2006.

[7] R. Barthelmie, S. Frandsen, M. Nielsen, S. Pryor, P. Rethore, and H. Jørgensen, "Modelling and measurements of power losses and turbulence intensity in wind turbine wakes at Middelgrunden offshore wind farm", *Wind Energy*, Vol. 10, No. 6, pp. 517-528, 2007.

[8] G. Bathurst, J. Weatherill, and G. Strbac, "Trading wind generation in short term energy markets," *IEEE Transactions on Power Systems*, vol. 17, pp. 782-789, 2002.

[9] M. J. A. Berry and G. S. Linoff, *Data Mining Techniques: For Marketing, Sales, and Customer Relationship Management (2nd ed)*, Wiley: New York, 2004.

[10] H. Bersini and F. Varela, "Hints for Adaptive Problem Solving Gleaned from Immune Network", *Proceedings of the First Conference on Parallel Problem Solving From Nature*, pp. 343-354, 1990.

[11] F. Besnard and L. Bertling, "An approach for condition-based maintenance optimization applied to wind turbine blades", *IEEE Transactions on Sustainable Energy*, Vol. 1, No. 2, pp. 77-83, 2010.

[12] R. Bessa, V. Miranda and J. Gama, "Entropy and Correntropy Against Minimum Square Error in Offline and Online Three-Day Ahead Wind Power Forecasting", *IEEE Transactions on Power Systems*, Vol. 24, pp. 1657-1666, 2009.

[13] S. Bhowmik, R. Spee and J. H. R. Enslin, "Performance Optimization for Doubly Fed Wind Power Generation Systems", *IEEE Transactions on Industry Applications*, Vol. 35, No. 4, pp. 949-958, 1999.

[14] B. Boukhezzar and H. Siguerdidjane, “Nonlinear control with wind estimation of a DFIG variable speed wind turbine for power capture optimization,” *Energy Conversion and Management*, Vol. 50, No. 4, pp. 885-892, 2009.

[15] B. Boukhezzar, H. Siguerdidjane and M. Hand, “Nonlinear Control of Variable-Speed Wind Turbines for Generator Torque Limiting and Power Optimization”, *ASME Transactions: Journal of Solar Energy Engineering*, vol. 128, pp. 516-530, 2006.

[16] D. Büche, P. Stoll, R. Dornberger and P. Koumoutsakos, “Multiobjective evolutionary algorithm for the optimization of noisy combustion processes,” *IEEE Transactions on Man, Control, and Cybernetics – Part C,* vol. 32, pp. 460-473, 2002.

[17] L. Breiman, "Random Forests," *Machine Learning*, Vol. 45, No. 1, pp. 5-32, 2001.

[18] L. Breiman, J. H. Friedman, R. A. Olshen, and C.J. Stone, *Classification and Regression Trees*. Monterey, CA: Wadsworth, Inc, 1984.

[19] E. F. Camacho and C. Bordons, *Model Predictive Control*. London, U.K.: Springer-Verlag, 1999.

[20] V. Calderaro, V. Galdi, A. Piccolo and P. Siano, “A fuzzy controller for maximum energy extraction from variable speed wind power generation systems”, *Electric Power Systems Research*, Vol. 78, No. 6, pp. 1109-1118, 2008.

[21] R. Cass and B. Radl, “Adaptive process optimization using functional-link networks and evolutionary optimization,” *Control Engineering Practice*, vol. 4, pp. 1579-1584, 1997.

[22] J. Z. Chu, S. S. Shieh, S. S. Jang, C. I. Chien, H. P. Wan, and H. H. Ko, “Constrained optimization of combustion in a simulated coal-fired boiler using artificial neural network model and information analysis,” *Fuel*, vol. 82, pp. 693-703, 2003.

[23] M. Clerc and J. Kennedy, “The Particle Swarm – Explosion, Stability, and Convergence in a Multidimensional Complex Space”, *IEEE Transactions on Evolutionary Computation*, Vol. 6, No. 1, pp. 58 – 73 , 2002.

[24] R.R. Coifman and M.V. Wickerhauser, “Entropy-based algorithms for best basis selection”, *IEEE Transactions on Information Theory*, Vol. 38, No. 2, pp. 713-718, 1992.

[25] I. G. Damousis, M. C. Alexiadis, J. B. Theocharis and P. S. Dokopoulos, “A fuzzy model for wind speed prediction and power generation in wind parks using spatial correlation”, *IEEE Transaction on Energy Conversion*, Vol. 19, pp. 352-361, 2004.

[26] D. Dasgupta, “An Artificial Immune System as a Multi-Agent Decision Support System”, *Proceedings of the IEEE International Conference on Systems, Man and Cybernetics*, 1998, pp. 3816-3820.

[27] I. Daubechies, *Ten Lectures on Wavelets*, Society for Industrial and Applied Mathematics, Philadelphia, PA, 1992.

[28] L. N. de Castro, “Immune, Swarm, and Evolutionary Algorithms Part II: Philosophical Comparisons”, *Proc. of the ICONIP Conference (International Conference on Neural Information Processing), Workshop on Artificial Immune Systems*, pp. 1469 – 1473, 2002.

[29] L. N. de Castro and J. Timmis, *Artificial Immune Systems: A New Computational Intelligence Approach*, London: Springer-Verlag, 2002a.

[30] L. N. de Castro and J. Timmis, “An Artificial Immune Network for Multimodal Optimization”, *Proceedings of the Congress on Evolutionary Computation*, 2002b, pp. 699-704.

[31] L. N. de Castro and F. J. Von Zuben, “Learning and Optimization Using the Clonal Selection Principle”, *IEEE Transactions on Evolutionary Computation*, Vol. 6, No. 3, pp. 239-251, 2002.

[32] M. A. Duran and I. E. Grossmann, “An Outer-Approximation Algorithm for a Class of Mixed-integer Nonlinear Programs”, *Mathematical Programming*, Vol. 36, No. 3, pp. 307–339, 1986.

[33] T. H. M. El-Fouly, E. F. El-Saadany and M. M. A. Salama, “One Day Ahead Prediction of Wind Speed and Direction”, *IEEE Transaction on Energy Conversion*, vol. 23, pp. 191 – 201, 2008.

[34] R. Fadaeinedjad, G. Moschopoulos, M. Moallem, “Investigation of voltage sag impact on wind turbine tower vibrations,” *Wind Energy*, Vol. 11, No. 4, pp. 351-375, 2008.

[35] C. Fang, J. Lee and M. A. Schilling, “Balancing Exploration and Exploitation Through Structural Design: The Isolation of Subgroups and Organizational Learning”, *Organization Science*, Vol. 21, No. 3, pp. 625 – 642, 2010.

[36] J. Farmer, N. Packard and A. Perelson, “The immune system, adaptation and machine learning”, *Physica D*, Vol. 2, No. 1-3, pp. 187-204, 1986.

[37] P. Flores, A. Tapia and G. Tapia, “Application of a control algorithm for wind speed prediction and active power generation”, *Renewable Energy*, vol. 30, pp. 523-536, 2005.

[38] S. Forrest, B. Javornik, R. E. Smith and A. S. Perelson, “Using Genetic Algorithms to Explore Pattern Recognition in the Immune System”, *Evolutionary Computation*, Vol. 1, No. 3, pp. 191-211, 1993.

[39] A. Fraser, “Simulation of genetic systems by automatic digital computers. I. Introduction”, *Australian Journal of Biological Sciences*, Vol. 10, pp. 484–491, 1957.

[40] J. H. Friedman, “Greedy function approximation: A gradient boosting machine,” *Ann. Statist.*, Vol. 29, No. 5, pp. 1189–1232, 2001.

[41] J. H. Friedman, “Stochastic gradient boosting,” *Comput. Statist. Data Anal.*, Vol. 38, No. 4, pp. 367-378, 2002.

[42] A. M. Geoffrion, "Generalized Benders Decomposition", *Journal of Optimization Theory and Applications*, Vol. 10, No. 4, pp. 237–260, 1972.

[43] R. Goldstein and W. Smith, "Water & Sustainability (Volume 4): U.S. Electricity Consumption for Water Supply & Treatment—The Next Half Century," Electric Power Research Institute, Inc. (EPRI), Palo Alto, California, Technical Report, 2002.

[44] P. V. Goosen, P. Riedel and J. W. Strauss, "GMPC enables energy transmission over interconnected SAPP grid", *IEEE Transactions on Power Delivery*, Vol. 18, No. 3, pp. 945 – 952, 2003.

[45] O. K. Gupta and A. Ravindran, "Branch and Bound Experiments in Convex Nonlinear Integer Programming", *Management Science*, Vol. 31, No. 12, pp. 1533–1546, 1985.

[46] M. H. Hansen, "Improved modal dynamics of wind turbines to avoid stall-induced vibrations", *Wind Energy*, Vol. 6, No. 2, pp. 179-195, 2003.

[47] L. K. Hansen and P. Salamon, "Neural Network Ensembles", *IEEE Transactions on Pattern Analysis and Machine Intelligence*, Vol. 12, No. 10, pp. 993-1001, 1990.

[48] M. H. Hansen, K. Thomsen, P. Fuglsang and T. Knudsen, "Two methods for estimating aeroelastic damping of operational wind turbine modes from experiments," *Wind Energy*, Vol. 9, No.1-2, pp. 179 – 191, 2006.

[49] J.A. Harding, M. Shahbaz, S. Srinivas, and A. Kusiak, "Data Mining in Manufacturing: A Review", *ASME Transactions: Journal of Manufacturing Science and Engineering*, Vol. 128, No. 4, pp. 969-976, 2006.

[50] D.-H. Hellmann, H. Rosenberger and E. F. Tusel, "Saving of energy and cost in seawater desalination with speed controlled pumps," *Desalinatio*, Vol. 139, No. 1 – 3, pp. 7 – 19, 2001.

[51] R. Houser, "Realizing energy saving through variable-speed pumping - A primer," *Water Environment and Technology*, Vol. 16, No. 4, pp. 51 - 54, 2004.

[52] G. Javier, M. R. Rocio, M. S. Luz and M. G. Alicia, "Stochastic Joint Optimization of Wind Generation and Pumped-Storage Units in an Electricity Market", *IEEE Transactions on Power Systems*, Vol. 23, No. 2, pp. 460-468, 2008.

[53] K. Johnson, L. Pao, M. Balas and L. Fingersh, "Control of variable-speed wind turbines: standard and adaptive techniques for maximizing energy capture," *IEEE Control Systems Magazine*, Vol. 26, pp. 70-81, 2006.

[54] N. Kakimoto, H. Satoh, S. Takayama and K. Nakamura, "Ramp-rate control of photovoltaic generator with electric double-layer capacitor", *IEEE Transactions on Energy Conversion*, Vol. 24, No. 2, pp. 465-473, 2009.

[55] M. S. Kang, "Generation Cost Assessment of an Isolated Power System With a Fuzzy Wind Power Generation Model", *IEEE Transactions on Energy Conversion*, Vol. 22, No. 2, pp. 397-404, 2007.

[56] G. N. Kariniotakis. G. *S.* Stavrakakis. and E. F. Nogaret, "Wind power forecasting using advanced neural networks models". *IEEE Transactions on Energy Conversion*, Vol.11, pp.762-761, 1996.

[57] J. Kennedy and R.C. Eberhart, "Particle swarm optimization", in *IEEE International Conference on Neural Networks*, 1995, pp. 1942-1948.

[58] H. Ko, K. Lee, M. Kang, H. Kim, "Power quality control of an autonomous wind-diesel power system based on hybrid intelligent controller," *Neural Networks*, Vol. 21, No. 10, pp. 1439-1446, 2008.

[59] M. Kobayashi, *Wavelets and their Applications: Case Studies*, 1st ed., Philadelphia: Society for Industrial and Applied Mathematics, 1998.

[60] R. Kohavi and G. H. John, "Wrapper for feature subset selection," *Artificial Intelligence*, Vol. 97, No. 1-2, pp. 273-324, 1997.

[61] A. Kusiak and M. Y. Li, "Reheat Optimization of the Variable-Air-Volume Box", *Energy*, Vol. 35, No. 5, pp. 1997 – 2005, 2010.

[62] A. Kusiak, M.Y. Li and Z. Zhang, "A Data-driven Approach for Steam-Load Prediction in Buildings", *Applied Energy*, Vol. 87, No. 3, pp. 925-933, 2010a.

[63] A. Kusiak, M.Y. Li and H. Zheng, "Virtual Models of Indoor-Air-Quality Sensors", *Applied Energy*, Vol. 87, No. 6, pp. 2087-2094, 2010b.

[64] A. Kusiak and Z. Song, "Clustering-Based Performance Optimization of the Boiler-Turbine System", *IEEE Transactions on Energy Conversion*, Vol. 23, No. 2, pp. 651-658, 2008.

[65] A. Kusiak, Z. Song, and H. Zheng, "Anticipatory Control of Wind Turbines with Data-Driven Predictive Models," *IEEE Transactions on Energy Conversion*, Vol. 24, No. 3, pp. 766-774, 2009a.

[66] A. Kusiak, Z. Song and H. Zheng, "Power Optimization of Wind Turbines with Data Mining and Evolutionary Computation", *Renewable Energy*, Vol. 35, No. 3, pp. 695-702, 2010c.

[67] A. Kusiak and Z. Zhang, "Analysis of Wind Turbine Vibrations Based on SCADA Data," *ASME Journal of Solar Engineering*, Vol. 132, No. 3, pp. 031008-1 - 031008-12, 2010a.

[68] A. Kusiak and Z. Zhang, "Short-Horizon Prediction of Wind Power: A Data-Driven Approach," *IEEE Transactions on Energy Conversion*, Vol. 25, No. 4, pp. 1112 - 1122, 2010b.

[69] A. Kusiak, Z. Zhang and M.Y. Li, "Optimization of Wind Turbine Performance with Data-Driven Models", *IEEE Transactions on Sustainable Energy*, Vol. 1, No. 2, pp. 66-76, 2010d.

[70] A. Kusiak and Z. Zhang, "Adaptive Control of a Wind Turbine with Data Mining and Swarm Intelligence", *IEEE Transactions on Sustainable Energy*, Vol. 2, No. 1, pp. 28 – 36, 2011.

[71] A. Kusiak and H. Y. Zheng, “Optimization of Wind Turbine Energy and Power Factor with an Evolutionary Computation Algorithm”, *Energy*, Vol. 35, No. 3, pp. 1324-1332, 2010.

[72] A. Kusiak, H. Zheng, and Z. Song, “Wind Farm Power Prediction: A Data-Mining Approach,” *Wind Energy*, Vol. 12, No. 3, pp. 275-293, 2009b.

[73] A. Kusiak, H. Zheng and Z. Song, “Short-Term Prediction of Wind Farm Power: A Data-Mining Approach,” *IEEE Transactions on Energy Conversion*, Vol. 24, No. 1, pp. 125-136, 2009c.

[74] A. Kusiak, H. Zheng and Z. Song, “On-line Monitoring of Power Curves,” *Renewable Energy*, Vol. 34, No. 6, pp. 1487-1493, 2009d.

[75] A. Kusiak, H. Zheng and Z. Song, “Models for Monitoring Wind Farm Power,” *Renewable* Energy, Vol. 34, No. 3, pp. 583-590, 2009e.

[76] D. Laino, C. Butterfield, R. Thresher, and D. Dodge, “Evaluation of select IEC standard wind turbine design cases on the combined experiment wind turbine model,” *Wind Energy*, American Society of Mechanical Engineers, Solar Energy Division (Publication) SED, Vol. 14, pp. 47-48, 1993.

[77] K. Y. Lee and J. B. Park, “Application of Particle Swarm Optimization to Economic Dispatch Problem: Advantages and Disadvantages”, *Power Systems Conference and Exposition*, pp. 188 – 192, 2006.

[78] T. Y. Lee, “Optimal spinning reserve for a wind-thermal power system using EIPSO”, *IEEE Transactions on Power Systems*, Vol. 22, No. 4, pp. 1612-1621, 2007.

[79] A. Leite, C. Borges, and D. Falcão, “Probabilistic Wind Farms Generation Model for Reliability Studies Applied to Brazilian Sites,” *IEEE Transactions on Power Systems*, Vol. 21, No. 4, pp. 1493-1501, 2006.

[80] W. Leithead and B. Connor, "Control of variable speed wind turbines: dynamic models," *International Journal of Control*, Vol. 73, No. 13, pp. 1173-1189, 2000.

[81] D. Li, C. He, and Y. Fu, “Optimization of internal electric connection system of large offshore wind farm with hybrid genetic and immune algorithm”, in *3rd International Conference on Deregulation and Restructuring and Power Technologies*, 2008, pp. 2476-2481.

[82] Z. Lian, S. Park and H. Qi, “Analysis on energy consumption of water-loop heat pump system in China,” *Applied Thermal Engineering*, Vol. 25, No. 1, pp. 73 – 85, 2005.

[83] C. E. Ling, Y. -W. Huang, H. L. Chow, and C. L. Huang, “A distribution system outage dispatch by data base method with real-time revision”, *IEEE Transactions on Power Delivery*, Vol. 4, No. 1, pp. 515 – 523, 1989.

[84] D. Liu, K. C. Tan, C. K. Goh and W. K. Ho, “A Multiobjective Memetic Algorithm Based on Particle Swarm Optimization”, *IEEE Transactions on Systems, Man, and Cybernetics*: Part B, Vol. 37, No. 1, pp. 42-50, 2007.

[85] G.P. Liu, *Nonlinear Identification and Control: A Neural Network Approach*, Springer, London, 2001.

[86] P. Louka, G. Galanis, N. Siebert, G. Kariniotakis, P. Katsafados, I. Pytharoulis, and G. Kallos, "Improvements in wind speed forecasts for wind power prediction purposes using Kalman filtering", *Journal of Wind Engineering and Industrial Aerodynamics*, vol. 96, pp. 2348-2362, 2008.

[87] C. H. Lu and C. C. Tsai, "Generalized predictive control using recurrent fuzzy neural networks for industrial processes", *Journal of Process Control*, Vol. 17, pp. 83-92, 2007.

[88] J. F. Manwell, J. G. McGowan, and A. L. Rogers, *Wind Energy Explained: Theory, Design and Application*, 1st Ed., London, John Wiley & Sons, 2002.

[89] J. G. March, "Exploration And Exploitation In Organizational Learning", *Organization Science*, Vol. 2, No. 1, pp. 71 – 87, 1991.

[90] S. Milgram, "The small world problem", *Psychology Today*, Vol. 1, No. 1, pp. 60 – 67, 1967.

[91] B. Mirzaeian, M. Moallem, V. Tahani, and C. Lucas, "Multiobjective Optimization Method Based on a Genetic Algorithm for Switched Reluctance Motor Design", *IEEE Transactions on Magnetics*, Vol. 38, No. 3, pp. 1524-1527, 2002.

[92] M. Molinas, J. A. Suul and T. Undeland, "Extending the Life of Gear Box in Wind Generators by Smoothing Transient Torque With STATCOM", *IEEE Transactions on Industrial Electronics*, Vol. 57, No. 2, pp. 476-484, 2010.

[93] J. Mora, J. Barón, J. Santos, and M. Payán, "An evolutive algorithm for wind farm optimal design," *Neurocomputing*, Vol. 70, No. 16, pp. 2651-2658, 2007.

[94] S. Morimoto, H. Nakayama, M. Sanada and Y. Takeda, "Sensorless output maximization control for variable-speed wind generation system using IPMSG", *IEEE Transactions on Industry Applications*, Vol. 41, No. 1, pp. 60-67, 2005.

[95] C. F. Moyano and J. A. Peças Lopes, "An optimization approach for wind turbine commitment and dispatch in a wind park", *Electric Power Systems Research*, Vol. 79, No. 1, pp. 71-79, 2009.

[96] E. Muljadi and C. P. Butterfield, "Pitch-controlled variable-speed wind turbine generation", *IEEE Transactions on Industry Applications*, Vol. 37, No. 1, pp. 240-246, 2001.

[97] I. Munteanu, N. Cutululis, A. Bratcu, and E. Ceanga, "Optimization of variable speed wind power systems based on a LQG approach," *Control Engineering Practice*, Vol. 13, No. 7, pp. 903-912, 2005.

[98] P.J. Murtagh, A. Ghosh, B. Basu, and B. M. Broderick, "Passive control of wind turbine vibrations including blade/tower interaction and rotationally sampled turbulence," *Wind Energy*, Vol. 11, No. 4, pp. 305-317, 2008

[99] Ö. Mutlu, E. Akpınar, and A. Balıkcı, "Power quality analysis of wind farm connected to Alaçatı substation in Turkey," *Renewable Energy*, Vol. 34, No. 5, pp. 1312-1318, 2009.

[100]T. Ogilvie, E. Swidenbank and B. W. Hogg, "Use of data mining techniques in the performance monitoring and optimisation of a thermal power plant", in *IEE Colloquium on Knowledge Discovery and Data Mining*, 1998, pp. 7/1-7/4.

[101]D. Ouelhadj and S. Petrovic, "A survey of dynamic scheduling in manufacturing systems," *Journal of Scheduling*, Vol. 12, pp. 417-431, 2009.

[102]W. L. Peterson and S. R. Brammer, "Capacity based Lagrangean relaxation unit commitment with ramp rate constraints", *IEEE Transactions on Power Systems*, Vol. 10, No. 2, pp. 1077-1084, 1995.

[103]V. S. Pappala and I. Erlich, "A new approach for solving the unit commitment problem by adaptive particle swarm optimization", *Proc. IEEE Power and Energy Soc. General Meeting—Conversion and Delivery of Electrical Energy in the 21st Century*, pp. 1 – 6, 2008.

[104]V. S. Pappala, I. Erlich, K. Rohrig and J. Dobschinski, "A Stochastic Model for the Optimal Operation of a Wind-Thermal Power System", *IEEE Transactions on Power Systems*, Vol. 24, No. 2, pp. 940 – 950, 2009.

[105]J. B. Park, K. S. Lee, J. R. Shin and K. Y. Lee, "A Particle Swarm Optimization for Economic Dispatch With Nonsmooth Cost Functions", *IEEE Transactions on Power Systems*, Vol. 20, No. 1, pp. 34 – 42, 2005.

[106]J. B. Park, Y. W. Jeong, J. R. Shin and K. Y. Lee, "An Improved Particle Swarm Optimization for Nonconvex Economic Dispatch Problems", *IEEE Transactions on Power Systems*, Vol. 25, No. 1, pp. 156 – 166, 2010.

[107]M. Prats, J. Carrasco, E. Galván, J. Sánchez, L. Franquelo and C. Batista, "Improving transition between power optimization and power limitation of variable speed, variable pitch wind turbines using fuzzy control techniques" in *IECON Proceedings (Industrial Electronics Conference)*, 2000, pp. 1497-1502.

[108]C. Potter and M. Negnevitsky, "Very Short-term Wind Forecasting for Tasmanian Power Generation", *IEEE Transactions on Power Systems*, vol. 21, 2006.

[109]A. Ratnaweera, S. K. Halgamuge and H. C. Watson, "Self-Organizing Hierarchical Particle Swarm Optimizer With Time-Varying Acceleration Coefficients", *IEEE Transactions on Evolutionary Computation*, Vol. 8, No. 3, pp. 240 – 254, 2004.

[110]B. Ren and C. Jiang, "A review on the economic dispatch and risk management considering wind power in the power market," *Renewable and Sustainable Energy Reviews*, Vol. 13, pp. 2169-2174, 2009.

[111]J. A. Rossiter, *Model-Based Predictive Control: A Practical Approach*. New York: CRC Press, 2003

[112]H. Rusinowski, M. Szega, A. Szlk and R. Wilk, "Methods of choosing the optimal parameters for solid fuel combustion in stoker-fired boilers," *Energy Conversion and Management*, vol. 43, pp. 1363-1375, 2002.

[113]K. Saranyasoontorn, and L. Manuel, "A comparison of wind turbine design loads in different environments using inverse reliability techniques," *Wind Energy*, Vol. 126, No. 4, pp. 1060-1068, 2004.

[114]B. Sareni, A. Abdelli, X. Roboam and D. Tran, "Model simplification and optimization of a passive wind turbine generator," *Renewable Energy*, Vol. 34, No.12, pp. 2640-2650, 2009.

[115]A. K. Saxena and M. Vora, "Novel Approach for the use of Small World Theory in Particle Swarm Optimization", *16th International Conference on Advanced Computing and Communications*, pp. 363 – 366, 2008.

[116]B. Schölkopf, C. J.C. Burges, and A. J. Smola, *Advances in Kernel Methods: Support Vector Learning*. Cambridge, MA: MIT Press, 1999.

[117]T. Senjyu, R. Sakamoto, N. Urasaki, T. Funabashi, H. Fujita, and H. Sekine, "Output power leveling of wind turbine generator for all operating regions by pitch angle control," *IEEE Transactions on Energy Conversion*, Vol. 21, No. 2, pp. 467-475, 2006.

[118]J. H. Seo, C. H. Im, C. G. Heo, J. K. Kim, H. K. Jung and C. G. Lee, "Multimodal Function Optimization Based on Particle Swarm Optimization", *IEEE Transactions on Magnetics*, Vol. 42, No. 4, pp. 1095 – 1098, 2006.

[119]S. Shah, A. Kusiak, and M. O'Donnell, "Patient-Recognition Data-Mining Model for BCG-plus Interferon Immunotherapy Bladder Cancer Treatment", *Computers in Biology and Medicine*, Vol. 36, No. 6, pp. 634-655, 2006.

[120]Shakhnarovish, Darrell, and Indyk, *Nearest-Neighbor Methods in Learning and Vision*. The MIT Press, 2005.

[121]S. K. Shevade, S. S. Keerthi, C. Bhattacharyya, and K. R. K. Murthy, "Improvements to the SMO algorithm for SVM regression", *IEEE Transactions on Neural Networks*, Vol. 11, No. 5, pp. 1188-1193, 2000.

[122]Y, Shi and R. Eberhart, "Parameter Selection in Particle Swarm Optimization," *Proceedings of the 7th Annual Conference on Evolutionary Programming*, 1998, pp. 591-600.

[123]H. Siahkali and M. Vakilian, "Electricity generation scheduling with large-scale wind farms using particle warm optimization," *Electric Power Systems Research*, Vol.79, pp. 826-836, 2009.

[124]G. Sideratos, and N.D. Hatziargyriou, "An Advanced Statistical Method for Wind Power Forecasting". *IEEE Transactions on Power Systems*, Vol.22, pp.258-265, 2007.

[125]H. Siegelmann and E. Sontag, "Analog computation via neural networks", *Theoretical Computer Science*, vol. 131, no. 2, pp. 331-360, 1994.

[126]M. Smith, *Neural Networks for Statistical Modeling*, Van Nostrand Reinhold, 1993.

[127]Z. Song and A. Kusiak, "Multi-Objective Optimization of Temporal Processes", *IEEE Transactions on Systems, Man, and Cybernetics: Part B*, Vol. 40, No. 3, pp. 845-856, 2010.

[128]C. M. Stein, "Estimation of the Mean of a Multivariate Normal Distribution", *The Annals of Statistics*, Vol. 9, No. 6, pp. 1135-1151, 1981.

[129]I. Steinwart and A. Christmann, *Support Vector Machines*. New York: Springer-Verlag, 2008.

[130]A. J. Svoboda, C. Tseng, C. Li and R. B. Johnson, "Short-term resource scheduling with ramp constraints", *IEEE Transactions on Power Systems*, Vol. 12, No. 1, pp. 77-83, 1997.

[131]D. J. Swider, "Compressed Air Energy Storage in an Electricity System with Significant Wind Power Generation", *IEEE Transactions on Energy Conversion*, Vol. 22, No. 1, pp. 95-102, 2007.

[132]Y. Y. Tang, L. H. Yang, J. Liu and H. Ma, *Wavelet Theory and its Application to Pattern Recognition*. 1st ed., Singapore: River Edge, New Jersey: World Scientific, 2000.

[133]J. Timmis, M. Neal and J. Hunt, "An artificial immune system for data analysis", *Biosystems*, Vol. 55, No. 1-3, pp. 143-150, 2000.

[134]U.S. Department of Energy, *20% Wind Energy by 2030 Report*, 2008.

[135]T. Ustüntas and A. D. Sahin, "Wind turbine power curve estimation based on cluster center fuzzy logic modeling", *Journal of Wind Engineering and Industrial Aerodynamics*, Vol. 96, No. 5, pp. 611 – 620, 2008.

[136]S. Y. Wang, G. L. Bai, Y. Cao and B. Li, "An algorithm of simulating human intelligent control for combustion system," in *IEEE International Conference on Intelligent Processing Systems*, 1997, pp. 786-771.

[137]Q. Wang and L. Chang, "An intelligent maximum power extraction algorithm for inverter-based variable speed wind turbine systems", *IEEE Transaction on Energy Conversion*, Vol. 19, No. 5, pp. 1242-1249, 2004.

[138]J. Wang, T. Chang and J. Chen, "An enhanced genetic algorithm for bi-objective pump scheduling in water supply", *Expert Systems with Applications*, Vol. 36, No. 7, pp. 10249 – 10258, 2009.

[139]S. J. Watson, B. J. Xiang, W. Yang, P. Tavner, and C. Crabtree, "Condition monitoring of the power output of wind turbine generators using wavelets", *IEEE Transactions on Energy Conversion*, Vol. 25, No. 3, pp. 715-721, 2010.

[140]D. J. Watts and S. H. Strogatz, "Collective dynamics of 'small-world' networks", *Nature*, Vol. 393, No. 6684, pp. 440 – 442, 1998.

[141]P. Welsby, M. Pezzani, S. Devotta, P.J. Diggory and J.J. Guy, "Steady- and dynamic-state simulations of heat-pumps. Part II: modeling of a motor driven water-to-water heat-pump," *Applied Energy*, Vol. 31, No. 4, pp. 239 – 262, 1988.

[142]T. Westerlund and F. Petersson, “A Extended Cutting Plane Method for Solving Convex MINLP Problems”, *Computers & Chemical Engineering*, Vol. 19, No. 1, pp. 131–136, 1995.

[143]I. H. Witten and E. Frank, *Data Mining: Practical Machine Learning Tools and Techniques.* 2nd ed. San Francisco, CA: Morgan Kaufmann, 2005.

[144]V. Wowk, *Machinery Vibration: Measurement and Analysis*, McGraw-Hill, 1991.

[145]W. Xuan, J. H. Chow, B. Fardanesh and A. -A. Edris, “A dispatch strategy for a unified power-flow controller to maximize voltage-stability-limited power transfer”, *IEEE Transactions on Power Delivery*, Vol. 20, No. 3, pp. 2022 – 2029, 2005.

[146]T. Yeh and L. Wang, “A Study on Generator Capacity for Wind Turbines Under Various Tower Heights and Rated Wind Speed Using Weibull Distribution”, *IEEE Transactions on Energy Conversion*, Vol. 23, No. 2, pp. 592 – 602, 2008.

[147]H. Y. Zheng and A. Kusiak, “Prediction of Wind Farm Power Ramp Rates: A Data-Mining Approach”, *ASME Journal of Solar Engineering*, Vol. 131, No. 3, pp. 031011-1- 031011-8, 2009.

[148]Wind Energy The Facts, “Economics of Wind Power”, http://www.wind-energy-the-facts.org/en/part-3-economics-of-wind-power/, Accessed in 2011

[149]AWEA, http://www.awea.org/, Accessed in 2011.

[150]World Meteorological Organization, “World Record Wind Gust: 408 km/h”, http://www.wmo.int/pages/mediacentre/infonotes/info_58_en.html.